POLY(ETHYLENE GLYCOL)-BASED MATERIALS AS NANOCARRIERS FOR SMALL MOLECULES AND MACROMOLECULES

By

Yu Ling Lien

A THESIS

Submitted to
Michigan State University
in partial fulfillment of the requirements
for the degree of

Chemistry – Master of Science

2015

ABSTRACT

POLY(ETHYLENE GLYCOL)-BASED MATERIALS AS NANOCARRIERS FOR SMALL MOLECULES AND MACROMOLECULES

By

Yu Ling Lien

Nanocarriers, the use of nanoparticles as a transport module for another substance, has been widely studied for their applications in biomedical and pharmaceutical fields. In our previous research, we have synthesized biocompatible and biodegradable poly(propargyl glycolide) (PPGL) polymer and its grafting derivatives and studied their ability to form unimolecular micelles and be used as nanocarriers. Moreover, the encapsulation of macromolecules using PPGL derivatives has inspired the thought of utilizing these materials as artificial chaperones for assisting protein refolding. A series of poly(ethylene glycol) (PEG) based analog, which will help us to further understand the role of degradability in PPGL derivatives, have been synthesized using a tetraoctylammonium bromide-triisobutylaluminum initiating system and the relationship between [monomer]/[initiator] ratio and molecular weights was studied. By increasing [monomer]/[initiator] ratio, the molecular weight of the resulting polymer also increases. In addition, copper(I)-catalyzed 1,3-dipolar cycloaddition of azides and alkynes "click" chemistry was used for the post-polymerization modification of these polymers. Water-soluble polymers that show lower critical solution temperature (LCST) behavior were obtained by varying the ratio between mDEG and decyl side chains. A relationship between cloud point temperatures and mol% mDEG in polymer was observed.

ACKNOWLEDGMENTS

I would like to thank my advisor, Dr. Milton R. Smith, who provided his knowledge and experiences and helped me overcome the issues during the research process. Thanks to my guidance committee, Dr. Xuefei Huang, Dr. James H. Geiger, Dr. Rémi Beaulac, for helpful discussions and suggestions.

Thanks to Dan Holmes, Kathy Severin, Dan Jones for teaching me various characterizations techniques. I would also like to thanks former and present group members form Smith group and Baker group as well as my dear friends, Budda, Dmitry, Sean, Gina, Wen, Hui Quanxuan, Heyi, Zhe, Greg, Behnaz, Salinda, Don, Kristin, Tim, Olivia, Kristen, Cathy, Tanner, Pengchao, Michelle for the assistance, the funny moments, and their friendship. They made my life at MSU enjoyable and interesting.

Finally, in memory of my former guidance committee member, Dr. Gregory Baker, for all I had learned from him before he left us forever.

TABLE OF CONTENTS

LIST OF TABLES

LIST OF FIGURES

LIST OF SCHEMES

Chapter 1 Introduction

The Study of Nanocarriers

In the past few decades, the rapid development of nanotechnology as well as nanomaterials has made a huge advance in material science. Generally, nanomaterials are defined as materials that have at least one dimension, which is sized between 1 to 100 nm and are composed of metals, ceramics, polymers, or composite materials.[1] Owing to their unique physicochemical properties, nanomaterials could be used in wide variety of applications such as electronics, solar cells, and medicine. The use of engineered functional nanoparticles has opened new avenues in biological and medical fields in the past two decades.[2] Nanoparticles have been shown to improve the solubility, diffusivity, and blood circulation half-life in drug delivery system.[2a, 3] Engineered functional nanoparticles could further provide the opportunity of tunable targeted delivery and controlled release of drugs and therapeutic biomolecules. Therefore, the study of different types of nanocarriers, which employ nanoparticles as a transport module for another substance, has drawn increasing attention in recent decades (Figure 1).[2a] Liposomes, polymeric micelles, and unimolecular micelles will be discussed as examples.

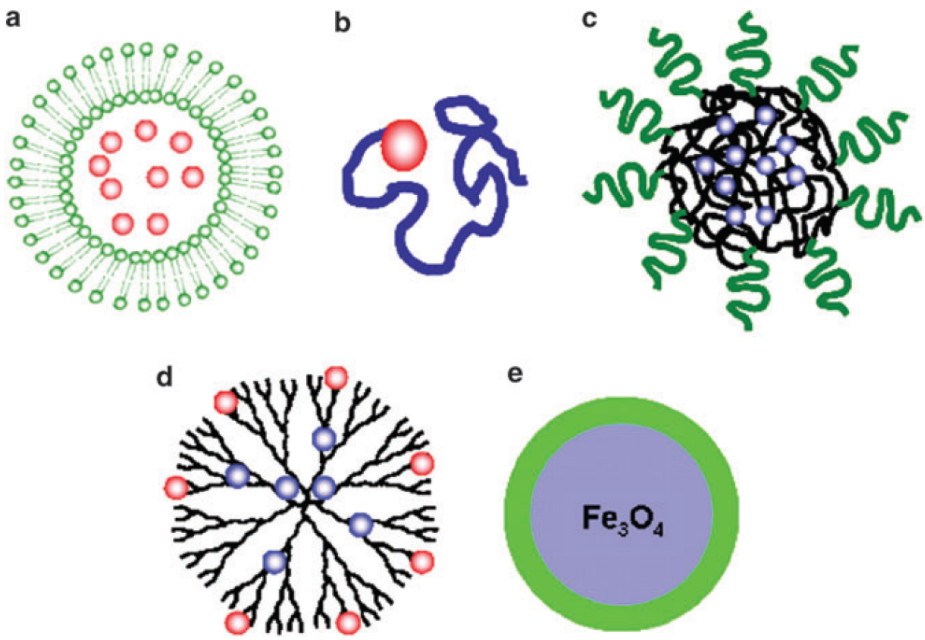

Figure 1. Schematic illustration of therapeutic nanoparticle platforms in preclinical development: (a) liposome, (b) polymer-drug conjugate, (c) polymeric nanoparticles, (d) dendrimer, and (e) iron oxide nanoparticle. The red dots represent hydrophilic drugs and the blue dots represent hydrophobic drugs. Reprinted from ref 2a. Copyright 2008 Nature Publishing Group.

Nanocarriers for Drug Delivery

Lipid-based carriers are especially attractive due to their biocompatible, non-toxic, and non-immunogenic nature.[3] Additionally; lipid-based carriers can entrap both hydrophobic and hydrophilic guest molecules. Liposomes are spherical vesicles that are typically formed from one phospholipid bilayer. Their similarity to cellular membranes makes it easier for liposomes to deliver the guest molecules to the cell; hence, liposomal formulations have been approved and widely utilized for *in vivo* delivery.[4] Although having many advantages, liposomes are not without disadvantages. For example, the common synthesis of liposomes first generates multilamellar vesicles (MLVs), which have several bilayers, and then the single vesicles are obtained via sonication with a broad size distribution.[5] Further processing is required for reducing their polydispersity.

The resulting vesicles are not very stable and tend to reform larger vesicles so additional stabilization techniques are needed. Moreover, the burst release of guest molecules results from the instability of liposomes also poses challenge in the use of liposomes for drug delivery.[3a, 6]

Polymeric micelles, formed by self-assembly of amphiphilic block copolymers in aqueous solutions, have also been explored for the use as nanocarriers.[2a, 3] Nanocarriers generated from amphiphilic block copolymers can be prepared in a simple and reproducible manner with precise control of morphology and architecture.[7] The most fascinating feature of polymeric micelle carriers is the ability to tune the sizes and the properties simply by changing the composition of amphiphilic block copolymers. Similar to micelles composed from conventional detergents, polymeric micelles consist of hydrophobic core and hydrophilic corona, but polymeric micelles are more stable compared to micelles composed from conventional detergents because of their lower critical micelle concentration (cmc).[7a]

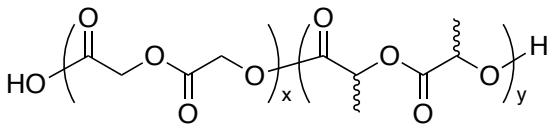

PGA-*b*-PLA (PLGA)
x = 0, PLA
y = 0, PGA

Figure 2. Structure of poly(lactic-*co*-glycolic acid) (PLGA).[8]

Biocompatibility and biodegradability are important criteria for a nanocarrier designed for medical uses; therefore, aliphatic polyesters derived from lactide, glycolide, and ε-caprolactone are especially attractive materials in drug and protein delivery applications.[9] Delivery devices composed of FDA (US Food and Drug Administration)-approved poly(lactic-*co*-glycolic acid) (PLGA) polymers have been an important

component in some commercialized drugs such as Lupron Depot and Decapeptyl (Figure 2).[8] Poly(ethylene glycol)/poly(ethylene oxide) (PEG/PEO) is one of the most studied non-degradable biocompatible polyethers and is widely used in composing nanocarriers. PEG is often used as a constituent with PLA in block copolymers because the hydrophilic PEG makes PLA-*b*-PEG polymers water soluble.[10] Amphiphilic block copolymers containing stimuli-responsive polymer have attracted special attention for undergoing conformational changes in response to external stimulus.[11] Thermally responsive poly(N-isopropylacrylamide) (PNIPAM) and its copolymers are one of the widely studied stimuli-responsive polymers in nanocarrier application since PNIPAM has a lower critical solution temperature (LCST) of 32 °C. Below this temperature it is water soluble and above PNIPAM precipitates.[12] In order to utilize the temperature difference between body temperature and target tissue to perform controlled release of the drug, incorporating PNIPAM in the system would be a convenient choice.[13] Although there have been many successes, the limitation cased by concentration dependent micelle formation behavior still poses challenges in the utility of polymeric micelles as nanocarriers (Scheme 1).[3a, 14]

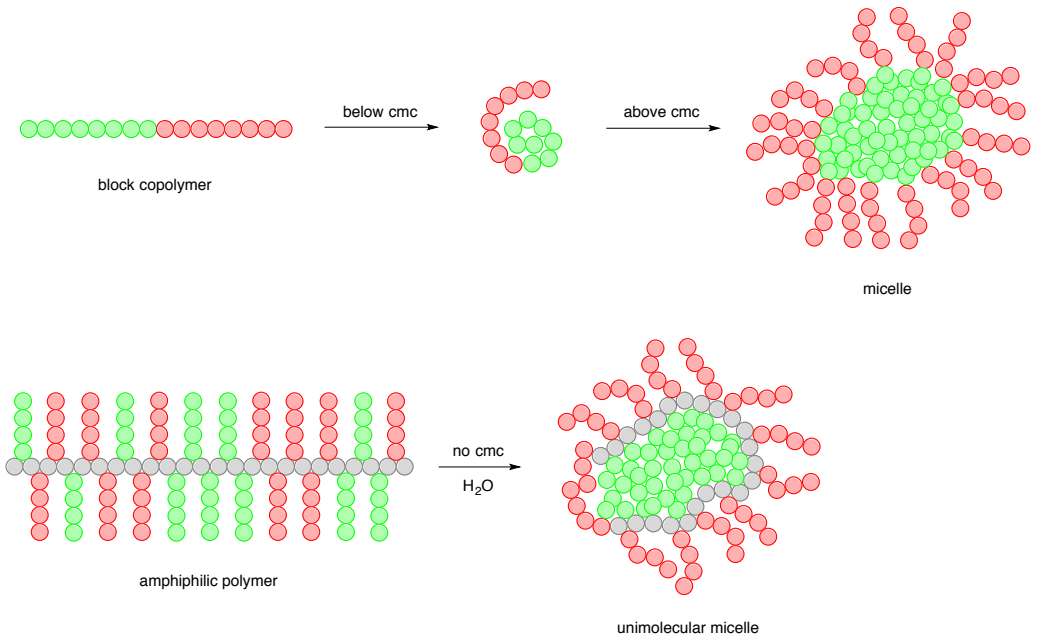

Scheme 1. Schematic illustration of the formation of polymeric micelle and unimolecular micelle.

Unimolecular micelles, first described by Newkome and co-workers,[15] have also been an attractive material for nanocarrier for their ability to form sub-20 nm size nanoparticles and their concentration independent micelle formation behavior.[16] Unimolecular micelles can be assembled by the intramolecular crosslinking of dendritic and linear polymer precursors. Two major strategies have been developed for dendrimer synthesis, divergent and convergent synthesis, since 1979.[17] The divergent method, also known as "inside-out" strategy, is the growth of a dendron from the core of the dendrimer to the molecular surface; on the other hand, the convergent method, also know as "outside-in" strategy, starts the synthesis from the molecular surface inward to the focal point at the core. Many studies have been done of dendritic nanocarriers; nonetheless, multiple-steps synthesis and inherent size restriction, which seldom exceed 10 nm, limit the usage of dendritic nanocarriers. Unimolecular micelles can also be prepared from the chain-collapse of single chain linear polymers and four approaches can be used.[16a] The

first approach is homofunctional chain-collapse where the polymer chain is functionalized with one kind of reactive pendent groups that could then react intramolecularly through covalent bonding or non-covalent interactions. In a second approach, the hetero-bifunctional chain collapse method, the polymer chain bears two functional groups, which could undergo intramolecular reaction. The third approach is the cross-linker mediated chain-collapse strategy, which involves the use of a monofunctional polymer and cross-linkers. The last approach is using any of the previous three methods on block copolymers and generating so-called molecular "tadpoles" or nanoparticle-coil copolymers.

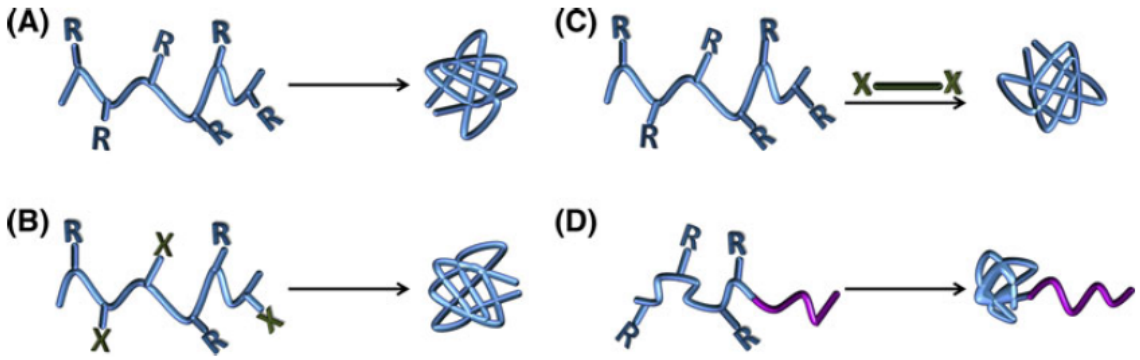

Figure 3. Schematic representation of the four strategies utilized for the synthesis of single-chain polymer unimolecular micelles: (a) homo-functional chain collapse, (b) hetero-functional chain collapse, (c) cross-linker-mediated chain collapse, and (d) one-block collapse of diblock or triblock copolymers. Reprinted from ref 16a. Copyright 2012 Springer Publishing.

In previous research, we have synthesized biocompatible, biodegradable, and tunable amphiphilic PEG/alkyl-grafted polymers of poly(propargyl glycolide) (PPGL), a substituted analog of PLA, which forms unimolecular micelles via hydrophobic interaction in aqueous solution.[18] PPGL-*g*-decyl/mPEG polymers were prepared by the post-polymerization modification of PPGL (Scheme 2). Interestingly, the resulting polymers could not only form unimolecular micelles, but it also exhibits a tunable LCST

behavior. These favorable properties give PPGL-*g*-decyl/mPEG polymers great potential for nanocarrier application; therefore, the encapsulation of hydrophobic and hydrophilic small guest molecules as well as macromolecules was performed and characterized.[18a] Azobenzene, a UV-active model for hydrophobic drugs, and Rodamine B, a hydrocarbon insoluble dye, were chosen as small guest molecules, also, an azobenzene taged poly(methyl methacrylate) (azobenzene-PMMA) was used as a guest macromolecule for encapsulation. The success of macromolecule encapsulation is an exciting result because it opens up the possibility of utilizing PPGL-*g*-decyl/mPEG polymers in biomacromolecule-related study such as nanocarriers for protein delivery and artificial chaperones for assisting protein refolding.

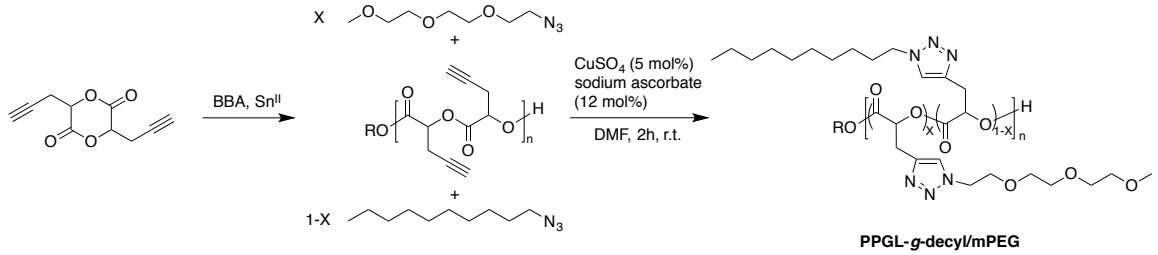

Scheme 2. Synthesis of PPGL-*g*-decyl/mPEG.

Protein Folding and Molecular Chaperones

How proteins fold and assemble from newly synthesized polypeptide chains into their native three-dimensional structures has been a topic of keen interest for several decades.[19] Christian Anfinsen and co-workers performed groundbreaking experiments in their protein folding studies in the early 1960s.[20] They conducted the experiments with ribonuclease A (RNase A), which catalyzes the cleavage of RNA into ribonucleotides. By adding and removing a denaturant and a reducing agent, the catalytic activity of RNase A was lost and restored, respectively. Under the assumption that the catalytic activity of RNase A could only be achieved when it folds into its proper three-dimensional structure,

a conclusion could be draw from Anfinsen's experiments that RNase A was unfolded and refolded reversibly *in vitro*. These results also demonstrated that the information needed for the native structure of RNase A is encoded in its amino acid sequence, which is matched with the thermodynamic hypothesis of protein folding. The thermodynamic hypothesis is the idea that the native structure of a protein is determined solely by the intrinsic properties of its amino acid sequence and is not the result of an external template.

It is believed that protein folding is governed by thermodynamics.[20c] The free-energy landscape of protein folding is described as a folding funnel, where the native state of a protein occupies a low energy state and the undesired aggregates, amyloid fibers, occupy a global energy minimum on the energy landscape.[21] On the other hand, the unfolded state of a protein corresponds to an ensemble of of different conformations with high internal energy, where each of the conformations folds along a unique pathway. This folding funnel energy landscape allows proteins to fold into their native structure within a reasonable amount of time. The major driving force of protein folding is hydrophobic interactions between hydrophobic residues, which lead to a gain of entropy as water molecules are expelled from the solvation sphere during the formation of the hydrophobic core.[22] Additionally, interactions such as hydrogen bonding,[22a] salt-bridge interaction,[23] and aromatic-aromatic interaction[24] between residues in the folded structure of the protein help stabilize the native structure. Although hydrophobic interactions are the key driving force for protein folding to their native state, they can also cause protein aggregation at higher concentrations of unfolded or partially folded proteins. If the concentration of unfolded or partially folded protein molecules is high enough, the exposed hydrophobic side chains in the protein molecules come in contact with each

other and form unwanted intermolecular aggregates. The aggregates in some proteins form irreversible ordered fibrils, known as amyloids, which are related to neurodegenerative diseases, such as Alzheimer's disease, Parkinson's diseases and spongiform neuro encephalopathies.[20c, 25] Although the formation of amyloids is irreversible, cells seem to have found strategies to avoid or reduce the formation of aggregates in the early stage.

Molecular chaperones are a group of functional related protein families, whose role includes preventing protein aggregation, assisting proper protein folding and assembly, and disassembling aggregates or misfolded proteins.[20c, 26] In general, molecular chaperones switch between two states, which is driven by adenosine triphosphate (ATP) binding and hydrolysis. In one state, chaperones have the ability to bind unfolded or partially folded polypeptides via hydrophobic interactions and hence prevent aggregation. In another state, the binding affinity of polypeptide chains decreases, causing the release of the protein. Not only can chaperones prevent protein aggregation by binding to the unfolded or partially folded polypeptides, but they can also unfold misfolded proteins by inducing conformational changes in the target protein; therefore, the successful folding can be achieved with the assistance of molecular chaperones. One of the most studied molecular chaperone families is a bacterial chaperonin system, known as GroEL and GroES.[20c, 21, 26] The term "GorE" is from the name of a bacterial gene that was discovered and the "L" and "S" in GroEL and GroES indicated the larger and the smaller of the two subunits. There are three structural domains, the apical, intermediate, and equatorial domain, in the GroEL. The apical domain contains binding sites for unfolded proteins and GroES and the equatorial domain contains the ATP-binding site. The internal

structure of GroEL is a hollow cylinder divided by the equatorial domain to form two cage-like chambers, known as Anfinsen cages. The co-chaperone GroES is a dome-like structure that acts as a cap while binding to GroEL. GroES and ATP are bound to GroEL after the unfolded polypeptide chain enters GroEL. This isolated environment allows polypeptides to fold into their native states without aggregation and the hydrolysis of ATP opens the chambers releasing the folded protein (Figure 4).[20c]

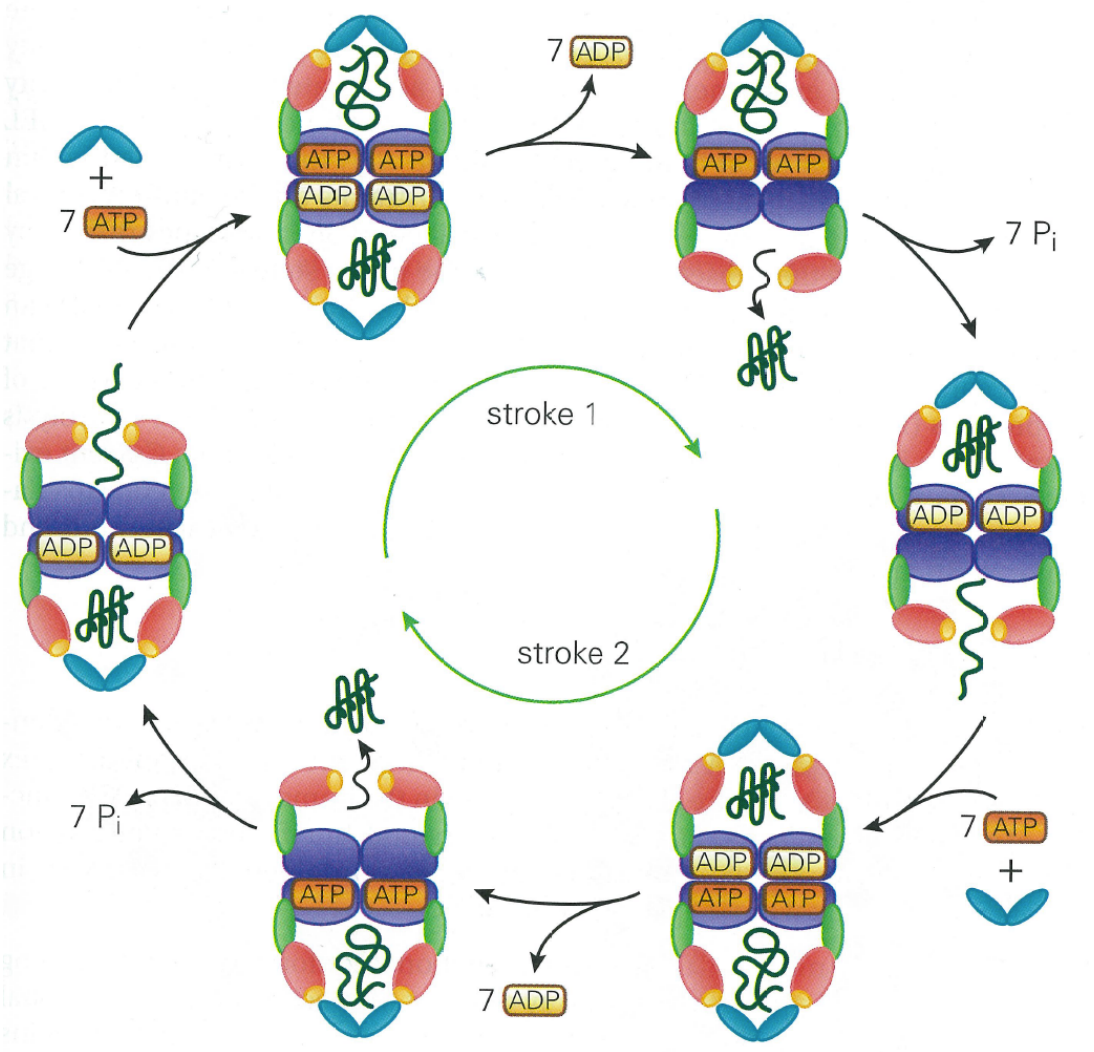

Figure 4. Schematic representation mechanism of GroEL/GroES chaperone-mediated protein folding. Reprinted from ref 20a. Copyright 2013 Garland Science, Taylor & Francis Group, LLC.

Artificial Chaperones

With the aid of molecular chaperones, aggregation during protein folding could be efficiently eliminated; however, in the absence of molecular chaperones, protein aggregation can be a serious problem *in vitro*. Hence, developing methods that efficiently produce proteins without aggregation has caught the attention of researchers in recent years. Inspired by molecular chaperones in living systems, artificial chaperones were first developed by Rozema and Gellman in 1995.[27] Similar to molecular chaperones, this artificial chaperone system consists of two consecutive steps. In the first step, a cationic detergent (cetyltrimethylammonium bromide, CTAB) is added to the denatured protein solution to form a protein-detergent complex and prevent denatured protein from aggregation from interprotein hydrophobic interactions. In the second step, *β*-cyclodextrin (*β*-CD) was introduced to the solution to strip the detergent away from the protein and allow for refolding of the protein. Figure 5 shows the schematic view of artificial chaperone-assisted protein refolding.

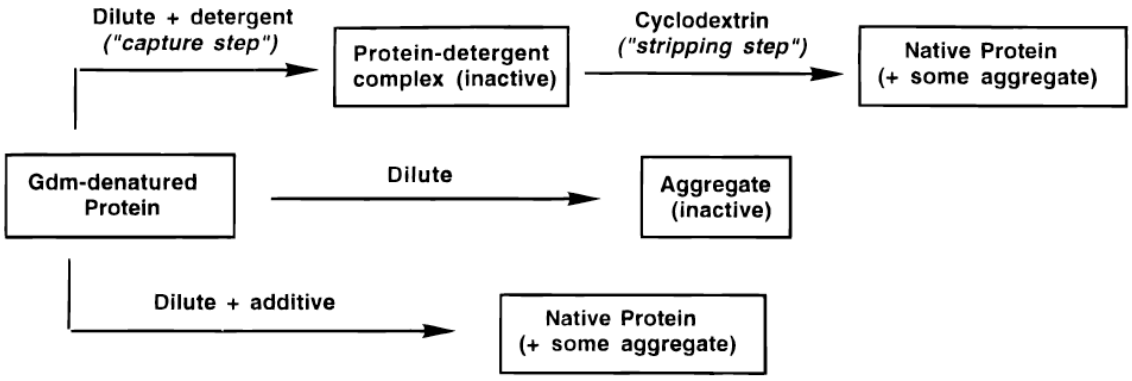

Figure 5. Schematic view of artificial chaperone-assisted protein refolding. Reprinted from ref 27b. Copyright 1996 American Chemical Society.

Following the work of Rozema and Gellman, Akiyoshi and co-workers developed self-assembled nanogels such as cholesteryl group-bearing pullulan (CHP)[28] and dodecyl group-bearing enzymatically synthesized glycogen (C_{12}ESG)[29] as artificial chaperones. These nanogels showed the ability to complex with denatured proteins and performed chaperone-like activity. Moreover, the addition of cyclodextrin was no longer required in the C_{12}ESG system to dissociate the nanogel from the protein (Figure 6). It is noteworthy that only one protein, carbonic anhydrase, was use in this study but the C_{12}ESG system showed promising results for one-step artificial chaperone-assisted protein refolding.

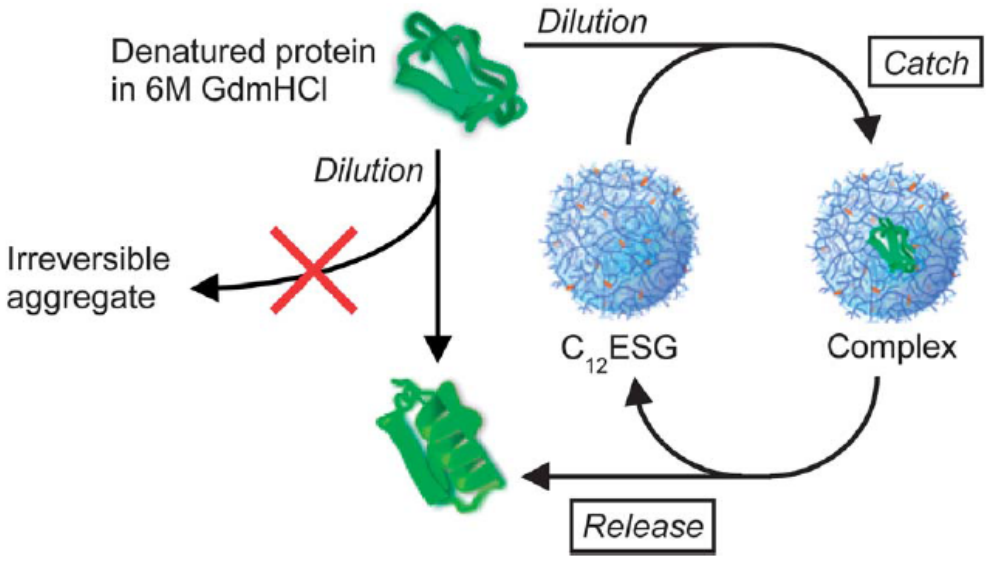

Figure 6. Schematic illustration of the C_{12}ESG nanogel-mediated one-step protein refolding system. Reprinted from ref 29. Copyright 2013 The Royal Society of Chemistry.

Recently, Shi and co-workers also established a one-step artificial chaperone system using a temperature-responsive mixed-shell polymeric micelle (MSPM).[30] This self-assembly micelle is composed of a mixture of two block copolymers, poly(lactide)$_{100}$-*b*-poly(ethylene oxide)$_{45}$ (PLA$_{100}$-*b*-PEG$_{45}$) and poly(lactide)$_{125}$-*b*-poly(N-isopropylacryamide)$_{180}$ (PLA$_{125}$-*b*-PNIPAM$_{180}$). The MSPMs evolve into core-shell-

corona micelles above the lower critical solution temperature of PNIPAM. The collapse of PNIPAM in the mixed shell leaves behind cavity-like spaces, which allow the denatured protein to enter, and the surrounding PEG chains serve as the inner wall of the cavities. They successfully demonstrated that MSPMs could effectively prevent the aggregation and assist the refolding of denatured carbonic anhydrase B (CAB) (Figure 7). However, the procedure required heating the MSPMs/CAB mixtures to 50 °C for collapsing PNIPAM and 70 °C for denaturing CAB, most of proteins would not survive these conditions.

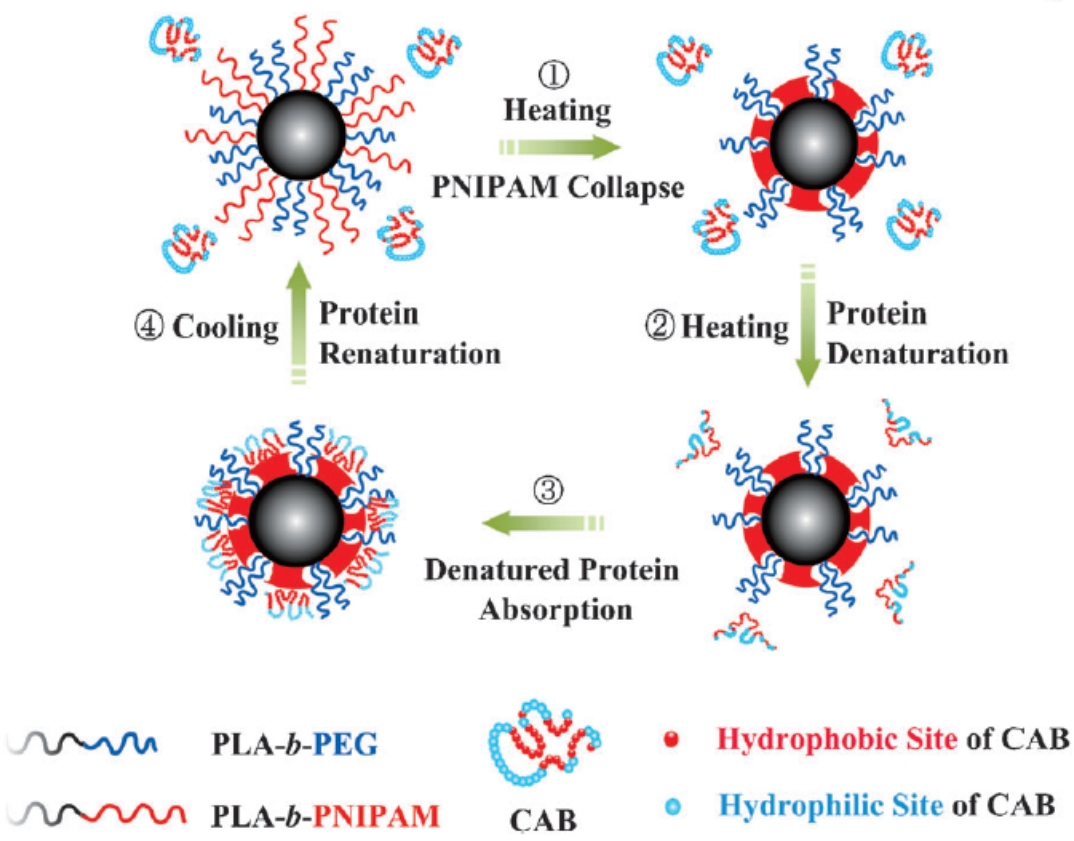

Figure 7. Schematic representation mechanism of MSPMs-assisted protein refolding. Reprinted from ref 30. Copyright 2013 Wiley-VCH Verlag GmbH & Co. KGaA, Weinheim.

The possibility of using biocompatible and biodegradable PPGL-*g*-PEG/alkyl polymers as artificial chaperones for assisting protein refolding has been an intriguing goal in our group since the tunable nature by modifying pendant groups on the polymer backbone could provide the opportunity to use PPGL-*g*-PEG/alkyl in different protein systems. The degradability would also add an advantage of releasing mechanism. However, the difficulty in long-term study also comes from the degradability of PPGL-*g*-PEG/alkyl polymers as well as the acidic microenvironment during degradation, which can cause protein denaturation and aggregation.[9] Herein, we describe synthesis of non-degradable poly(propargyl(glycicylether)) (PPGE) analogs of of PPGL from the polymerization of proparglycidyl ethers to probe the role of degradability in delivery system and artificial chaperones. These can be viewed as substituted PEGs, the parent compounds of which are well known for their non-toxic and non-immunogenic nature.[10] PEG is usually synthesized via anionic ring-opening polymerization of ethylene oxide in the presence of metal hydroxide or alkoxide initiator.[31] Recently, several groups have broadened the application scope by using functionalized epoxides (Scheme 3) to synthesize functionalized PEG-based polymers.[32] Since the material properties are related to the nature of functional groups on the polymers, the variety of functional groups as well as the possibility of post-polymerization modifications can provide a broader range of potential applications.

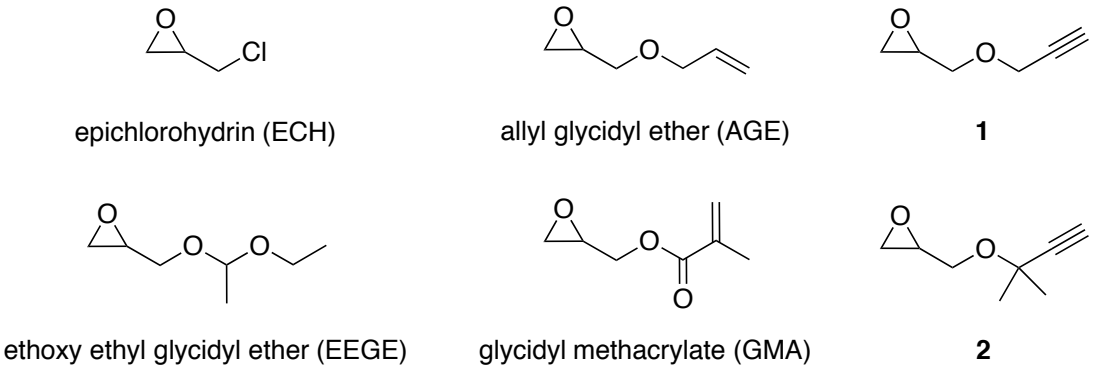

Scheme 3. Examples of functionalized epoxides.

The grafting of PPGE was performed using the same post-polymerization modification, copper(I)-catalyzed 1,3-dipolar cycloaddition (CuAAC) of azides and alkynes, as PPGL. The thermal-responsive behavior of the resulting polymers was also studied. The results of the polymerization and the properties of unmodified and modified polymers will be presented.

Chapter 2 Results and Discussion

Polymerization Method

Anionic ring-opening polymerization of epoxides is one of the most studied and important methods for epoxide polymerization. Recently, Carlotti, Deffieux and co-workers reported a new living/controlled polymerization of functionalized epoxides, which operates via an anionic coordination mechanism.[33] In the reports, the authors used triisobutylaluminum (*i*-Bu_3Al) as the catalyst and tetraoctylammonium bromide (Oct_4NBr) as the initiator, which resulted in controlled molecular weight polymers under moderate conditions. Scheme 4 shows the plausible mechanism of the ring-opening polymerization of functionalized epoxides.[33a] The authors proposed that two events, which include the formation of initiating complex and the activation of the monomer, would occur in the initiation step. When the catalyst and initiator ratio is greater than one, the initiating complex will be formed and the excess catalyst will activate the corresponding monomer by coordinating with the oxygen atom on the epoxide. Nonetheless, to the best of our knowledge, there is no spectroscopic evidence for the bromide end group in these polymers.

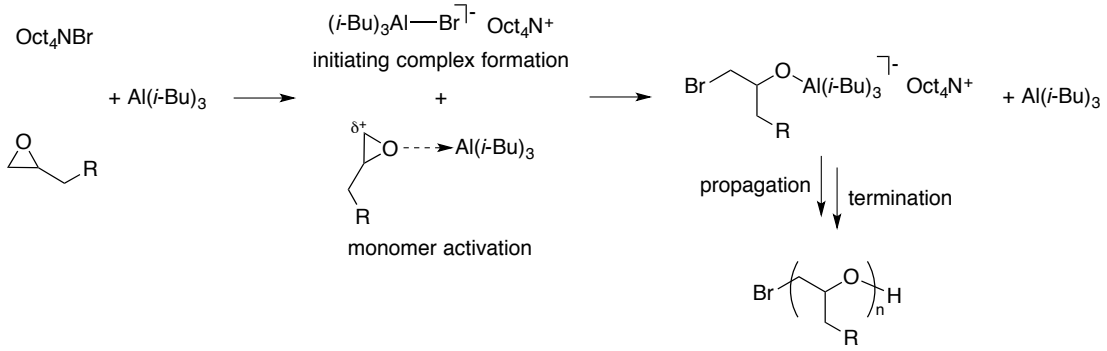

Scheme 4. Proposed mechanism of ring-opening polymerization of functionalized epoxides using triisobutylaluminum and tetraoctylammonium bromide.

Because of the controlled and living-like nature, this tetraoctylammonium bromide-triisobutylaluminum initiating system was applied for the ring-opening polymerization of alkyne-functionalized epoxides in our laboratory. However, low molecular weight polymers were obtained in the initial attempts. Therefore, for proof of concept, the ring-opening polymerization of allyl glycidyl ether (AGE), which is chosen for the backbone structural similarity with alkyne-functionalized epoxides, was performed. And the results were compared with the literature results published by Carlotti, Deffieux and co-workers.[33c]

Ring-opening Polymerization of Allyl Glycidyl Ether (AGE)

The ring-opening polymerization of AGE was performed using *i*-Bu_3Al as the catalyst and Oct_4NBr as the initiator. To decrease the initial rate, the initiation of polymerization was conducted at -35 °C. Then the reaction was allowed to reach the room temperature for a desired period of time. In order to make a comparison with the results published by Carlotti, Deffieux and co-workers, certain ratios of [*i*-Bu_3Al]/[Oct_4NBr] and reaction times were used.[33c] The results of polymerization are presented in Table 1. Conversion of monomer to polymer was calculated by comparing the ^1H NMR integration of the epoxide peaks at 2.57 ppm with those on polymer backbone at 3.43-3.62 ppm (see Figure A1, Appendix). The molecular weights and polydispersities were measured by GPC in THF. The GPC traces are shown in Figure A7. Comparison of results shows that the conversion can reach higher than 90% within 2 hours for most of the polymerization reactions (Table 1). Notably, higher molecular weight polymers were obtained by using a higher [*i*-Bu_3Al]/[Oct_4NBr] ratio (entry 5 and 6).

Table 1. Polymerizations of AGE

Entry	[M]: [Al]: [I]	Time (h)	Conversion (%)[a]	Yield (%)	M_n^{calc} (g mol^{-1})[b]	M_n^{exp} (g mol^{-1})[c]	PDI
1	50: 2: 1	1.5	> 99	91	5700	9000	1.54
2	100: 2: 1	1.5	98	98	11000	10000	1.14
3	200: 2: 1	1.5	96	84	22000	26000	1.09
4	500: 2: 1	1.5	91	77	52000	24000	1.32
5	750: 3:1	2	95	54	81000	55000	1.22
6	1000: 4: 1	4	75	89[d]	86000	71000	1.22

[a] Determined by ^{1}H NMR. [b] Calculated from the monomer to initiator ratio and corrected for conversion. [c] Measured by GPC in THF via light scattering. [d] Crude yield without purification.

Based on literature results, a higher [*i*-Bu_3Al]/[Oct_4NBr] ratio was needed to obtain a higher molecular weight polymer and keep the reaction time short. In addition, no polymerization occurs when the [*i*-Bu_3Al]/[Oct_4NBr] ratio equals one.[33a] This result is consistent with the proposed mechanism, where the excess of *i*-Bu_3Al acts as a monomer activator. Table 2 contains the present results and the reported literature results.[33c] Although the molecular weights of polymers in our work were lower than those in the literature, our results still show a controlled and living polymerization process with no appearance of undesired reactions. These results boded favorably for applying the same catalytic system our propargyl substituted monomers.

The structure of poly(allyl glycidyl ether) (PAGE) was confirmed by ^{1}H and ^{13}C NMR spectra (see Figure A1 and A2, Appendix). The absence of epoxide protons at 2.50-3.20 ppm supports ring-opening of the epoxide. In addition, the protons of the pendant allyl group are observed as a doublet at 5.11 ppm, a doublet of doublets at 5.21 ppm, and a multiplet at 5.80-5.88 ppm. Also, two singlet peaks at 116.6 ppm and 134.9 ppm in ^{13}C NMR spectrum are assigned to the sp^2 carbons of the pendant allyl group.

Table 2. The results of polymerization of AGE from this work and the literature

Entry	[M]: [Al]: [I]	Time (h)	M_n^{calc} (g mol^{-1})[a]	M_n^{exp} (g mol^{-1})[b]	PDI	M_n^{lit} (g mol^{-1})[c]	PDI^{lit}
1	50: 2: 1	1.5	5700	9000	1.54	6900	1.08
2	100: 2: 1	1.5	11000	10000	1.14	14500	1.07
3	200: 2: 1	1.5	22000	26000	1.09	30000	1.05
4	500: 2: 1	1.5	52000	24000	1.32	70000	1.22
5	750: 3:1	2	81000	55000	1.22	72000	1.40
6	1000: 4: 1	4	86000	71000	1.22	109000	1.32

[a] Calculated from the monomer to initiator ratio and corrected for conversion. [b] Measured by GPC in THF via light scattering. [c] Ref. 31c.

Ring-opening Polymerization of Alkyne-functionalized Epoxides

The preparation of monomers **1** and **2** and their polymerization is shown in Scheme 5. Synthesis of 2-[(prop-2-yn-1-yloxy)methyl]oxirane (**1**) was modified from literature.[34] Monomer **1** was obtained from the reaction of (±)-epichlorohydrin and propargyl alcohol under basic conditions in the presence of a phase transfer reagent, tetrabutylammonium hydrogensulfate (TBAHS). Purification by distillation gave a colorless liquid in 76% yield. To obtain monomer 2-{[(2-methylbut-3-yn-2-yl)oxy]methyl}oxirane (**2**), a similar reaction was performed between (±)-epichlorohydrin and 2-methyl-3-butyn-2-ol. However, because of the steric hindrance of the two methyl groups, the reaction took 24 hours to complete. Monomer **2** was obtained as a colorless oil in 50% yield by distillation from the crude mixture.

The ^{1}H NMR spectrum of **1** is shown in Figure 8. The acetylene proton (H_e) appears as a doublet of doublets centered at 2.49 ppm. This splitting pattern was caused by ^4J coupling with the methylene protons on the propargyl group. Two doublets centered at 4.07 ppm and 4.08 ppm correspond to propargyl group methylene protons (H_d, $H_{d'}$) and their appearance is caused by their diastereotopic nature. Likewise the methylene protons

(H_c, $H_{c'}$) alpha to the epoxide appear as two doublets of doublets centered at 3.34 ppm and 3.69 ppm. Two triplets (H_a and $H_{a'}$) are assigned as the methylene protons on the expoxide and the ^3J coupling constants are 2.5 Hz (H_a) and 4.4 Hz ($H_{a'}$) for trans and cis to the methine proton (H_b), respectively.

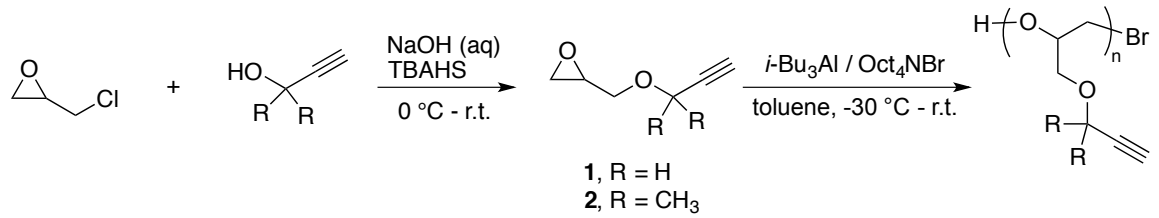

Scheme 5. Synthesis and polymerization of monomer **1** and **2**.

Polymerization of **1** was initiated using *i*-Bu_3Al as the catalyst and Oct_4NBr as the initiator at -35 °C and reaction was continued at room temperature for a desired period of time. Poly(2-[(prop-2-yn-1-yloxy)methyl]oxirane) (poly(**1**)) was obtained in good yields and the results are shown in Table 3. The [*i*-Bu_3Al]/[Oct_4NBr] ratio was 2:1 for all polymerizations of **1**. Conversions of monomer to polymer were calculated by comparing the ^1H NMR integration of the epoxide peaks at 2.66 ppm with those on the polymer backbone at 3.52-3.63 ppm (Figure 8). The pendant propargyl groups of poly(**1**) are can be quantified by the characteristic shift of H_e in the ^1H NMR at 2.44 ppm, as well as in the ^{13}C NMR at 74.6 ppm (C_6) and 79.1 ppm (C_5) (see Figure A4, Appendix). Also, it is worth mentioning that, in ^{13}C NMR spectrum of poly(**1**), a low intensity signal at 29.6 ppm is observed, which could arise from a bromomethyl end group. The intergration of H_e, $H_{d,\,d'}$, and $H_{a\text{-}c}$ is 0.9, 1.0, and 5.0, respectively. The slightly smaller intergration of H_e is the result of insufficient relaxation time.

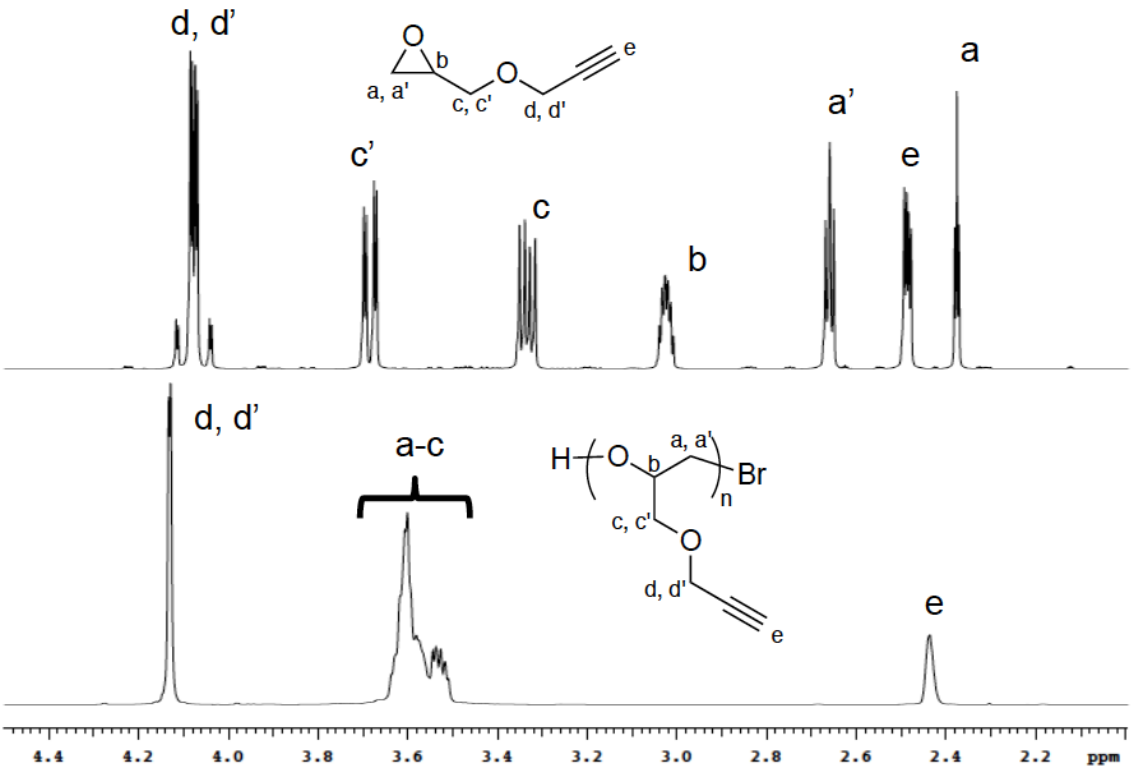

Figure 8. 500 MHz ^{1}H NMR spectra of **1** and poly(**1**).

The molecular weights of poly(**1**) were measured by GPC in THF and the obtained values are comparable with the theoretical values with fairly narrow polydispersities (Table 3 and Figure A8, Appendix). The increasing of the [monomer]/[initiator] ratio did result in an increase in molecular weight. Therefore, the tetraoctylammonium bromide-triisobutylaluminum initiating system was successfully applied to the polymerization of alkyne-functionalized epoxides without noticeable undesired exchange reactions.

Table 3. Polymerizations of **1**

Entry	[M]: [Al]: [I]	Time (h)	Conversion (%)[a]	Yield (%)	M_n^{calc} (g mol^{-1})[b]	M_n^{exp} (g mol^{-1})[c]	PDI
1	50: 2: 1	2	98	97	5500	6000	1.32
2	100: 2: 1	2	98	90	11000	11000	1.19
3	200: 2: 1	6	97	73	22000	18000	1.35
4	200: 2: 1	2.5	97	89	22000	19000	1.26

[a] Determined by ^{1}H NMR. [b] Calculated from the monomer to initiator ratio and corrected for conversion. [c] Measured by GPC in THF via light scattering.

To eliminate the possibility of alkyne-allene isomerization and ensure the stability of the pendant alkyne functional group, 2-{[(2-methylbut-3-yn-2-yl)oxy]methyl}oxirane (**2**) was synthesized. Figure 9 shows the ^{1}H NMR spectrum of **2**. As opposed to **1**, the peak of the acetylene proton (H_e) appears as a singlet at 2.35 ppm because of the lack of ^4J coupling. Also, the two diastereotopic methyl groups (H_d, $H_{d'}$) are observed as two overlapping singlets at 1.32 ppm and 1.33 ppm. Moreover, the diastereotopic methylene protons (H_c, $H_{c'}$) are shown as two doublet of doublets centered at 3.41 ppm and 3.62 ppm.

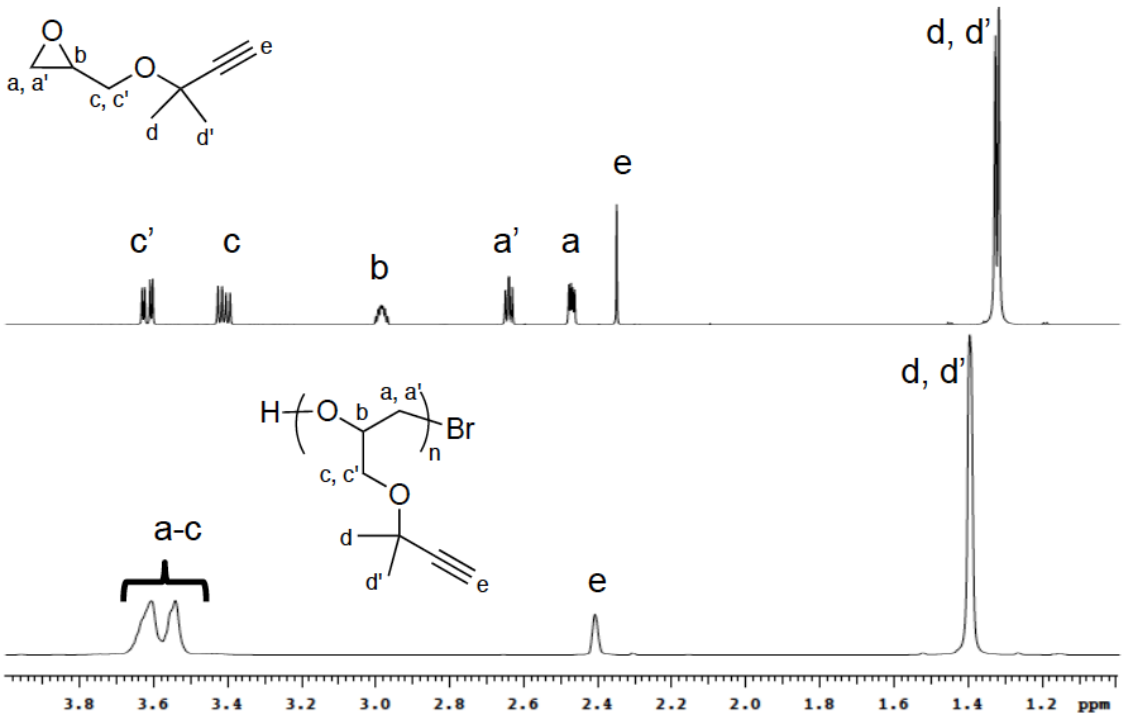

Figure 9. 500 MHz ^{1}H NMR spectra of **2** and poly(**2**).

The tetraoctylammonium bromide-triisobutylaluminum initiating system was also applied to the polymerization of **2**. The reaction was initiated at -35 °C and was then allowed to reach room temperature. After it stirred for a desired period of time, poly(2-{[(2-methylbut-3-yn-2-yl)oxy]methyl}oxirane) (poly(**2**)) was produced. Ratios of 2:1 and 3:1 for [*i*-Bu_3Al]/[Oct_4NBr] were used for polymerizations of **2**. Conversion of monomer to polymer was calculated by comparing the ^{1}H NMR integration of the residual epoxide peak at 2.64 ppm with those on polymer backbone at 3.56-3.63 ppm (Figure 9). The pendant alkyne group was confirmed by ^{1}H and ^{13}C NMR spectra (Figure 9 and Figure A6, Appendix). The acetylene proton (H_e) is observed at 2.43 ppm and the alkyne carbons appear at 74.6 ppm (C_6) and 79.1 ppm (C_5). The intergration of H_e, $H_{d, d'}$, and H_{a-}

$_c$ is 0.9, 6.0, and 5.0, respectively. The slightly smaller intergration of H_e is the result of insufficient relaxation time.

Typical results for the polymerization of **2** are listed in Table 4. The GPC traces are shown in Figure A9, Appendix. Similar to the polymerization of **1**, the molecular weights of poly(**2**) are comparable with the theoretical values with narrow polydispersities except for entry 5. When the [*i*-Bu_3Al]/[Oct_4NBr] ratio equals to 2, no conversion was observed in the ^1H NMR spectrum after 48 hours. Therefore, in entry 5, the 3:1 ratio of *i*-Bu_3Al and Oct_4NBr is essential for the polymerization to undergo. The results shown in entry 5 suggests that an even higher [*i*-Bu_3Al]/[Oct_4NBr] ratio might be needed to shorten the reaction time and increase the conversion.

Table 4. Polymerizations of **2**

Entry	[M]: [Al]: [I]	Time (h)	Conversion (%)[a]	Yield (%)	M_n^{calc} (g mol^{-1})[b]	M_n^{exp} (g mol^{-1})[c]	PDI
1	50: 2: 1	2	> 99	99	7000	7000	1.15
2	100: 2: 1	2	> 99	95	14000	12000	1.17
3	200: 2: 1	14.5	96	64	27000	24000	1.11
4	200: 2: 1	2.5	> 99	85	28000	20000	1.22
5	500: 3:1	24	76	31	53000	32000	1.58

[a] Determined by ^1H NMR. [b] Calculated from the monomer to initiator ratio and corrected for conversion. [c] Measured by GPC in THF via light scattering.

As expected, an increased [monomer]/[initiator] ratio results in a higher molecular weight. A similar trend was also observed in the polymerizations of AGE and **1**. Hence, it is reasonable to say that the polymerization of **1** and **2** share the same mechanism, which is a controlled and living anionic ring-opening polymerization, with the polymerization of AGE.

Post-polymerization Modification via "Click" Chemistry

Post-polymerization modification is an effective approach to tune the properties of polymers. Not only does this approach overcome the limited functional group tolerance of many common polymerization techniques, but it also reduces the number of synthetic steps when new polymers are synthesized.[35] Scheme 6 shows a generic illustration of the post-polymerization modification. First, monomers with functional groups that are inert toward polymerization conditions are polymerized. Then, in the following step, functional groups are modified carrying functional group transformations.

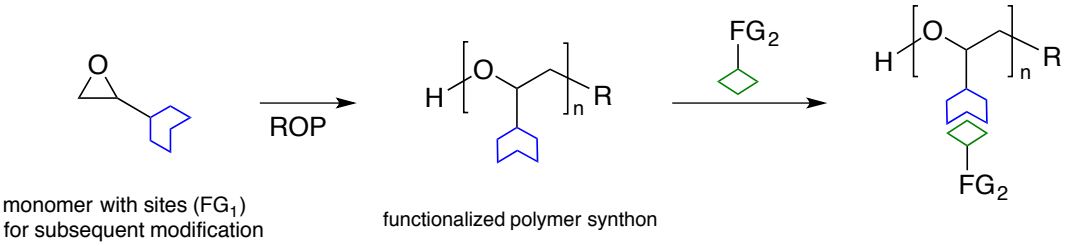

Scheme 6. Post-polymerization modification of PEG-based polymers.

"Click" chemistry, which was developed simultaneously by Sharpless and co-workers[36] and Meldal and co-workers,[37] has been utilized as a post-polymerization modification in recent research. The advantages of using "click" chemistry include broad scope, high yields, and regioselectivity. There are different "click" reactions that have been used for post-polymerization modifications such as thio-ene, thio-yne, and copper(I)-catalyzed 1,3-dipolar cycloaddition of azides and alkynes.[36-38] Due to its high functional group tolerance, copper(I)-catalyzed 1,3-dipolar cycloaddition (CuAAC) of azides and alkynes is one of the most widely used "click" reactions. Fokin and co-workers had recently found direct evidence of a dinuclear copper intermediate in copper(I)-catalyzed 1,3-dipolar cycloaddition.[39] Scheme 7 shows the proposed mechanisms of CuAAC from Fokin and co-workers. The reaction begins with the

coordination of the acetylene to the first copper (Cu^a) followed by the coordination of the second copper (Cu^b), results in the formation of Cu^a acetylide, and forms the active complex in the catalytic cycle. Then, the reversible coordination of the organic azide to the active complex results in the formation of the dinuclear copper intermediate. After the generation of C-N bond and the leaving of one copper, the triazolyl-copper derivative is formed. Protonation of Cu-C bond releases triazole product and reforms the initial copper catalyst.

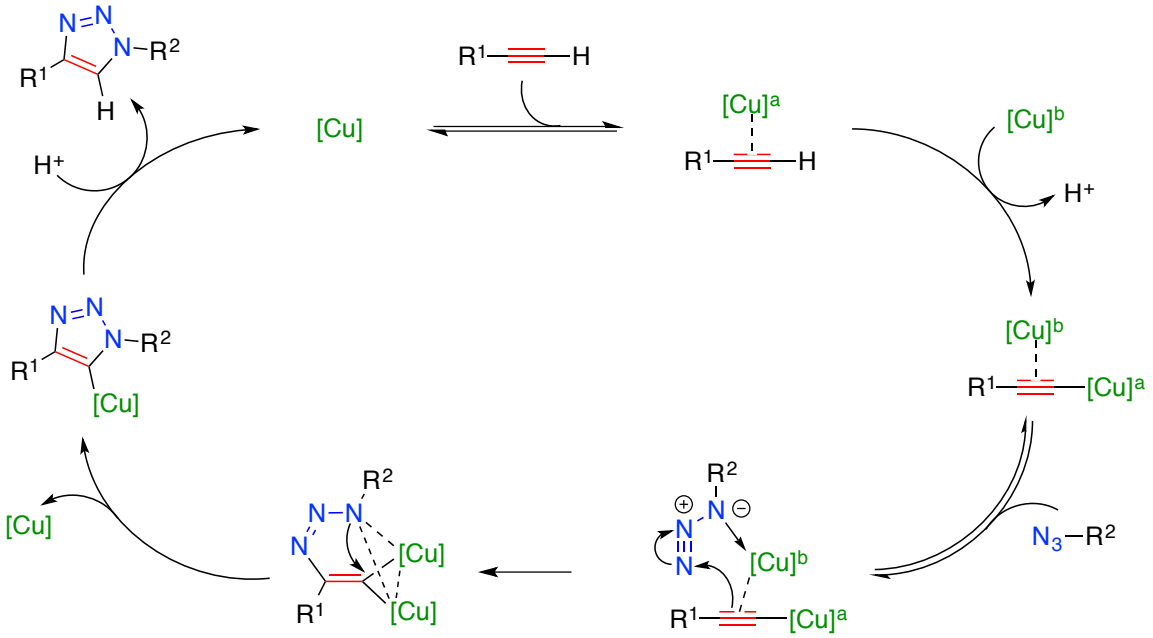

Scheme 7. Proposed mechanism of copper(I)-catalyzed 1,3-dipolar cycloaddition via dinuclear copper intermediate.[39]

To further extend the scope of the polymer properties, "click" chemistry, specifically copper(I)-catalyzed 1,3-dipolar cycloaddition of azides and alkynes,[37b, 38] was carried out for post-polymerization modification of poly(**1**) and poly(**2**). The synthesis of "click" modified polymers is illustrated in Scheme 8. The "click" reaction was carried out in the presence of $CuSO_4 \bullet 5H_2O$ and sodium ascorbate in DMF at room temperature. 1-(2-

Azidoethoxy)-2-(2-methoxyethoxy)ethane (mDEG-azide) was synthesized from triethylene glycol monomethyl ether and sodium azide.[18a] Also, 1-azidodecane was synthesized from 1-bromodecane and sodium azide.[18a, 40] To synthesize amphiphilic PEG/alkyl-grafted polymers of poly(**1**), polymer **3**, poly(**1**) (M_n = 50000, PDI = 1.35 or M_n = 52000, PDI = 1.26, Figure A8, Appendix), the desired amount of mDEG-azide and/or 1-azidodecane, and 12 mol% sodium ascorbate were dissolved in DMF (all equivalents and mole percentages are with respect to acetylene units in poly(**1**)). Then, 5 mol% of $CuSO_4 \bullet 5H_2O$ in DMF was added via syringe. After reaction time, the residual copper was removed by stirring the polymer solution with ion exchange resin beads (Amberlite® IRC-748 ion exchange resin) for 12-24 hours. The polymers were purified via dialysis (molecular weight cutoff (MWCO) = 6-8 kD).[18b] Similar procedures were followed to synthesize polymer **4** from poly(**2**) (M_n = 51000, PDI = 1.11, Figure A9, Appendix). By varying the ratio of mDEG-azide and 1-azidodecane, a series of polymers $\mathbf{3_X}$ and $\mathbf{4_X}$ (X = mole fraction of mDEG-azide) were obtained.

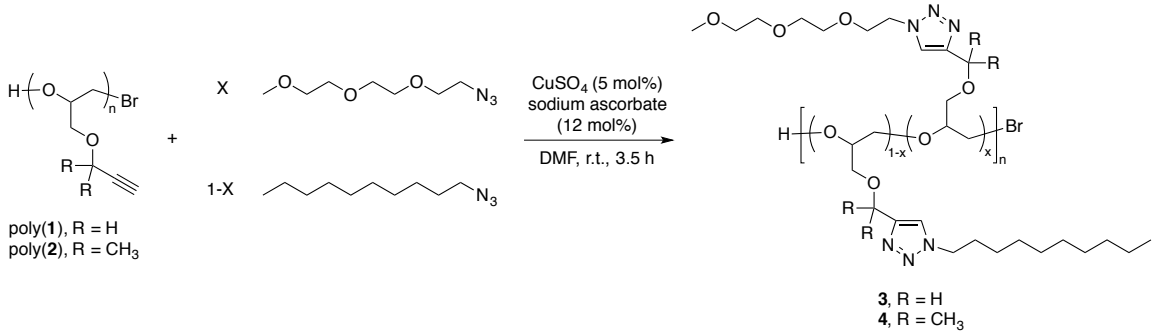

Scheme 8. Synthesis of "click" modified polymers.

In the ^{1}H NMR spectrum, the absence of an acetylene protons at 2.44 ppm (poly(**1**)) and 2.43 ppm (poly(**2**)) confirmed that the reactions were complete after 3.5 hours (Figure 10 and Figure A10 and A11, Appendix). As shown in Figure 10a, the new peak(s)

for the proton on the triazole ring appear(s) at 7.64 ppm and/or 7.74 ppm. Also, the appearance of the triazole proton at 7.57 ppm and/or 7.65 ppm is observed in Figure 10b. Moreover, the ^{1}H NMR proves that the side-chain composition in polymer **3** and **4** is comparable with the azide ratio used.

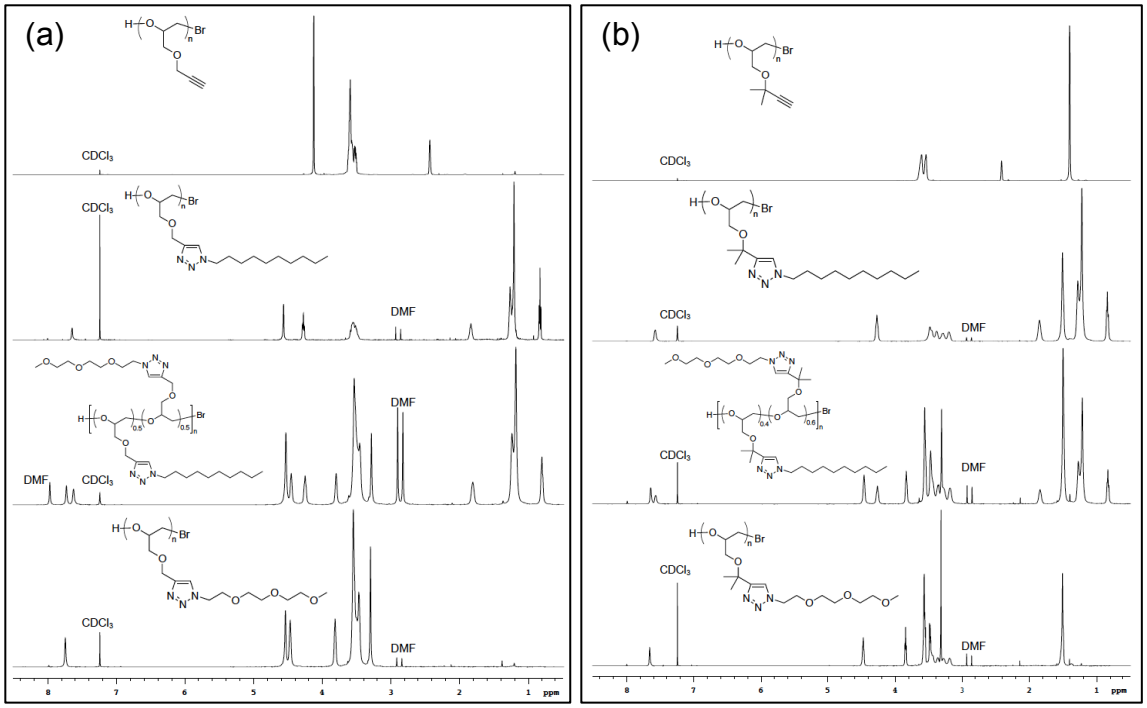

Figure 10. 500 MHz ^{1}H NMR spectra of (a) poly(**1**), polymer $\mathbf{3}_{\mathbf{0.00}}$, $\mathbf{3}_{\mathbf{0.50}}$, and $\mathbf{3}_{\mathbf{1.00}}$ (also see Figure A10, Appendix) (b) poly(**2**), polymer $\mathbf{4}_{\mathbf{0.00}}$, $\mathbf{4}_{\mathbf{0.60}}$, and $\mathbf{4}_{\mathbf{1.00}}$ (also see Figure A11, Appendix).

The increase in the molecular weight of the resulting polymer $\mathbf{3}_{\mathbf{0.0}}$ and $\mathbf{4}_{\mathbf{0.0}}$ was confirmed by GPC (Figure 11 and Figure A12 and A13, Appendix). The GPC trace shows a noticeable change in molecular weight of polymer $\mathbf{3}_{\mathbf{0.00}}$ ($M_{\mathrm{n,\ theor.}}$ = 132000, M_{n} = 137000, PDI = 1.21). In addition, a significant change in molecular weight of polymer $\mathbf{4}_{\mathbf{0.00}}$ ($M_{\mathrm{n,\ theor.}}$ = 118000, M_{n} = 118000, PDI = 1.14) with a slight change in PDI is observed (Figure 11b). Although the theoretical and experimental value of molecular

weights of polymer $\mathbf{3}_{0.00}$ and $\mathbf{4}_{0.00}$ are close, the GPC traces of polymer $\mathbf{3}_{0.00}$ do not seem to support this result (Figure 11a). It is believed that there are issues in how the light scattering molecular weights were calculated using the instrument software. Polymer **3** and **4** with various ratios of mDEG and decyl pendent groups were synthesized and characterized by NMR spectroscopy. However, the molecular weight characterization via gel permeation chromatography (GPC) is still an on-going process.

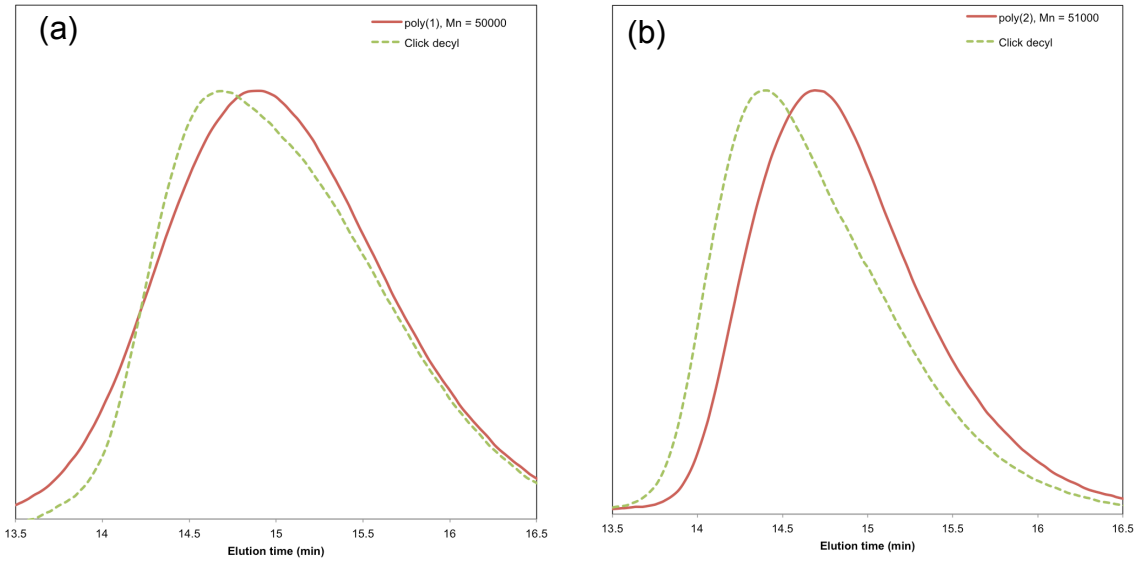

Figure 11. GPC traces of (a) poly(**1**) (solid line) and polymer $\mathbf{3}_{0.00}$ (dash line) (b) poly(**2**) (solid line) and polymer $\mathbf{4}_{0.00}$ (dash line). The polymers were analyzed in THF at 35 °C, at 1 mL/min flow rate.

Materials that have lower critical solution temperature (LCST) behavior are interesting for their potential applications in the biomedical area.[12] At LCST, these materials undergo a solution-gel transition that is driven by entropic gain as water molecules are expelled from the polymer solvation sphere. It was shown in our previous report that the cloud point temperatures have a linear relationship with mole fraction of

mDEG in polyglycolide systems.[18b] Hence, the LCST behavior of the PEG-based alkyne-functionalized polymers was investigated. The solubility tests show that polymer **3** containing more than 55% mDEG and polymer **4** containing more than 60% mDEG are soluble in water at room temperature. Also, polymer $\mathbf{3_{0.50}}$ and polymer $\mathbf{4_{0.55}}$ were soluble in ice-cold water. To perform the preliminary experiments of cloud point determination, 15 mg of polymer samples were dissolved in 1 mL of Milli-Q water and heated in water bath to observe the solution turbidity. Results of the preliminary experiments are presented in Figure 12. The cloud points are between 13.8 and 85.5 °C for polymer **3** and, between 18.0 and 55.5 °C for polymer **4**, Moreover, there is an increasing trend of cloud points versus mol% of mDEG for both polymer **3** and **4**. Figure 13 shows the representitive photographs of LCST behavior of polymer $\mathbf{3_{0.5}}$ and $\mathbf{4_{0.8}}$. Below the LCST, the aqueous solutions of $\mathbf{3_{0.5}}$ and $\mathbf{4_{0.8}}$ were transparent and turned cloudy above the LCST, showing the increased turbidity.

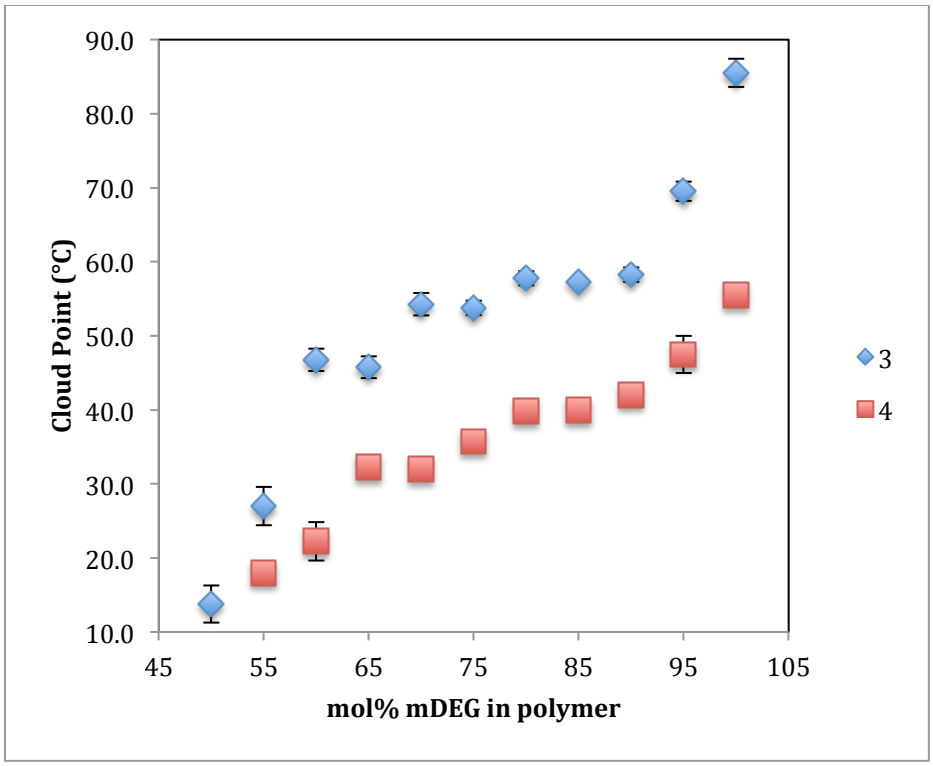

Figure 12. Results of preliminary experiments of cloud point investigation.

To further investigate the LCST behavior, polymers were dissolved in Milli-Q water and solution turbidity was monitored by measuring the absorbance at 450 nm as a function of temperature. As shown in representative graph, Figure A22, the absorbance increases dramatically during gel formation upon heating over temperature range of 10 °C. The relationship between the cloud point temperatures and mol% of mDEG in polymer **4** is shown in Figure 14(a). The increasing trend of cloud points versus mol% of mDEG in polymer was still seen but the LCST as a function of mDEG is not as linear as in the propargyl glycolide case. This is in agreement with our previous research on "click" modified poly(propargyl) glycolide (PPGL) (Figure 14(b)).[18b] Thus, this result shows the solubility and the LCST behavior is sensitive to the nature of the side chains and not the polymer backbone.

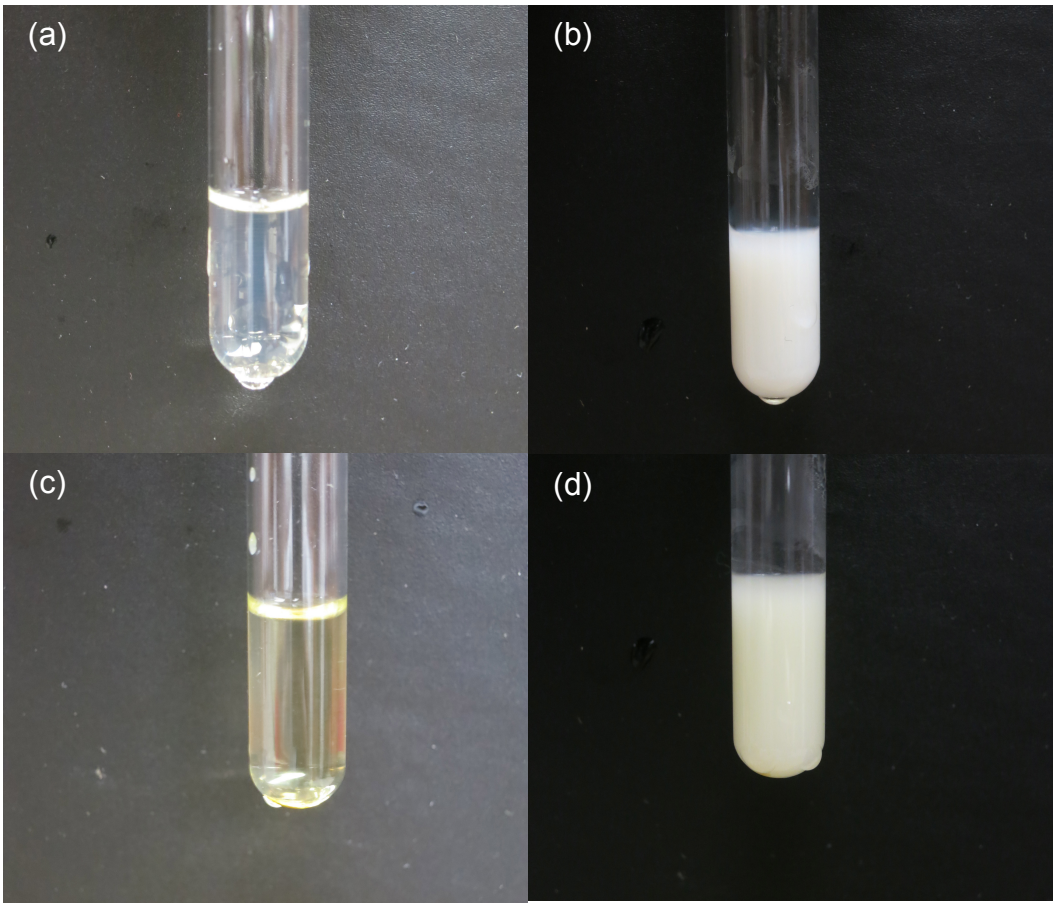

Figure 13. Photographs of the lower critical solution temperature behavior of polymers $\mathbf{3}_{0.50}$ and $\mathbf{4}_{0.80}$ in Milli-Q water. (a) polymer $\mathbf{3}_{0.50}$ below LCST (14°C) (b) polymer $\mathbf{3}_{0.50}$ above LCST (22 °C) (c) polymer $\mathbf{4}_{0.80}$ below LCST (37 °C) (d) polymer $\mathbf{4}_{0.80}$ above LCST (40°C).

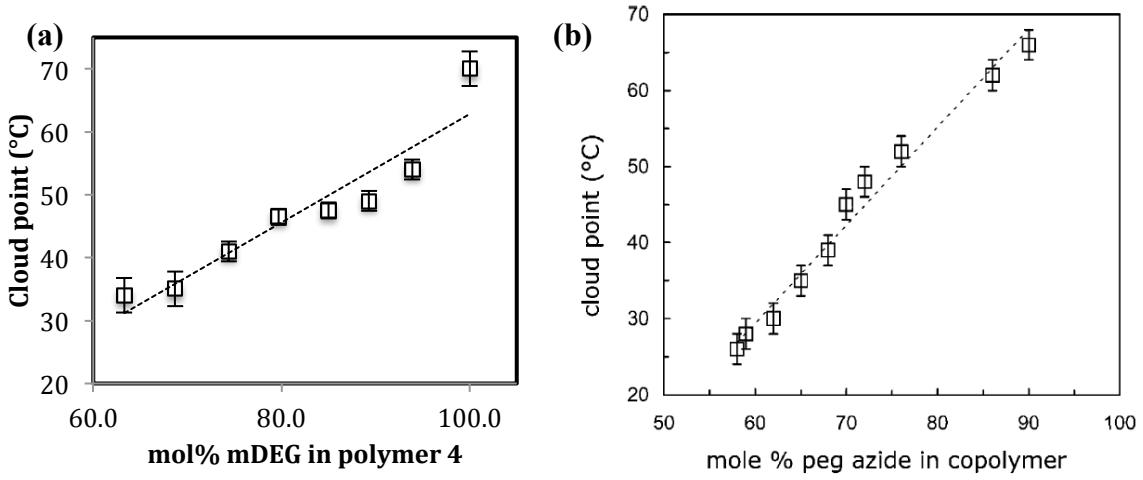

Figure 14. Relationship between the cloud point observed at 450 nm and mol% mDEG in (a) polymer **4** and (b) "click" modified PPGL.[18b]

Characterization of the Formation of Unimolecular Micelles

Micelles are dynamic aggregates of surfactant molecules above the critical micelle concentration (cmc). Dynamic light scattering (DLS) is often used to determine the cmc. By illuminating particles with a laser, DLS measures the intensity fluctuation caused by Brownian motion in the scattered light, and one can calculate the hydrodynamic radius (R_h) of the particles via the Stokes-Einstein equation. When traditional micelles reach the cmc, there is a dramatic change in the hydrodynamic radius. However, previous work on "clickable" polyglycolides showed that hydrodynamic radius of the poly(propargyl glycolide)-*graft*-poly(ethylene glycol) monoethyl ether (PPGL-*g*-mPEG) polymers was unaffected by polymer concentration, which suggested the formation of unimolecular micelles.[18a] To perform the unimolecular micelle study on polymer **3** and **4**, the polymer samples were dissolved in a small amount of acetone (< 1 mL) and dispersed into ice-cold Milli-Q water. The acetone was then removed by passing a stream of nitrogen through the solution. Prior to analysis, the samples were filtered through 0.2 μm Whatman PTFE (poly(tetrafluoroethylene)) filter and the analysis was done at a temperature below the LCST of the sample. Similar to PPGL-*g*-mPEG system, the preliminary DLS data shows that the hydrodynamic radius of the particles at different concentrations was relatively similar, which indicates the formation of unimolecular micelles (Figure 15 and S23). The hydrodynamic radius of polymer $\mathbf{3_{0.55}}$ is 18.55 ± 2.36 nm and is 20.45 ± 1.75 nm for polymer $\mathbf{4_{0.60}}$. Although our preliminary results seem promising, wider concentration ranges and more systematic characterization via DLS will help verify these conclusions.

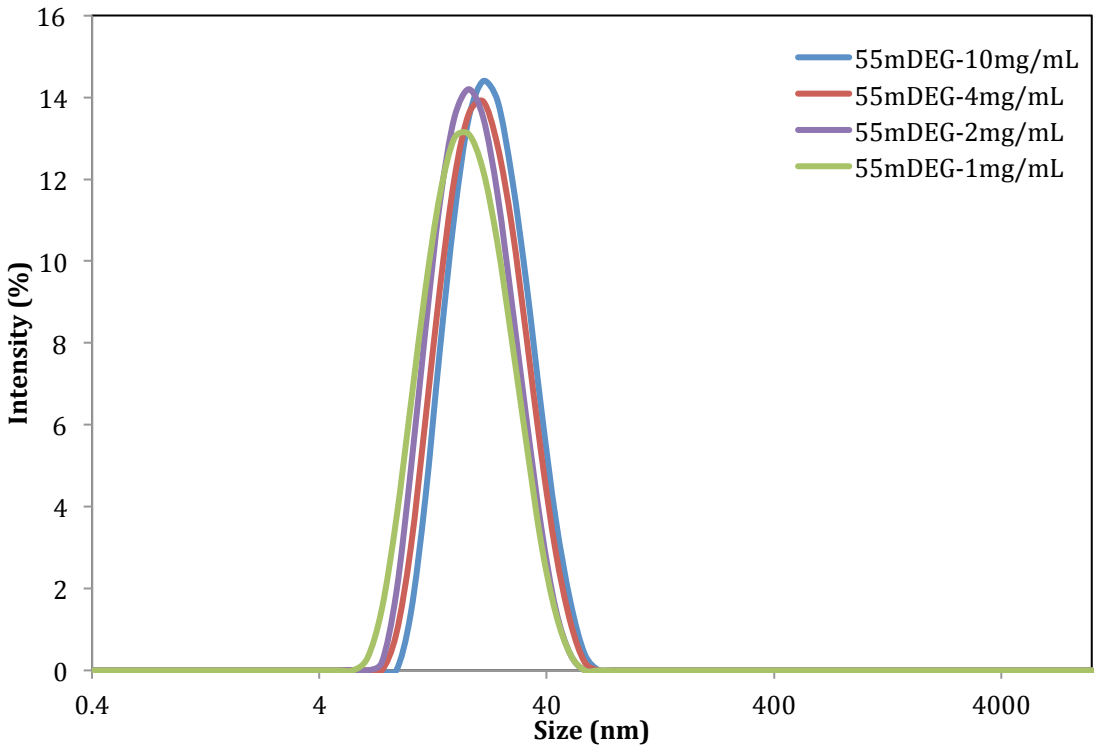

Figure 15. Hydrodynamic radius of polymer $\mathbf{3}_{\mathbf{0.55}}$ determined by DLS.

The size of the particles can also be examined by transmission electron microscopy (TEM). Samples were prepared by dropping an aqueous solution of polymer onto a Formvar-coated copper grid. After water was evaporated, the sample was negatively stained with 2% uranyl acetate solution. For the LCST behavior study, two samples were prepared with the same method below the LCST of the polymer. However, instead of evaporating the excess water, one of the samples was heated above its LCST via hot plate before staining. The TEM experiments are in progress but particle aggregation above the LCST was observed.

Encapsulation of Hydrophobic Guest Molecules

PEG-based materials have long been studied for their application in controlled drug delivery.[2a, 3, 7a] Polymers that form unimolecular micelles are promising as drug carriers

because they can be prepared by controlled polymerization methods and are not subject to cmc. As a proof of concept, azobenzene, which is a UV-active model for hydrophobic drugs, was chosen as a hydrophobic guest molecule to be encapsulated in the unimolecular micelles (Scheme 9). For preliminary experiment, azobenzene and polymer $\mathbf{3}_{0.55}$ were dissolved in acetone (< 1 mL) and dispersed into ice-cold Milli-Q water. The acetone was removed by passing a stream of nitrogen through the solution followed by filtration to remove unencapsulated azobenzene. The resulting solution appeared yellow which indicates the encapsulation of azobenzene. Also, as shown in Figure 16, the characteristic absorbance at 425 nm in UV spectrum confirmed that azobenzene was encapsulated in the micelles.

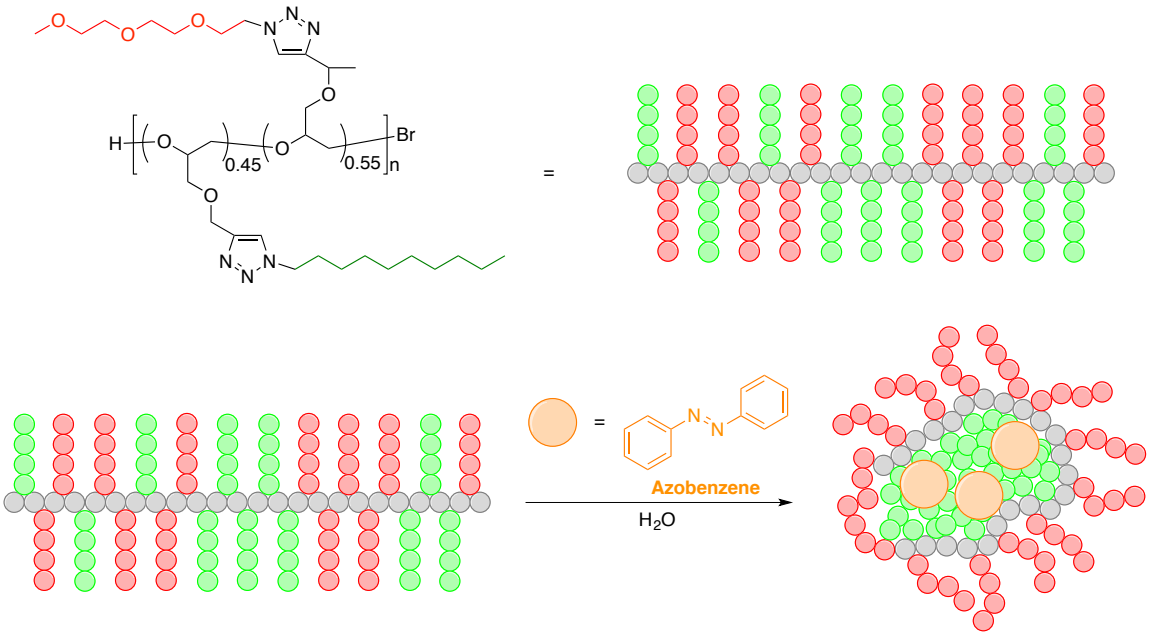

Scheme 9. Schematic representative of azobenzene encapsulation.

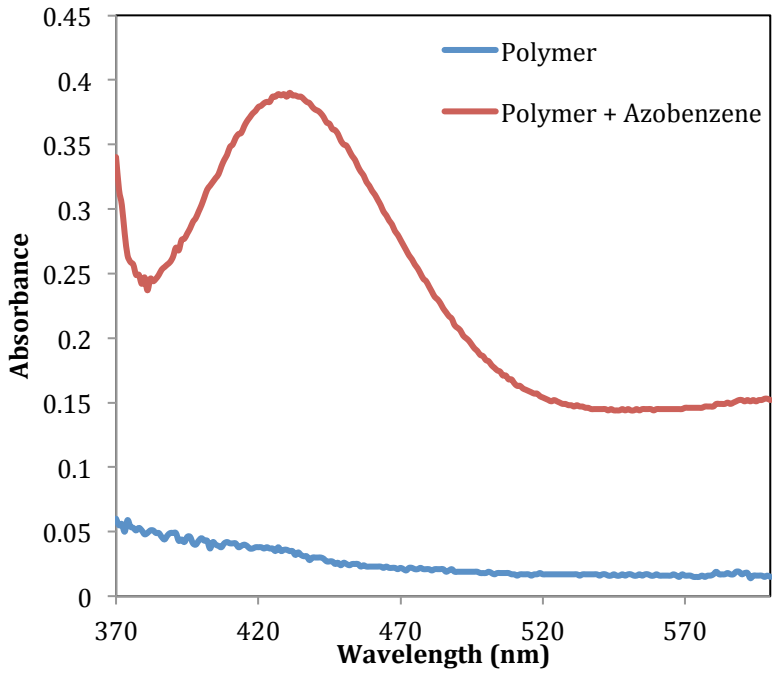

Figure 16. UV-vis spectra of azobenzene loaded polymeric micelles (top, red) and polymeric micelles (bottom, blue) in Milli-Q water at room temperature.

Chapter 3 Conclusions

A series of PEG-based alkyne-functionalized polymers have been synthesized using a tetraoctylammonium bromide-triisobutylaluminum initiating system developed by Carlotti, Deffieux and co-workers. A relationship between [monomer]/[initiator] ratio and molecular weights was studied. By increasing [monomer]/[initiator] ratio, the molecular weight of the resulting polymer also increases. In addition, "click" chemistry was applied for the post-polymerization modification of these polymers. Water-soluble polymers that show lower critical solution temperature (LCST) behavior were obtained by varying the ratio between mDEG and decyl side chains. A relationship between cloud point temperatures and mol% mDEG in polymer was observed. Significantly, the LCST results were comparable with our previous research.[18b] Therefore, a conclusion could be drawn that the LCST behavior is related to the nature of the side chains rather than the nature of the polymer backbone. Preliminary results have shown that these "click" modified PEG-base polymers have the ability to form unimolecular micelles and to encapsulate azobenzene. More detailed studies should be performed to understand the properties of these unimolecular micelles.

Chapter 4 Future Work

Systematic Follow-up Experiments

Although high molecular weight poly(**2**) was obtained when the [monomer]/[initiator] ratio equals 500, a lower conversion was noticed with a longer reaction time. This might mean that the living ring-opening polymerization process was compromised when the [monomer]/[initiator] ratio is higher than 500 in our monomer system. Further investigation through systematic experiments is necessary to understand the reason behind this result. In addition, a kinetic study of polymerization should be done to understand the mechanism and to prove the living ring-opening polymerization behavior. Moreover, to the best of our knowledge, there is no other evidence in literature to confirm the existence of the bromine end-group in these PEG-based polymers; hence, a reaction between polymer and triphenylphosphine could be performed (Scheme 10). If there were a bromine end-group, the ^{31}P NMR spectrum of the product would display strong spectroscopic evidence. Another approach would be the synthesis of low molecular weight oligomers and analysis via mass spectrometry to evaluate the incorporation of bromine.

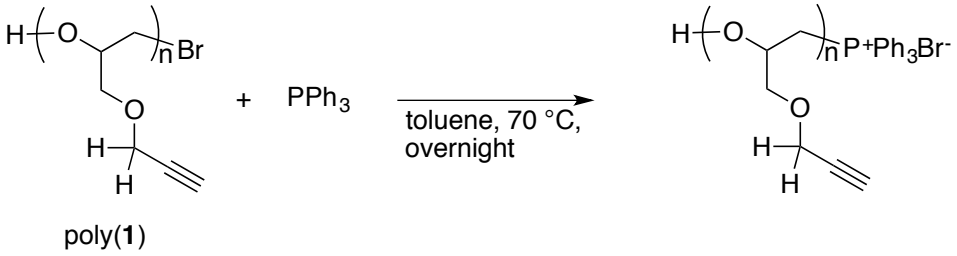

Scheme 10. Reaction between poly(**1**) and triphenylphosphine.

As for "click" modified polymers, **3** and **4**, the LCST behavior study via UV-vis spectroscopy should be continued to obtain statistically valid data. Also, our preliminary results have shown the ability of these polymers to form unimolecular micelles. To fully confirm and understand the unimolecular micelle behavior of our materials, wider concentration range DLS experiments need to be performed on the whole series of water-soluble polymers. By comparing results with TEM experiments, the size of unimolecular micelles and the LCST behavior can be further confirmed.

It is a promising result that azobenzene can be encapsulated inside the polymeric unimolecular micelles. In order to further understand the trends between different polymer compositions, their ability to encapsulate small molecules should be examined. Furthermore, the release of azobenzene should be studied to understand if azobenzene molecules would escape from micelles over time. Our previous research has shown that cross-linked particles had slower release rate of azobenzene than non-cross-linked particles. Therefore, cross-linkable PEG-based polymers should be synthesized for studying the effect on the encapsulation ability and the possibility of leakage.

Artificial Chaperone

Our previous research on PPGL-*g*-mPEG system has shown that this polymer has the ability to encapsulate poly(methyl methacrylate) (PMMA) in micelles.[18a] The idea of utilizing these biocompatible materials on the encapsulation of biological macromolecules has occurred to us ever since. However, the degradability of PPGL-*g*-mPEG system is a drawback for preliminary studies, because degradation cannot be avoided and it can be difficult to assay. The newly developed non-degradable PEG-based system would allow us to assess the role that functionality grafted to the PEG chain has

on the ability of nanomicelles to function as artificial chaperones. Once the non-degradable systems have been optimized, it may be possible to construct degradable analogs for "catch and release" applications. Since our preliminary results have suggested "click" modified PEG-based system shares the similar properties with PPGL-*g*-mPEG system, and it is reasonable to assume that these PEG-based amphiphilic polymers could also encapsulate macromolecules. Thus, we would like to apply these materials as artificial chaperones on biological macromolecule study.

Chaperones are proteins that assist and facilitate the proper folding of nascent and partially folded polypeptides into their three-dimensional structure to prevent aggregation and misfolding. The aggregation and misfolding of proteins is the suspected cause of many diseases such as Alzheimer's disease, Parkinson's disease, and type II diabetes.[25, 26b, 26c] Encapsulating unfolded proteins in unimolecular micelles could be a way to prevent the aggregation of unfolded proteins. Also, it might shine a light on the mechanism of protein aggregation.

As a proof of concept, the encapsulation of cellular retinol binding protein II (CRBP II) will be performed. CRBP II is a relatively small monomeric protein that participates in the metabolism of vitamin A and the transportation of retinol. While studying the structure of CRBP II, our collaborator, Professor James Geiger and co-workers in Department of Chemistry at Michigan State University, observed the presence of domain swapped dimer after the refolding process of a single mutant denatured protein. Interestingly, they found that if the refolding process occurred at a relatively low protein concentration, it resulted in the formation of monomeric species only.[41] The λ_{max} of monomers and dimers is 496 nm and 514 nm, respectively, which makes it a great system

for assessing the aggregation via UV-vis spectrometry. As a result, we propose to introduce our amphiphilic polymers as an artificial chaperone during the protein refolding process at a relatively high concentration to alter the protein-folding pathway and prevent the formation of dimers (Scheme 11).

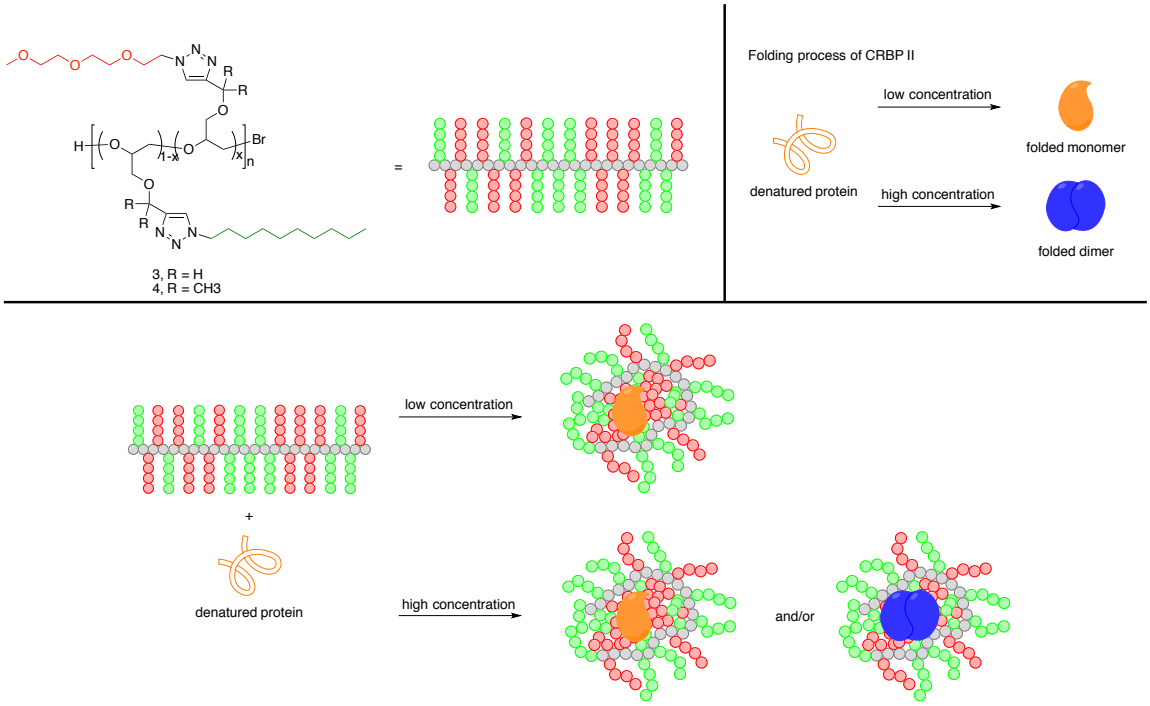

Scheme 11. Schematic folding process of CRBP II and proposed experiments of artificial chaperones.

Two approaches could be used to examine this proposal. First, as a control experiment, the encapsulation of CRBP II during the refolding process at various protein concentrations should be conducted. It is possible that there is not enough driving force to encapsulate denatured protein molecules at low protein concentration. It is also possible that more than one denatured protein molecule will be encapsulated in the same micelle and form the dimer. So this experiment could set up a baseline protein concentration for our future studies. In addition, it is worthwhile to study the relationship between

molecular weight and particle size, as well as the effect on protein refolding, with different sizes of artificial chaperones. For this reason, polymers with different molecular weights should be used as artificial chaperones. The ratio of hydrophobic and hydrophilic side chains might affect the encapsulation efficiency; therefore, the experiments should also be performed using polymers with various ratios of hydrophobic side chains.

The second approach is to introduce amphiphilic polymers at a high protein concentration during the protein refolding process. We believe that by varying the relative concentration between polymers and proteins, it might be possible to control the ratio of monomer and dimer. With a higher polymer loading, there is a higher possibility to exclusively obtain monomers. Hence, the experiments should be performed with different polymer to protein ratio such as 1:1, 1:2, and 2:1 to study the effect of polymer loading. All experiments could be examined by UV-vis spectrometry, in which the characteristic absorption of monomers is 496 nm and the characteristic absorption of dimers is 514 nm.

Chapter 5 Experimental Section

Materials

(±)-Epichlorohydrin (≥98%, Fluka), propargyl alcohol (99%, Aldrich), 2-methyl-3-butyn-2-ol (98%, Aldrich), and tetrabutylammonium hydrogensulfate (TBAHS, 97%, Aldrich) were used without further purification. Allyl glycidyl ether (AGE) was purified by distillation from CaH_2 and stored in glove box under nitrogen atmosphere at room temperature in vials. Triisobutylaluminum (*i*-Bu_3Al, 1 mol/L in toluene, Aldrich) was used as received. Tetraoctylammonium bromide (Oct_4NBr, 98%, Aldrich) was stored in glove box under nitrogen atmosphere. Ion exchange resin beads (Amberlite® IRC-748) were purchased from Alfa Aesar and soaked in DMF prior to use. 1-azidodecane was obtained from group member, Georgina Comiskey and used without further purification. Toluene was dried by refluxing over sodium benzophenone ketyl and stored in an air-free flask, which contained activated 4 Å molecular sieves.

Characterization

The molecular weights of polymers were determined by gel permeation chromatography (GPC) at 35 °C using two PLgel 10μ mixed-B columns in series (manufacturer stated linear molecular weight range of 500-10,000,000 g/mol) with THF as the eluent solvent at a flow rate of 1 mL/min. A Waters 2410 differential refractometer was used as the detector. An Optilab rEX (Wyatt Technology Co.) and a DOWN EOS 18-angle light scattering detector (Wyatt Technology Co.) with a laser wavelength of 684 nm were used to calculate absolute molecular weights. Monodisperse polystyrene standards were used to calibrate the molecular weights. The concentration of polymer

solutions used for GPC was 1-4 mg/mL and all samples were filtered through a 0.2 μm Whatman PTFE syringe filter. UV-Vis spectrua were recorded with Thermo Evolution 600. Dynamic light scattering (DLS) data were obtained using a temperature-controlled Malvern Zetasizer Nano ZS spectrometer. ^{1}H NMR (500 MHz) and ^{13}C NMR (125 MHz) spectra were acquired using either a Varian Inova-500 spectrometer or Agilent DirectDrive2 500 spectrometer. Chemical shifts for ^{1}H and ^{13}C spectra were recorded in parts per million relative to the residual ^{1}H and ^{13}C of $CDCl_3$ (δ 7.24, 77.0).

General Procedure of Polymerization

All polymerizations were performed using standard Schlenk techniques at 25 °C in an atmosphere of high-purity nitrogen. The Schlenk flasks were dried in the oven at 115 °C for overnight and cooled down prior to use. Monomer(s), tetraoctylammonium bromide (initiator), and triisobutylaluminum (catalyst) were transferred into Schlenk flasks in glove box under nitrogen atmosphere, and then the catalyst solution in toluene was transferred into the monomer and initiator mixture in toluene at -35 °C. After it has reached room temperature, the reaction mixture was stirred for the desired reaction time. A small amount of ethanol was then added to stop the reaction. Toluene was removed *in vacuo*. The conversions of polymerization were determined by NMR spectroscopy.

General Procedure for "Click" Functionalization

The desired amount of acetylene-functionalized polymer, azide (1 equiv. with respect to acetylene groups), and 12 mol% sodium ascorbate were dissolved in DMF. The resulting solution was transferred to a Schlenk flask and deoxygenated by three freeze-pump-thaw cycles. After the solution had warmed to room temperature, a 0.1 M solution of $CuSO_4 \bullet 5H_2O$ in deoxygenated DMF (5 mol% with respect to the acetylene groups)

was added under nitrogen, and the reaction mixture was then stirred at room temperature for desired time. At the end of the reaction, the solids in the reaction mixture were removed by filtration and ion exchange resin beads (Amberlite® IRC-748 ion exchange resin) were added to the solution for 12-24 hours to remove residual copper. The ion exchange resin beads were removed by filtration and DMF was removed *in vacuo*. The polymer was purified via dialysis (MWCO = 6-8 kD) in acetone/water mixture (9:1 v/v) overnight and then dried under vacuum.

Synthesis of 2-[(prop-2-yn-1-yloxy)methyl]oxirane (1)

In an Erlenmeyer flask, (±)-epichlorohydrin (98.53 g, 1.06 mol) and TBAHS (1.6 g, 4.71 mmol) were added to 40% NaOH aqueous solution (60 mL) at 0 °C. Propargyl alcohol (14.85 g, 0.27 mol) was added dropwise into above mixture at 0 °C and then the mixture was allowed to reach room temperature. After 3 h, water was added to the reaction mixture to quench the reaction. The aqueous phase was extracted with diethyl ether (3×50 mL) and the organic phase was dried over Na_2SO_4. The product was purified by vacuum distillation (bp = 72 °C, 30 torr) to obtain a colorless liquid of **1** (22.57 g, 0.20 mol, 76% yield). ^{1}H NMR ($CDCl_3$, 500 MHz) δ 2.38 (t, 1H, *J* = 2.5 Hz), 2.49 (dd, 1H, *J* = 3.0 Hz), 2.66 (t, 1H, *J* = 4.4 Hz), 3.01-3.04 (m, 1H), 3.34 (dd, 1H, *J* = 5.9 and 11.3 Hz), 3.69 (dd, 1H, *J* = 2.9 and 11.2 Hz), 4.07 (d, 1H, *J* = 1.9 Hz), 4.08 (d, 1H, *J* = 2.4 Hz). ^{13}C NMR ($CDCl_3$, 125 MHz) δ 43.8, 50.1, 58.0, 70.0, 74.6, 79.1.

Synthesis of 2-{[(2-methylbut-3-yn-2-yl)oxy]methyl}oxirane (2)

In an Erlenmeyer flask, (±)-epichlorohydrin (98.04 g, 1.06 mol) and TBAHS (3.2 g, 9.42 mmol) were added to 25% NaOH aqueous solution (240 mL) at 0 °C. 2-Methyl-3-butyn-2-ol (44.56 g, 0.53 mol) was added dropwise into above mixture at 0 °C and then

the mixture was allowed to reach room temperature. After 24 h, water was added to the reaction mixture to quench the reaction. The aqueous phase was extracted with diethyl ether (3×100 mL) and the organic phase was dried over Na_2SO_4. The product was purified by vacuum distillation (bp = 60 °C, 10 torr) to obtain a colorless liquid of **2** (37.54 g, 0.27 mol, 50 % yield). ^{1}H NMR ($CDCl_3$, 500 MHz) δ 1.32 (s, 3H), 1.33 (s, 3H), 2.55 (s, 1H), 2.46 (dd, 1H, *J* = 2.9 and 5.4 Hz), 2.64 (dd, 1H, *J* = 3.9 and 4.9 Hz), 2.98-3.00 (m, 1H), 3.41 (dd, 1H, *J* = 5.4 and 10.8 Hz), 3.62 (dd, 1H, *J* = 3.5 and 10.8 Hz). ^{13}C NMR ($CDCl_3$, 125 MHz) δ 28.2, 28.4, 44.4, 50.5, 65.0, 70.1, 72.1, 85.3.

Synthesis of 1-(2-azidoethoxy)-2-(2-methoxyethoxy)ethane (mDEG-azide)

Triethylene glycol monomethyl ether (20.00 g, 0.12 mol) in THF (60 mL) was added dropwise to a solution of NaOH (14.60g, 0.37 mol) in a water/THF mixture (6:4 v/v, 200 mL) at 0 °C. The mixture was stirred at 0 °C for 30 minutes and then *p*-toluenesulfonic chloride (23.00 g, 0.12 mol) in THF (100 mL) was added dropwise. The mixture was stirred at 0 °C for 3 h and then at room temperature for 6 h. The mixture was poured into ice water (30 mL). The water layer was extracted with diethyl ether (3×100 mL). The combined organic layers were washed with saturated aqueous NaCl solution and dried over $MgSO_4$. Diethyl ether was evaporated and the tosylate product was used without further purification (32.86 g, 0.10 mol, 85% yield).

The tosyl PEG (32.86 g, 0.10 mol) and sodium azide (13.43 g, 0.20 mol) were dissolved in DMF (200 mL) and the solution was heated to 60 °C. After 15 h, the solution was cooled to room temperature and was added to water (100 mL). The solution was extracted with diethyl ether (4×100 mL). The combined organic layers were washed with saturated aqueous NaCl solution (2×100 mL) and dried over $MgSO_4$. Diethyl ether was

evaporated and the product was purified via vacuum distillation (bp = 197 °C, 50 torr) to obtain a clear liquid of 1-(2-azidoethoxy)-2-(2-methoxyethoxy)ethane (10.93g, 0.06 mol, 60% yield). ^{1}H NMR ($CDCl_3$, 500 MHz) δ 3.25-3.28 (m, 5H), 3.42-3.45 (m, 2H), 3.52-3.57 (m, 8H). ^{13}C NMR ($CDCl_3$, 125 MHz) δ 50.4, 58.6, 69.7, 70.3, 70.3, 70.4, 71.6.

Formation of Unimolecular Micelles (1 mg/mL solution)

A solution of poly(propargyl glycolide)-*graft*-poly(ethylene glycol) monoethyl ether (PPGL-*g*-mPEG) (20 mg) in 0.5 mL acetone was slowly added dropwise to stirred ice-cold Milli-Q water (20 mL) in a Schlenk flask. The solution was allowed to stir for 30 minutes before the acetone was removed under a stream of nitrogen or *in vacuo*.

Azobenzene Encapsulation

Azobenzene (10 mg) and poly(propargyl glycolide)-*graft*-poly(ethylene glycol) monoethyl ether (PPGL-*g*-mPEG) (5 mg) were dissolved in acetone (<1 mL) and the solution was slowly added dropwise to stirred ice-cold Milli-Q water (5 mL) in a Schlenk flask. The acetone was removed under a stream of nitrogen or *in vacuo* and the solution was filtered to remove unencapsulated azobenzene. The characteristic absorbance at 425 nm in UV spectrum confirmed that azobenzene was encapsulated in the micelles.

APPENDIX

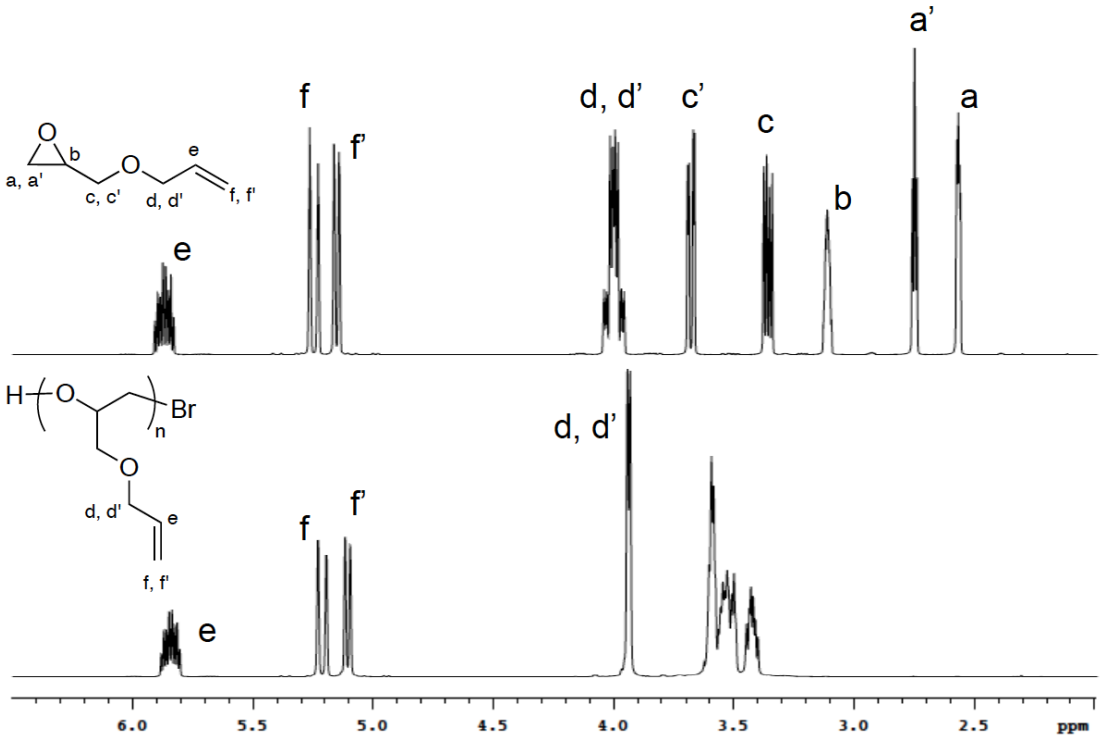

Figure A1. 500 MHz ^{1}H NMR spectra of AGE and PAGE.

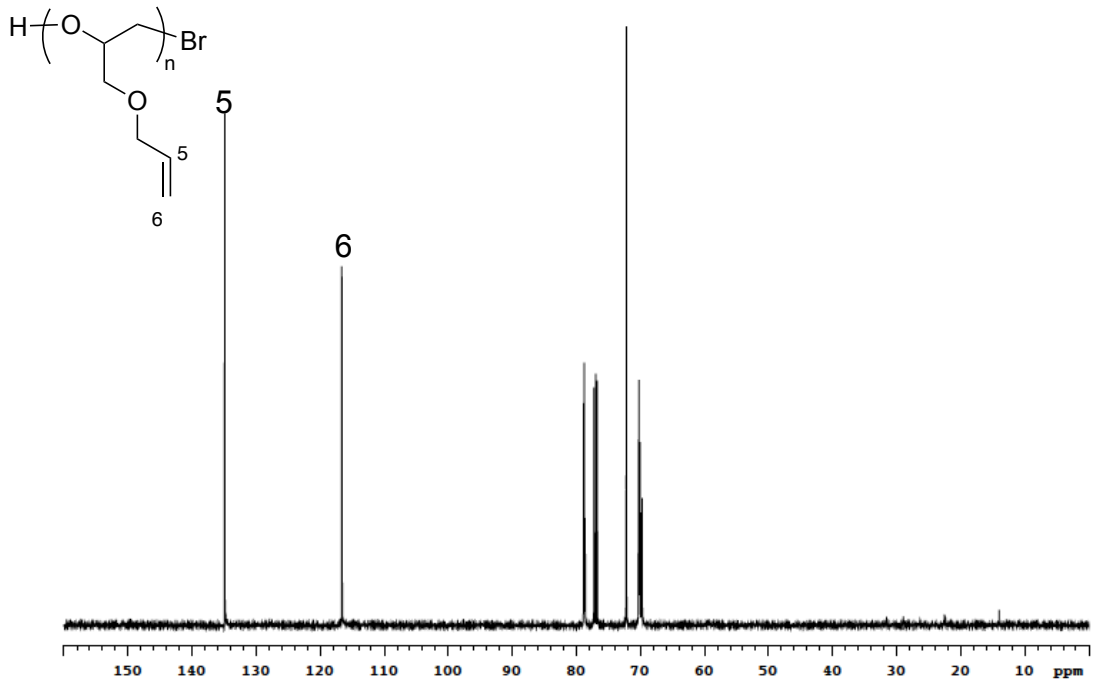

Figure A2. 125 MHz ^{13}C NMR spectrum of PAGE.

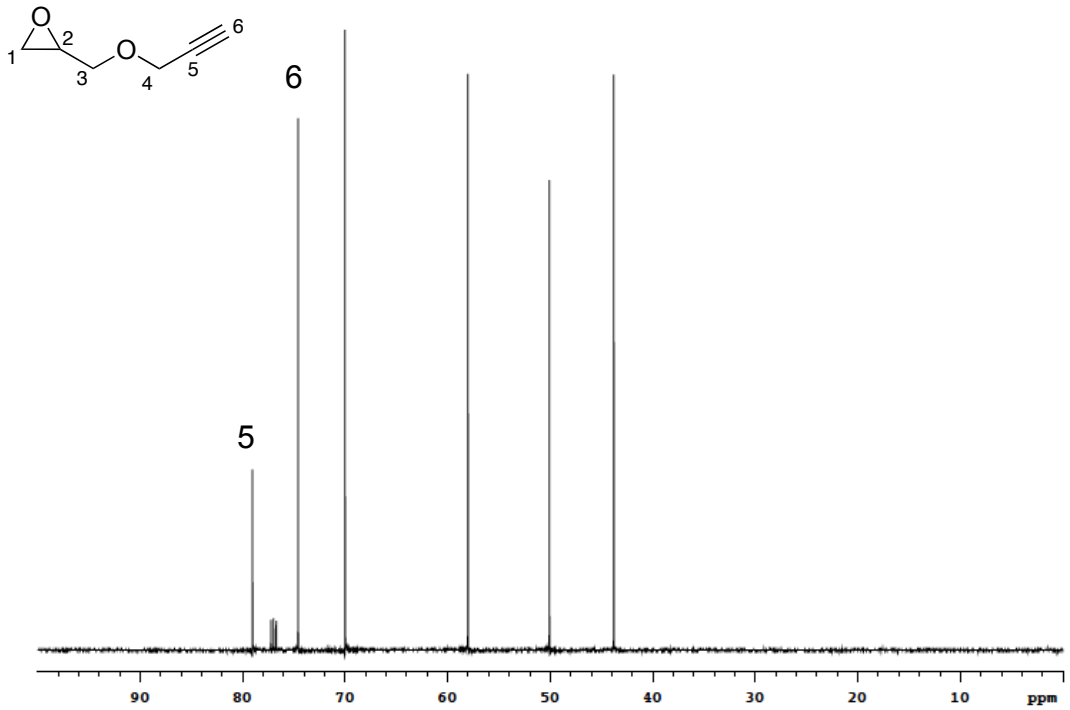

Figure A3. 125 MHz ^{13}C NMR spectrum of **1**.

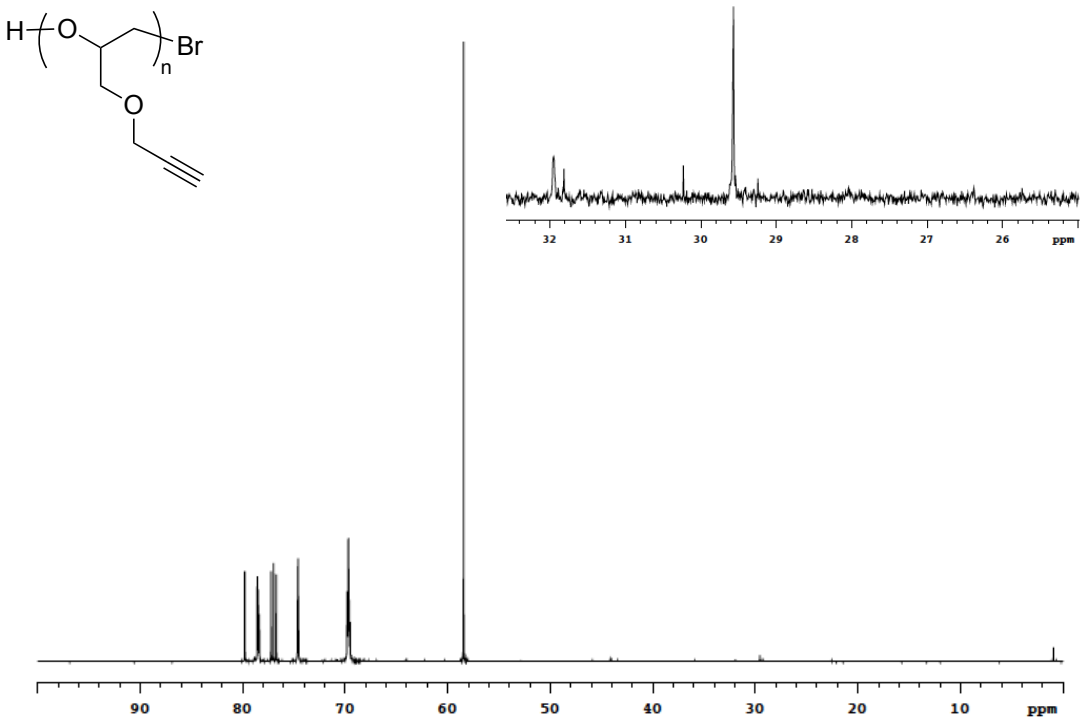

Figure A4. 125 MHz ^{13}C NMR spectrum of poly(**1**).

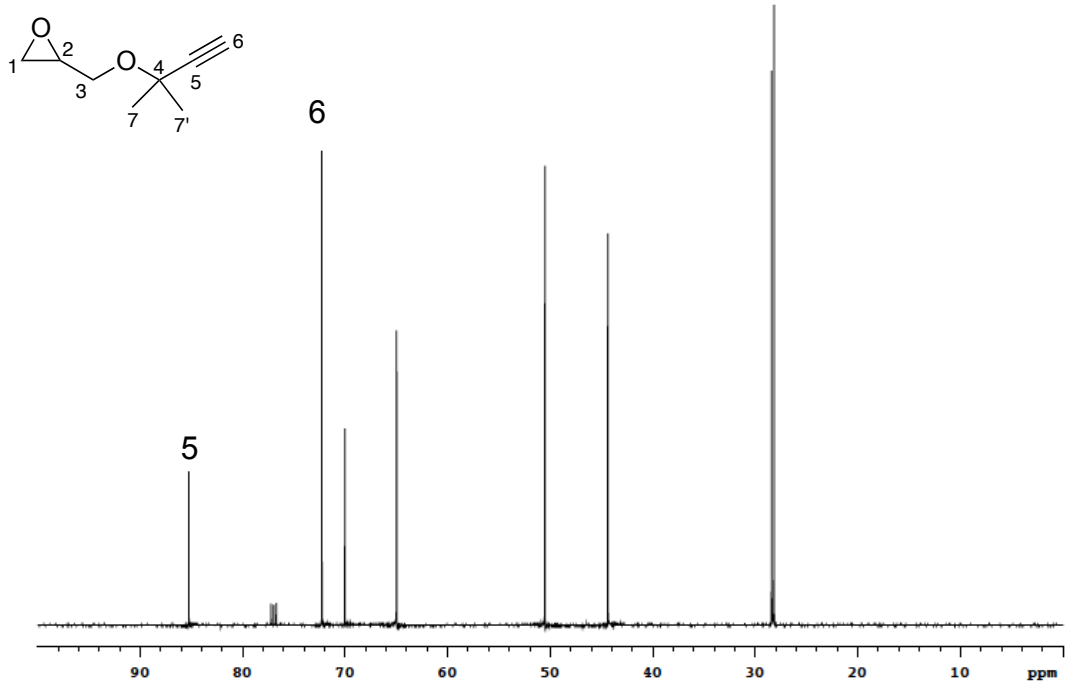

Figure A5. 125 MHz ^{13}C NMR spectrum of **2**.

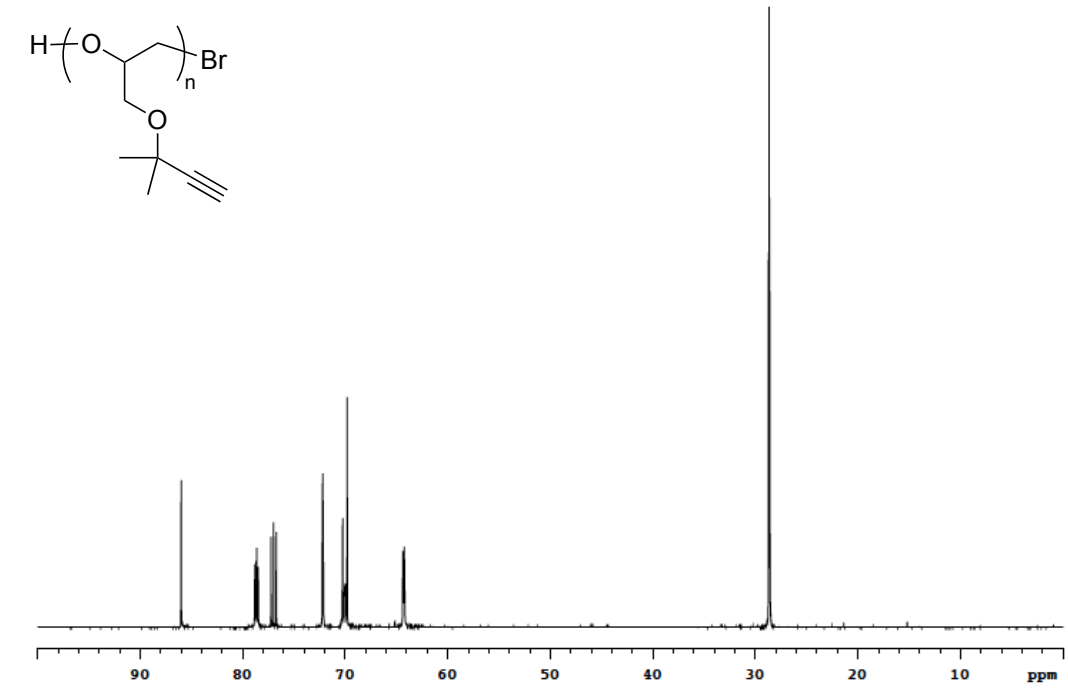

Figure A6. 125 MHz ^{13}C NMR spectrum of poly(**2**).

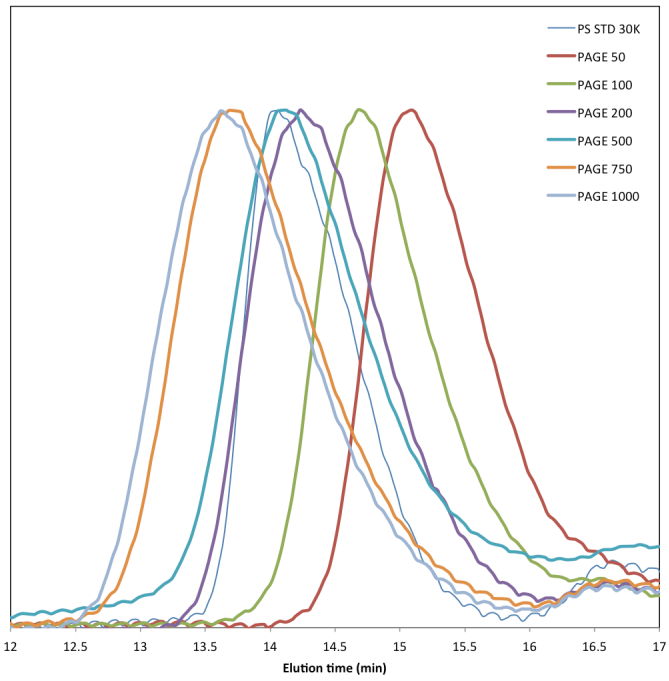

Figure A7. GPC traces of PAGE. The polymers were analyzed in THF at 35 °C, at 1 mL/min flow rate.

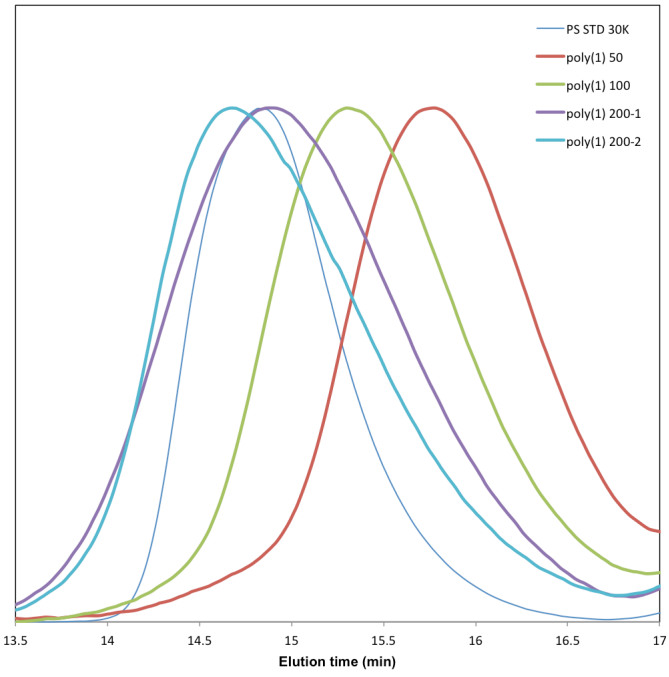

Figure A8. GPC traces of poly(**1**). The polymers were analyzed in THF at 35 °C, at 1 mL/min flow rate.

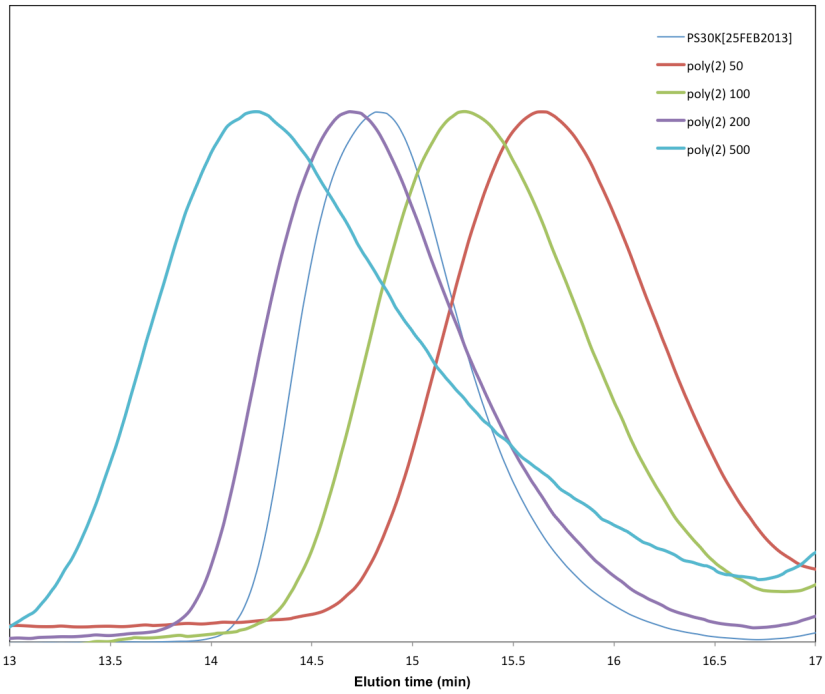

Figure A9. GPC traces of poly(**2**). The polymers were analyzed in THF at 35 °C, at 1 mL/min flow rate.

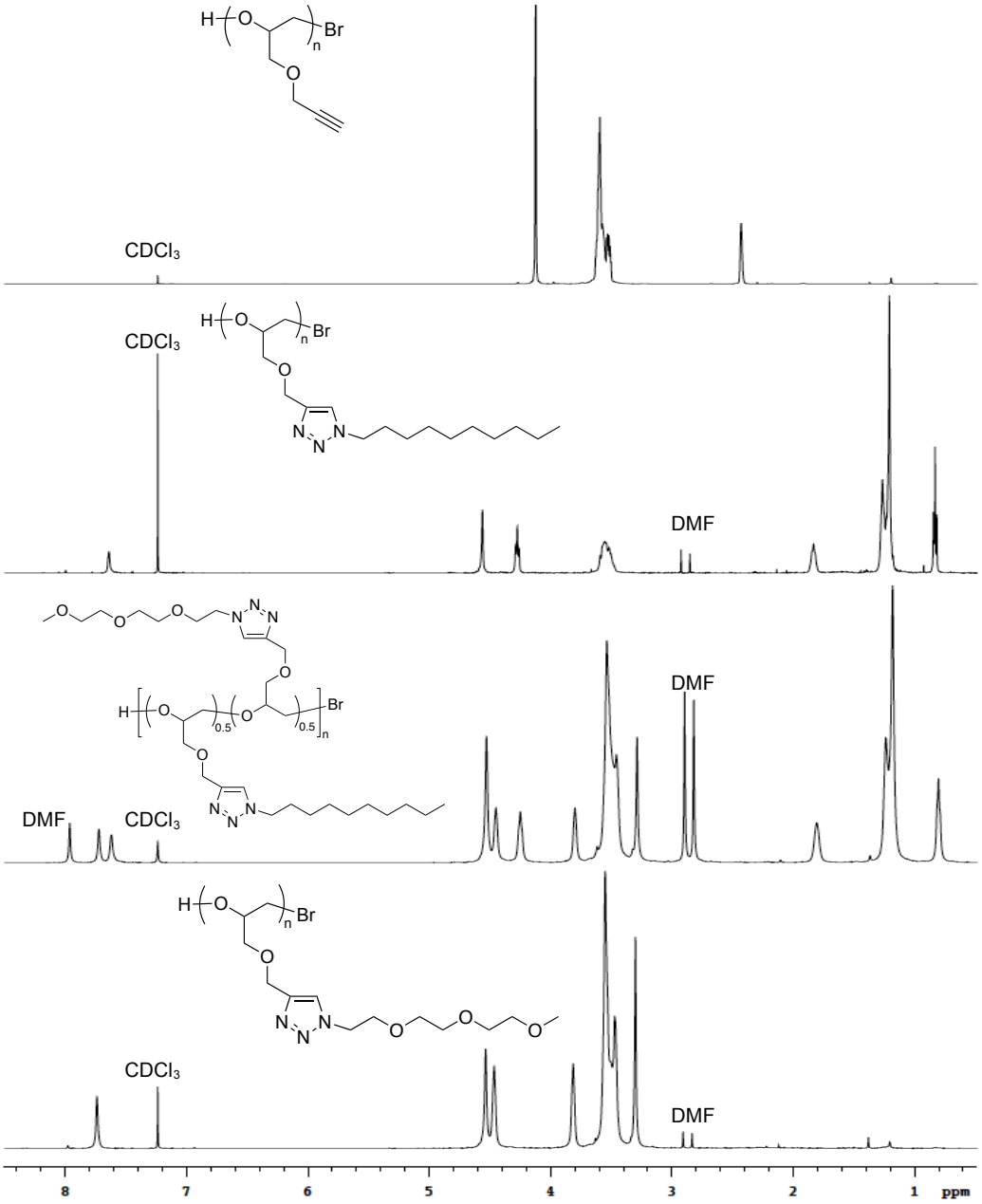

Figure A10. 500 MHz ^{1}H NMR spectra of poly(**1**), polymer $\mathbf{3}_{\mathbf{0.00}}$, $\mathbf{3}_{\mathbf{0.50}}$, and $\mathbf{3}_{\mathbf{1.00}}$.

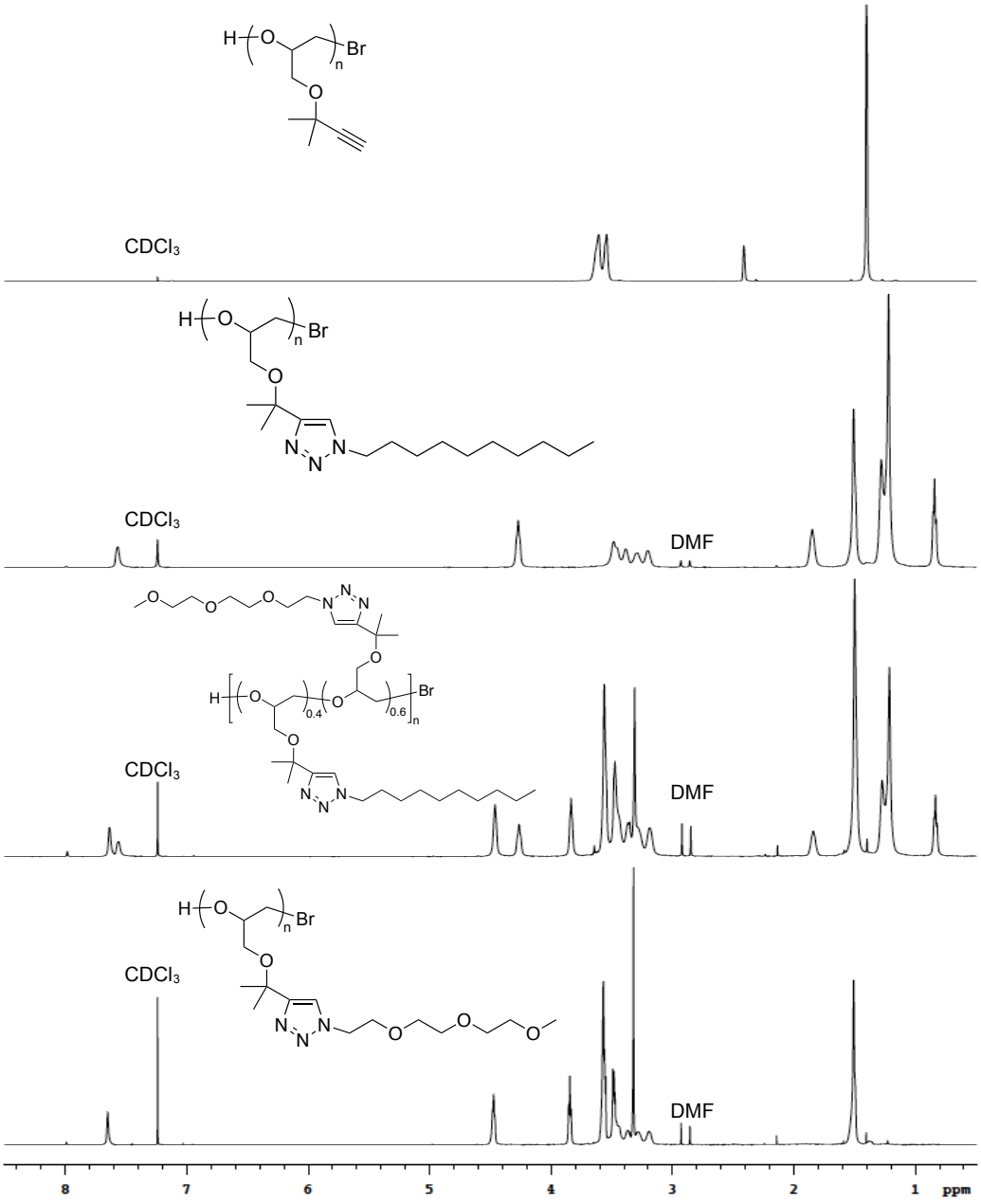

Figure A11. 500 MHz ^{1}H NMR spectra of poly(**2**), polymer $\mathbf{4}_{\mathbf{0.00}}$, $\mathbf{4}_{\mathbf{0.60}}$, and $\mathbf{4}_{\mathbf{1.00}}$.

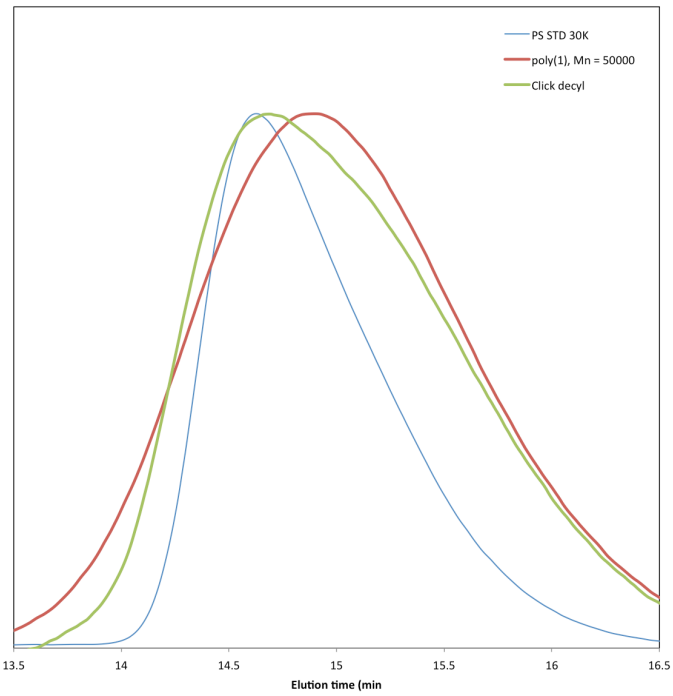

Figure A12. GPC traces of poly(**1**) and polymer $\mathbf{3_{0.0}}$. The polymers were analyzed in THF at 35 °C, at 1 mL/min flow rate.

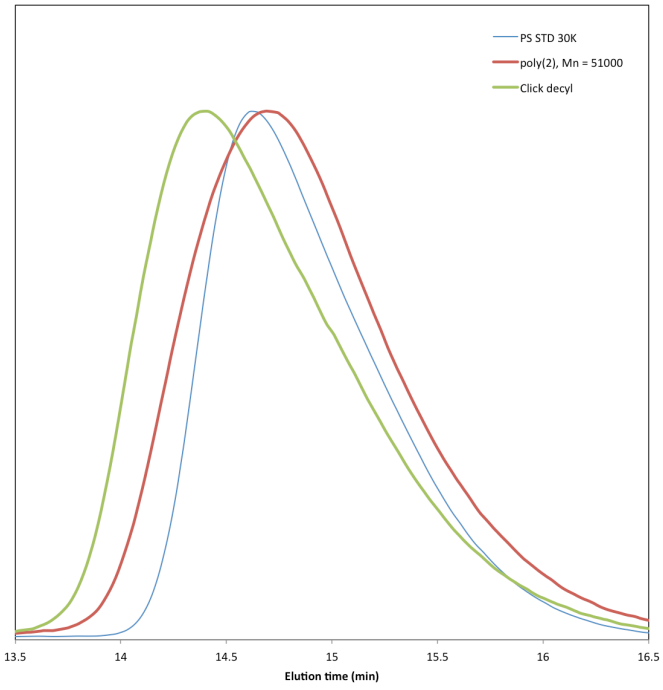

Figure A13. GPC traces of poly(**2**) and polymer $\mathbf{4_{0.0}}$. The polymers were analyzed in THF at 35 °C, at 1 mL/min flow rate.

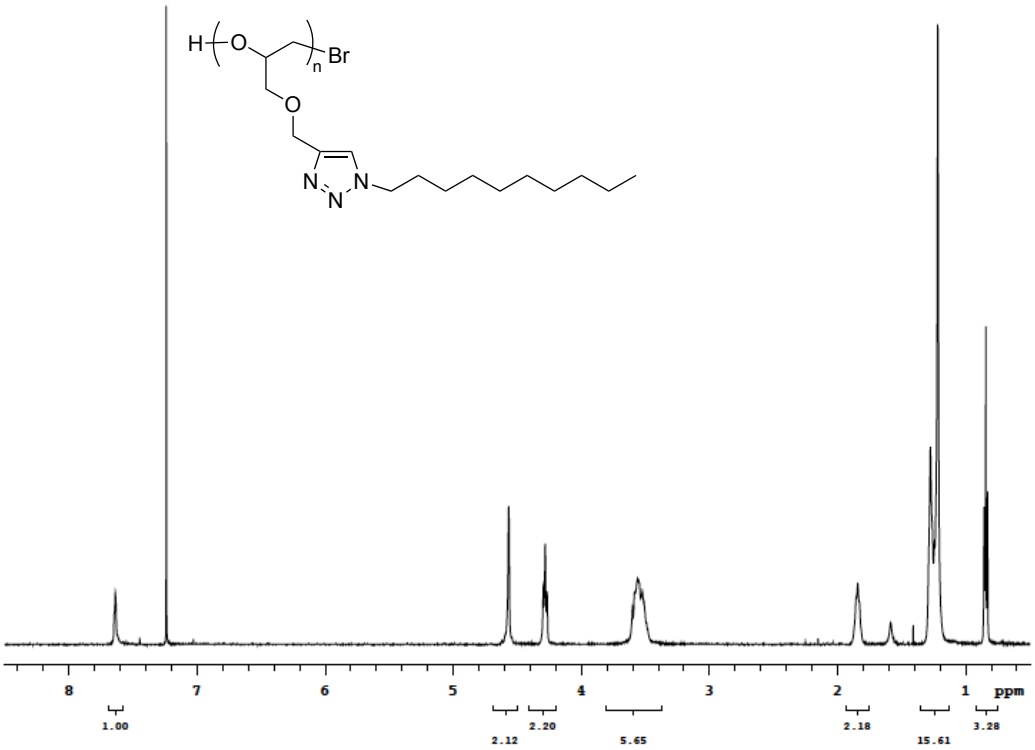

Figure A14. 500 MHz ^{1}H NMR spectra of polymer $\mathbf{3_{0.00}}$.

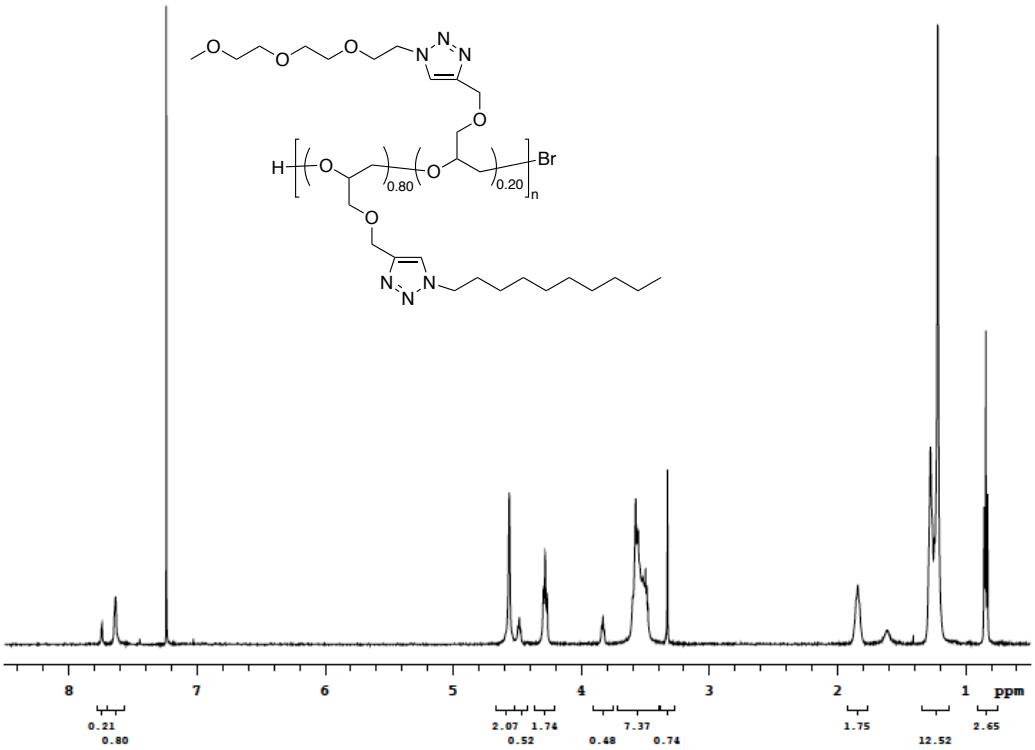

Figure A15. 500 MHz ^{1}H NMR spectra of polymer $\mathbf{3_{0.20}}$.

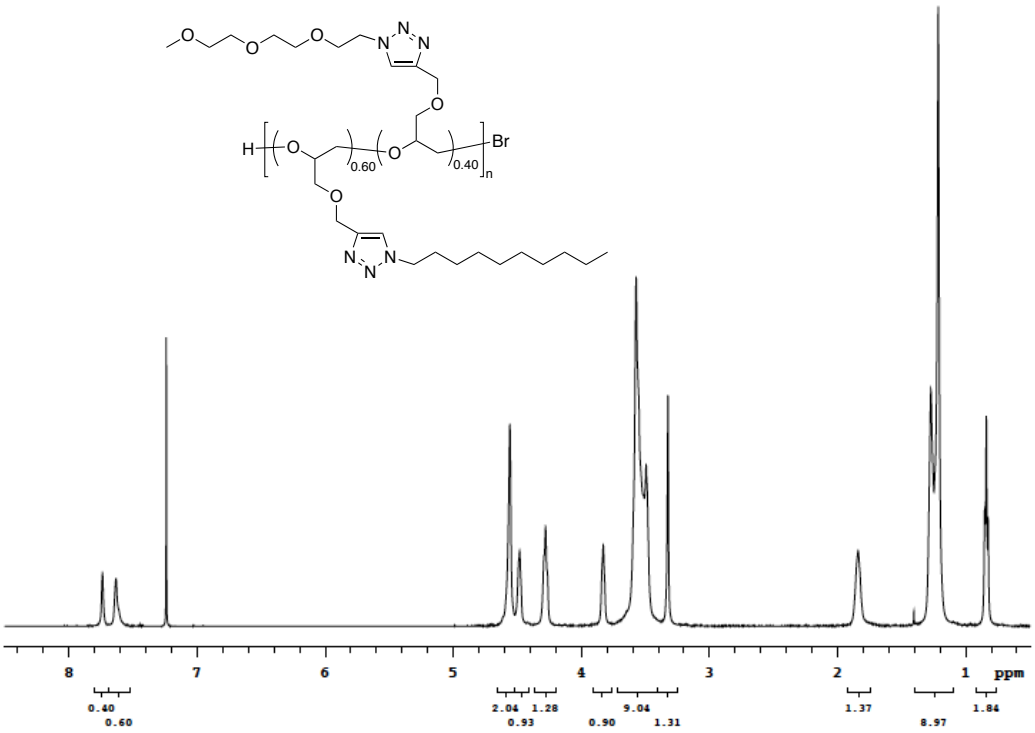

Figure A16. 500 MHz ^{1}H NMR spectra of polymer $\mathbf{3}_{\mathbf{0.40}}$.

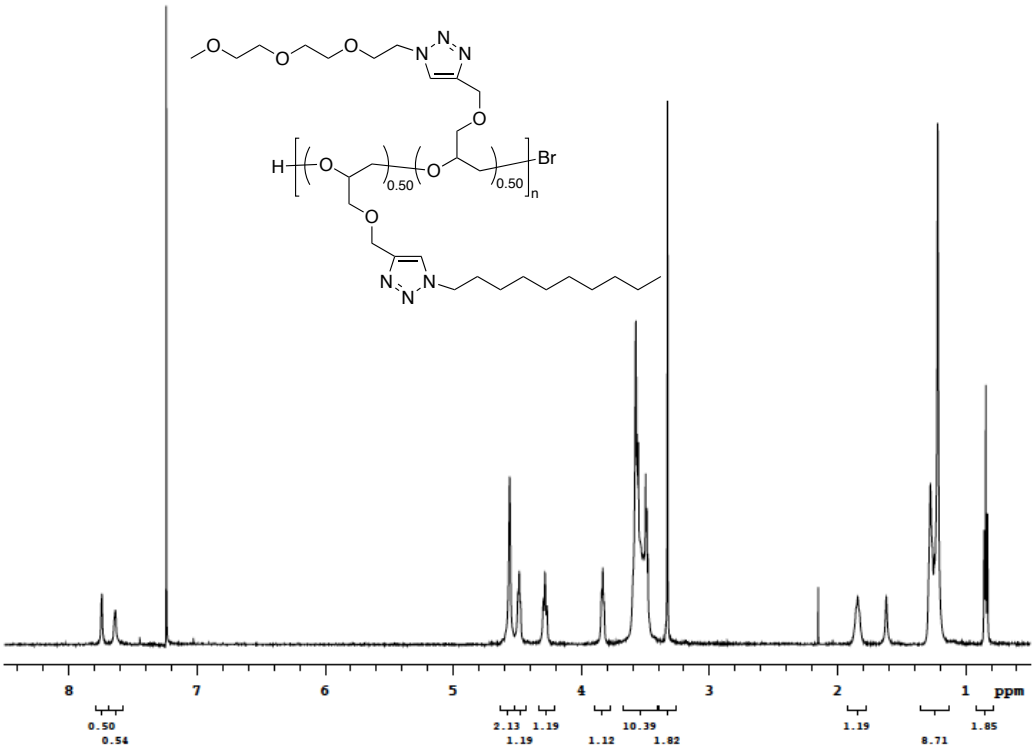

Figure A17. 500 MHz ^{1}H NMR spectra of polymer $\mathbf{3}_{\mathbf{0.50}}$.

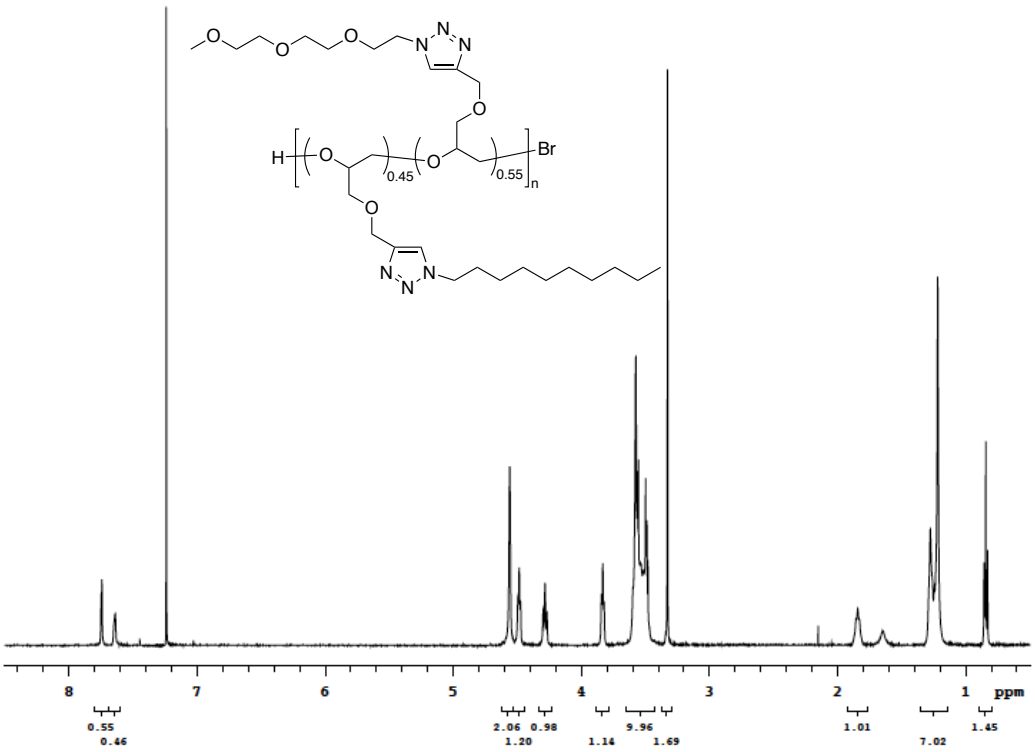

Figure A18. 500 MHz ^{1}H NMR spectra of polymer $\mathbf{3}_{\mathbf{0.55}}$.

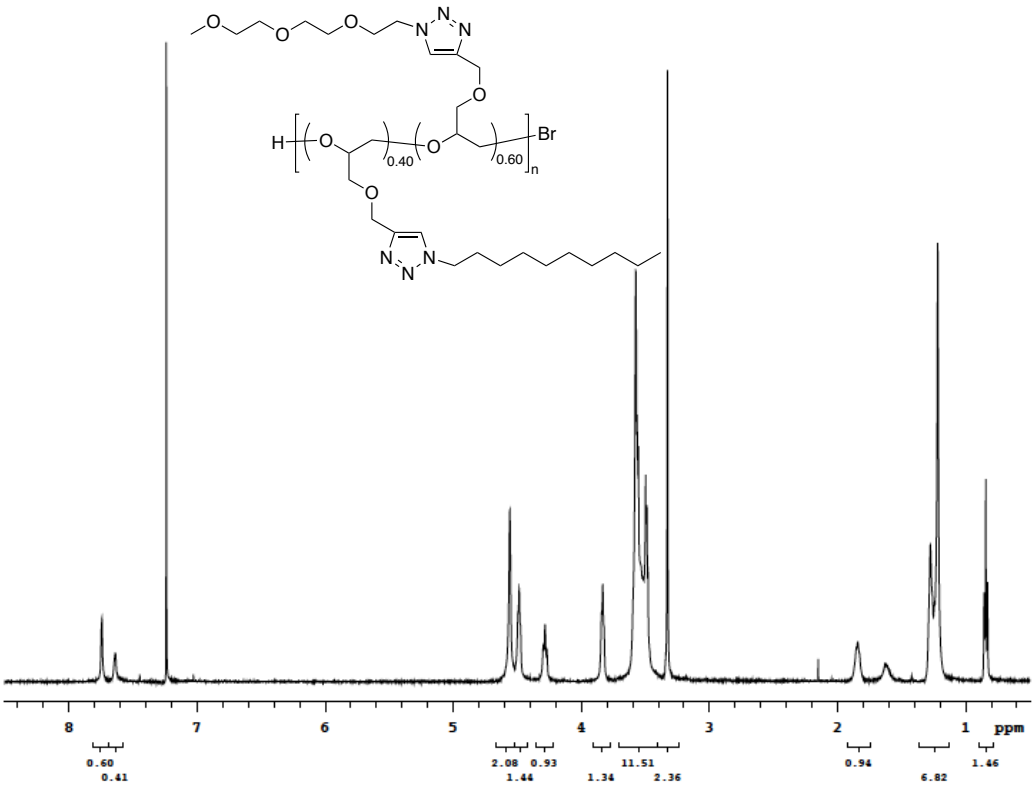

Figure A19. 500 MHz ^{1}H NMR spectra of polymer $\mathbf{3}_{\mathbf{0.60}}$.

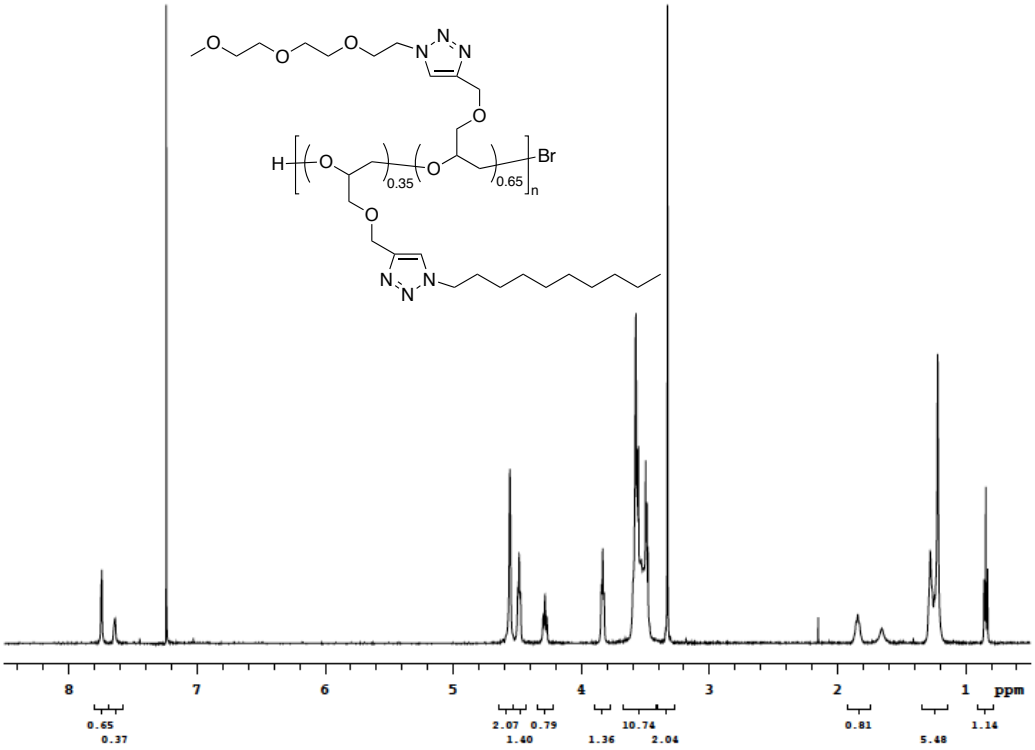

Figure A20. 500 MHz ^{1}H NMR spectra of polymer $\mathbf{3}_{\mathbf{0.65}}$.

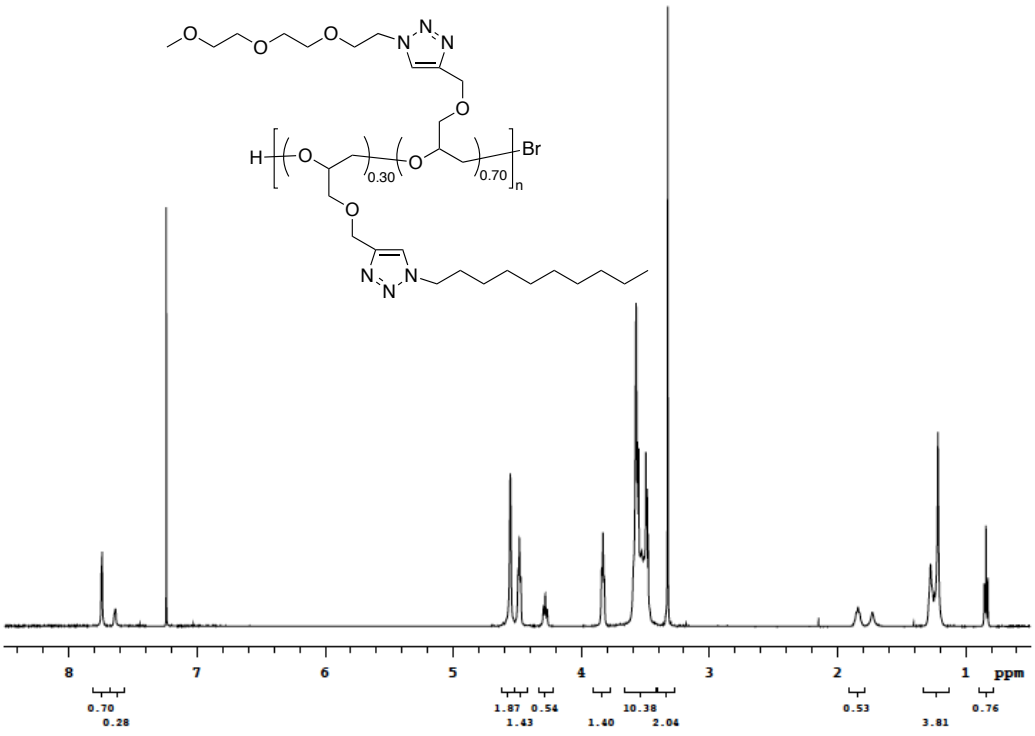

Figure A21. 500 MHz ^{1}H NMR spectra of polymer $\mathbf{3}_{\mathbf{0.70}}$.

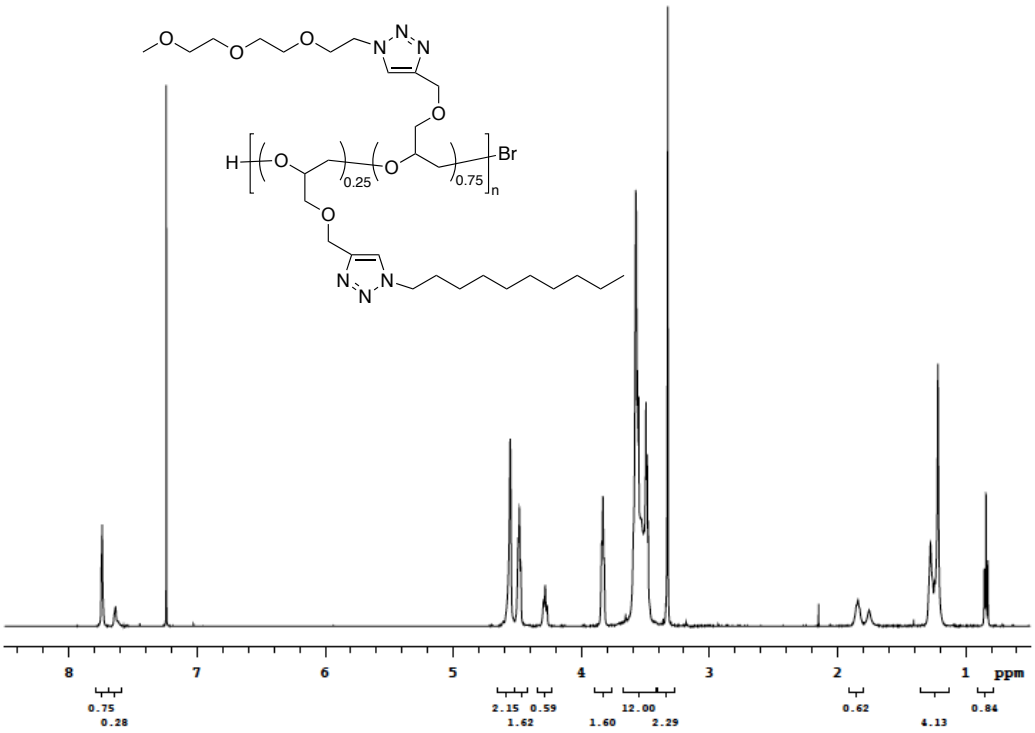

Figure A22. 500 MHz ^{1}H NMR spectra of polymer $\mathbf{3}_{\mathbf{0.75}}$.

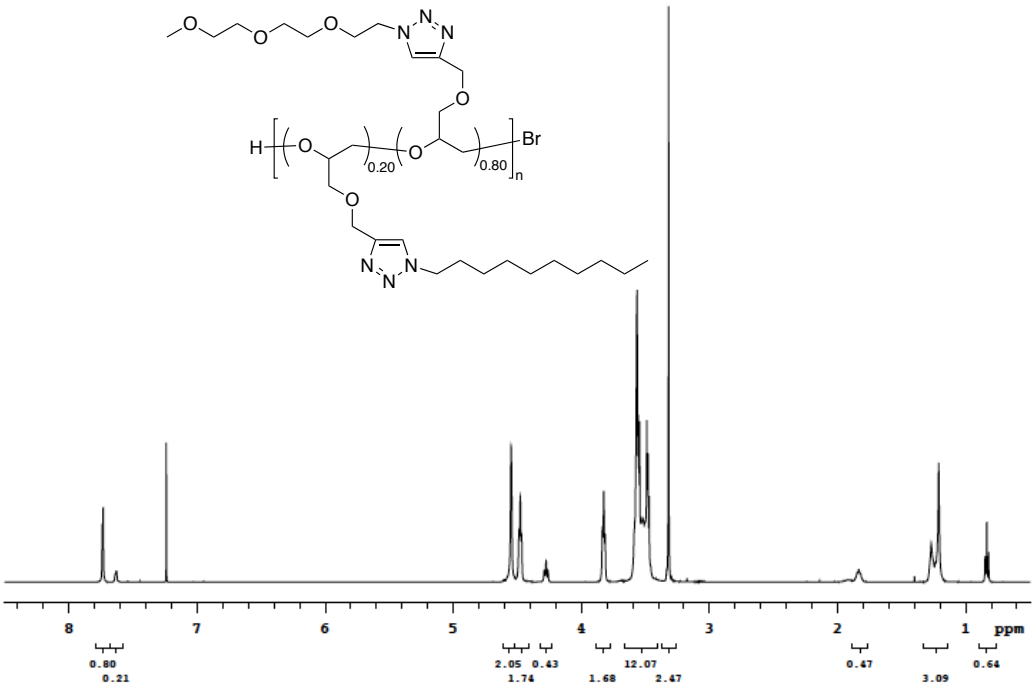

Figure A23. 500 MHz ^{1}H NMR spectra of polymer $\mathbf{3}_{\mathbf{0.80}}$.

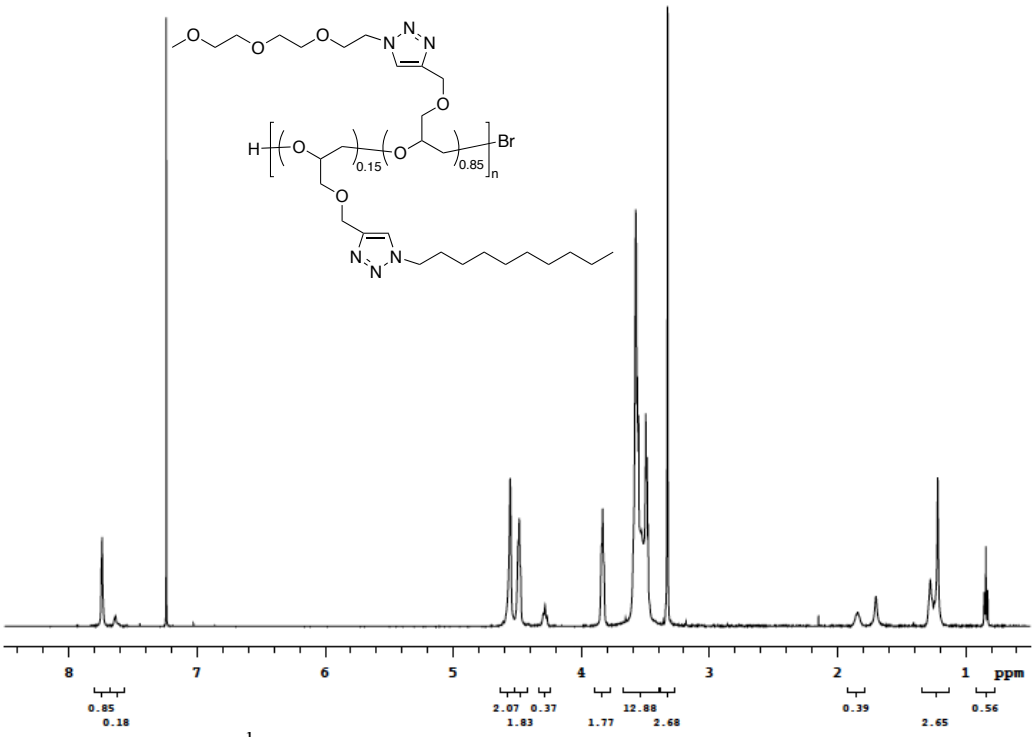

Figure A24. 500 MHz ^{1}H NMR spectra of polymer $\mathbf{3}_{\mathbf{0.85}}$.

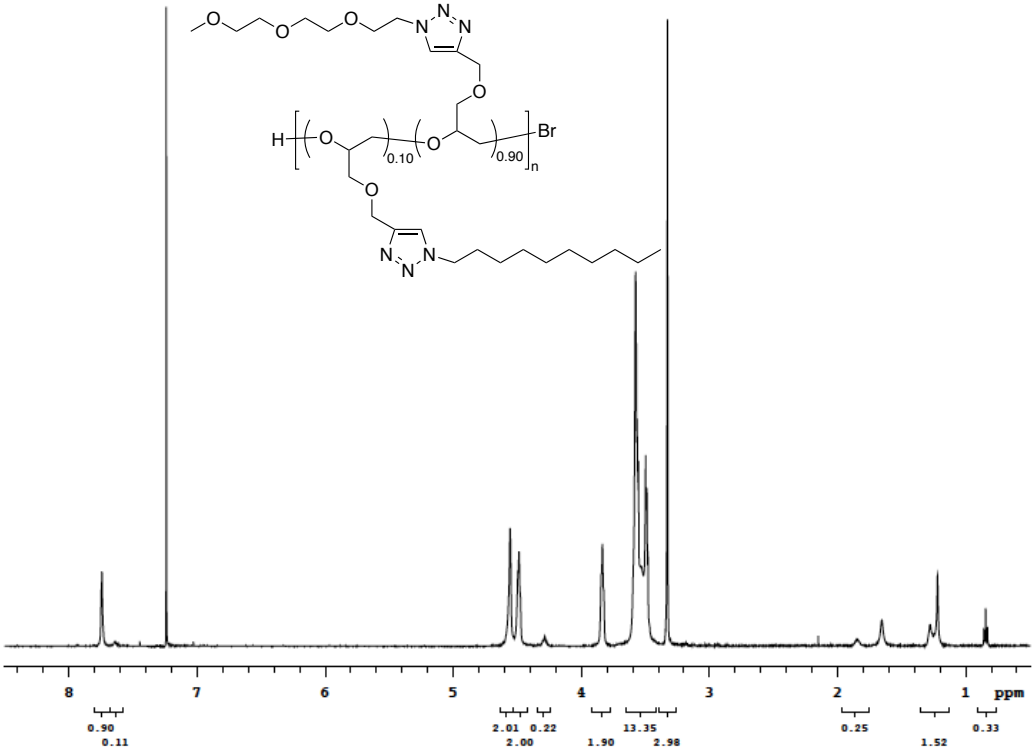

Figure A25. 500 MHz ^{1}H NMR spectra of polymer $\mathbf{3}_{\mathbf{0.90}}$.

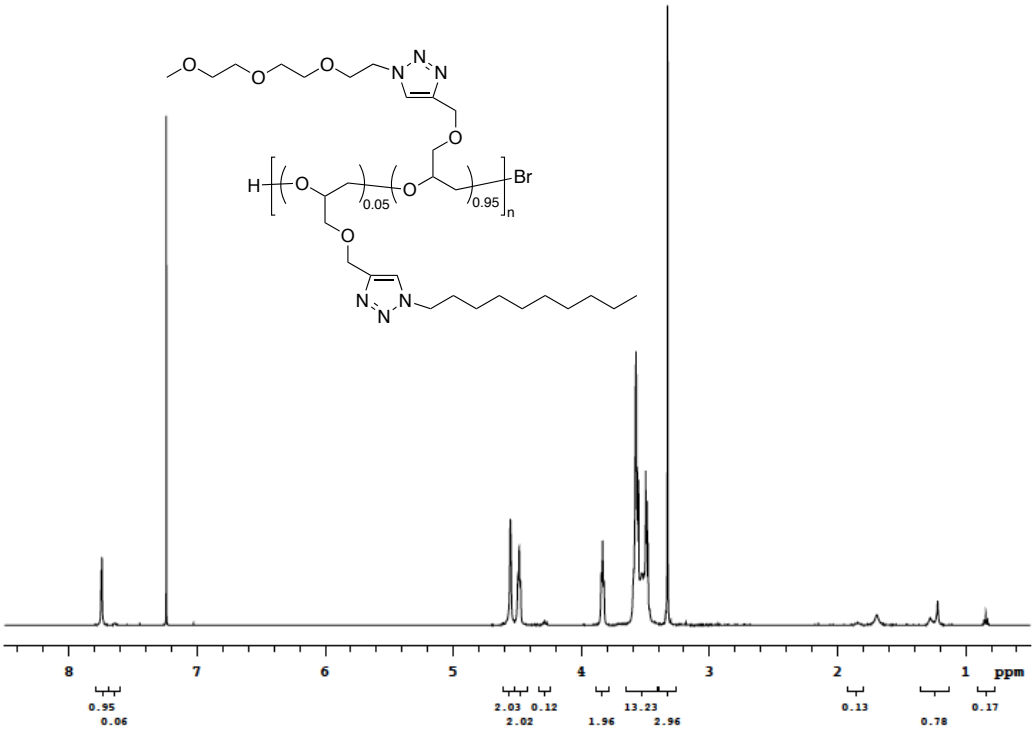

Figure A26. 500 MHz ^{1}H NMR spectra of polymer $\mathbf{3}_{\mathbf{0.95}}$.

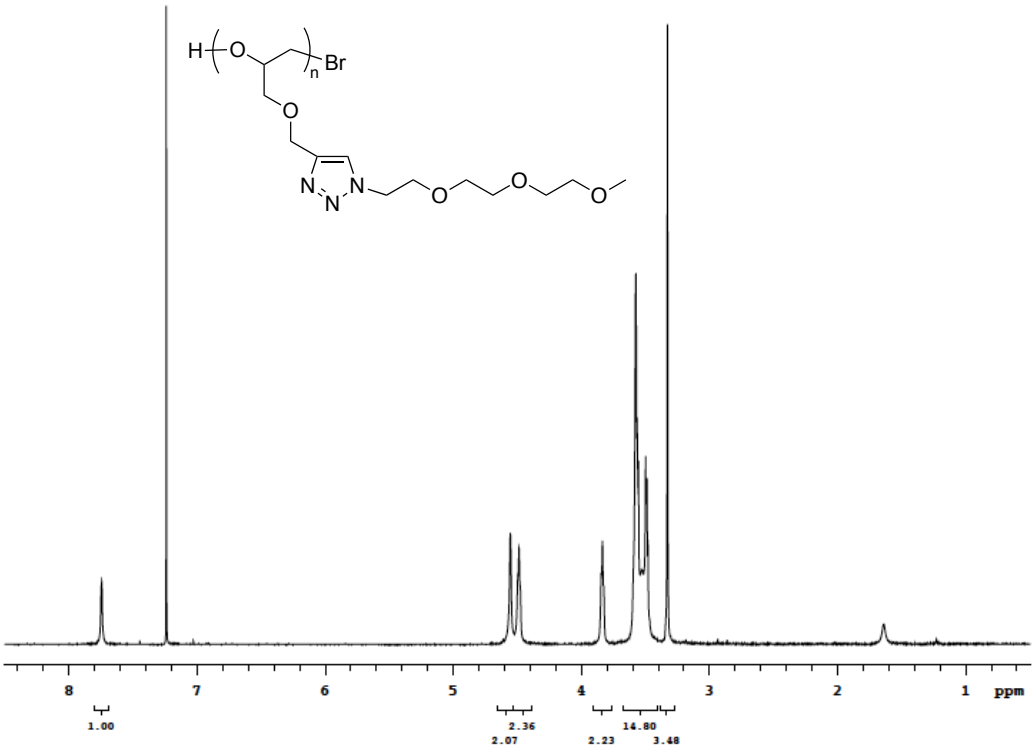

Figure A27. 500 MHz ^{1}H NMR spectra of polymer $\mathbf{3}_{\mathbf{1.00}}$.

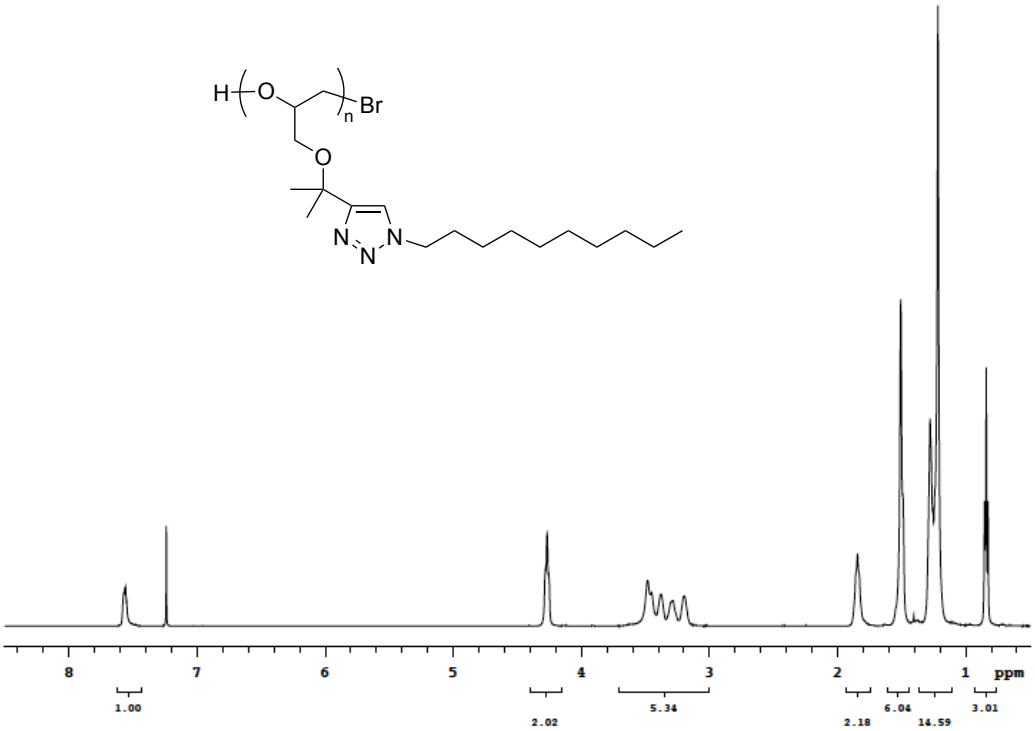

Figure A28. 500 MHz ^{1}H NMR spectra of polymer $\mathbf{4_{0.00}}$.

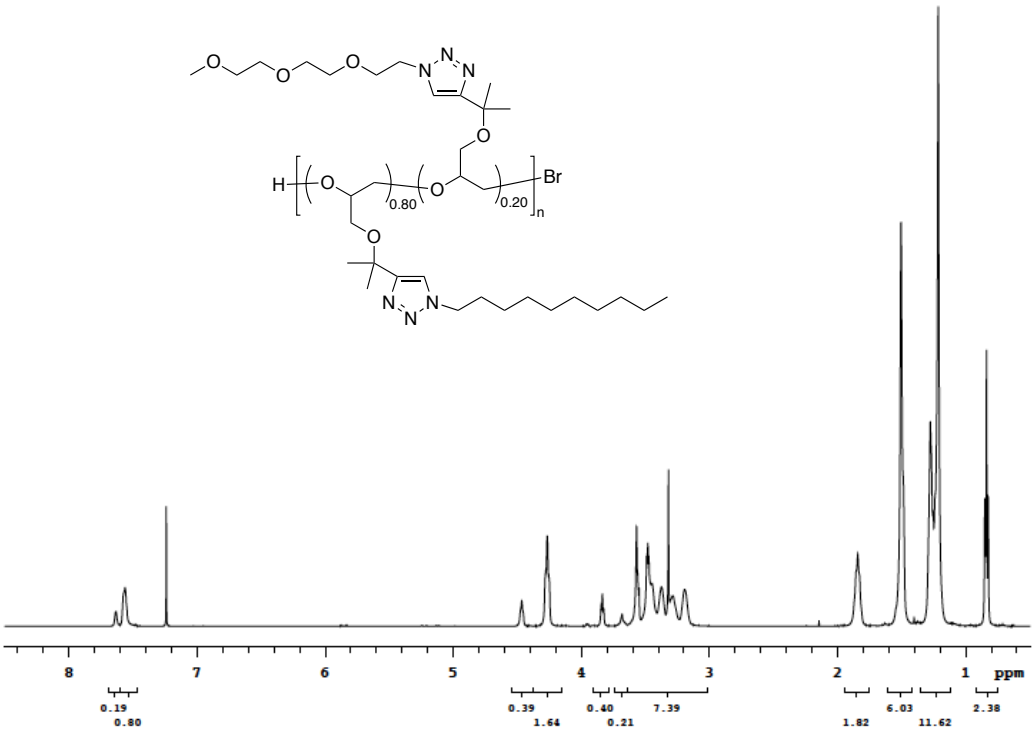

Figure A29. 500 MHz ^{1}H NMR spectra of polymer $\mathbf{4_{0.20}}$.

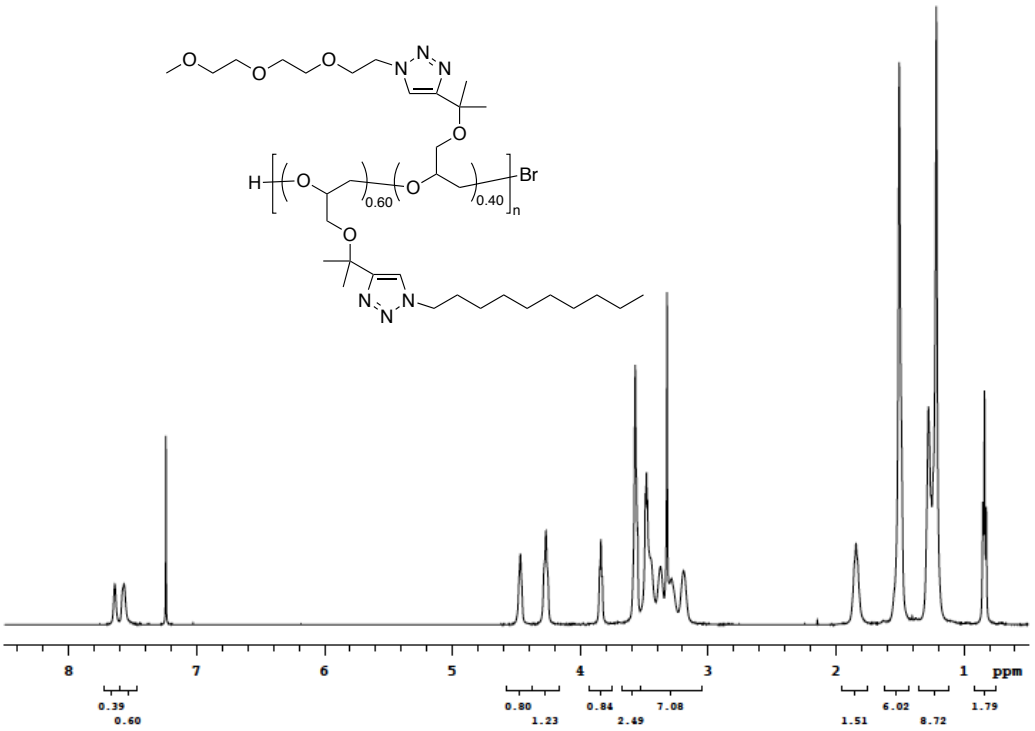

Figure A30. 500 MHz ^{1}H NMR spectra of polymer $\mathbf{4}_{\mathbf{0.40}}$.

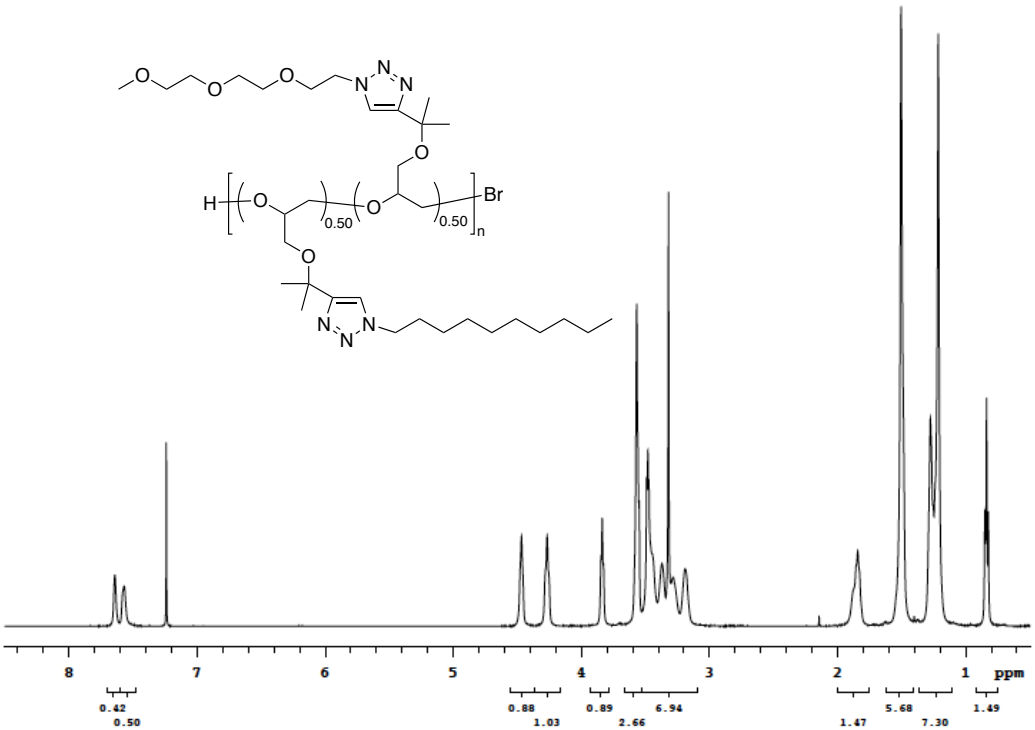

Figure A31. 500 MHz ^{1}H NMR spectra of polymer $\mathbf{4}_{\mathbf{0.50}}$.

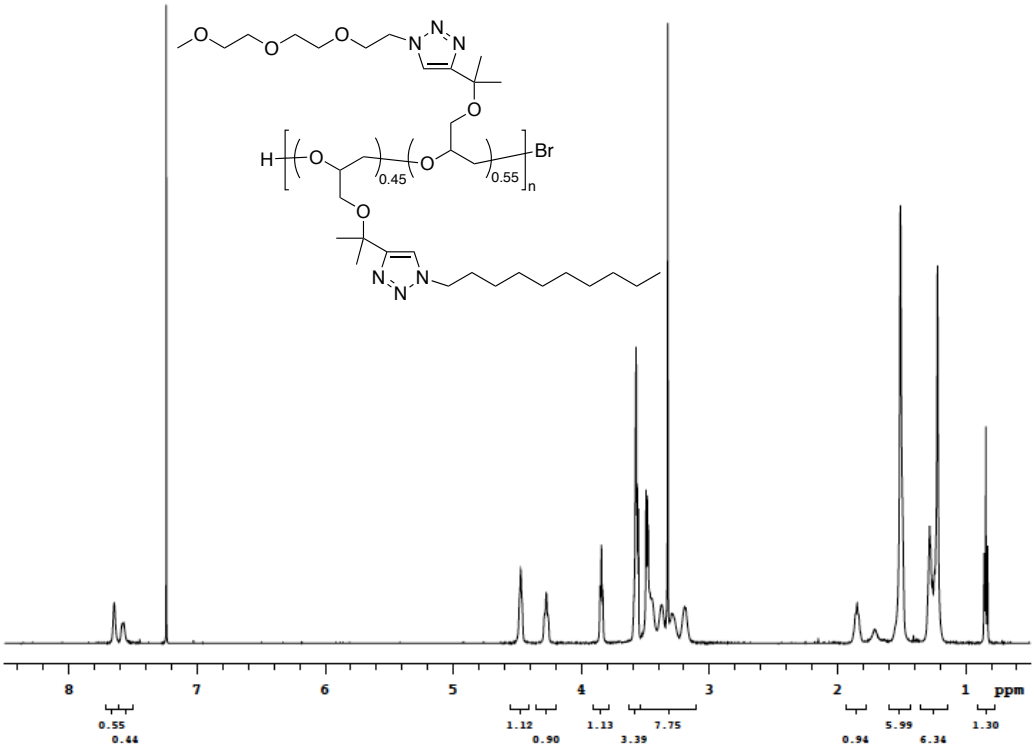

Figure A32. 500 MHz ^{1}H NMR spectra of polymer $\mathbf{4}_{\mathbf{0.55}}$.

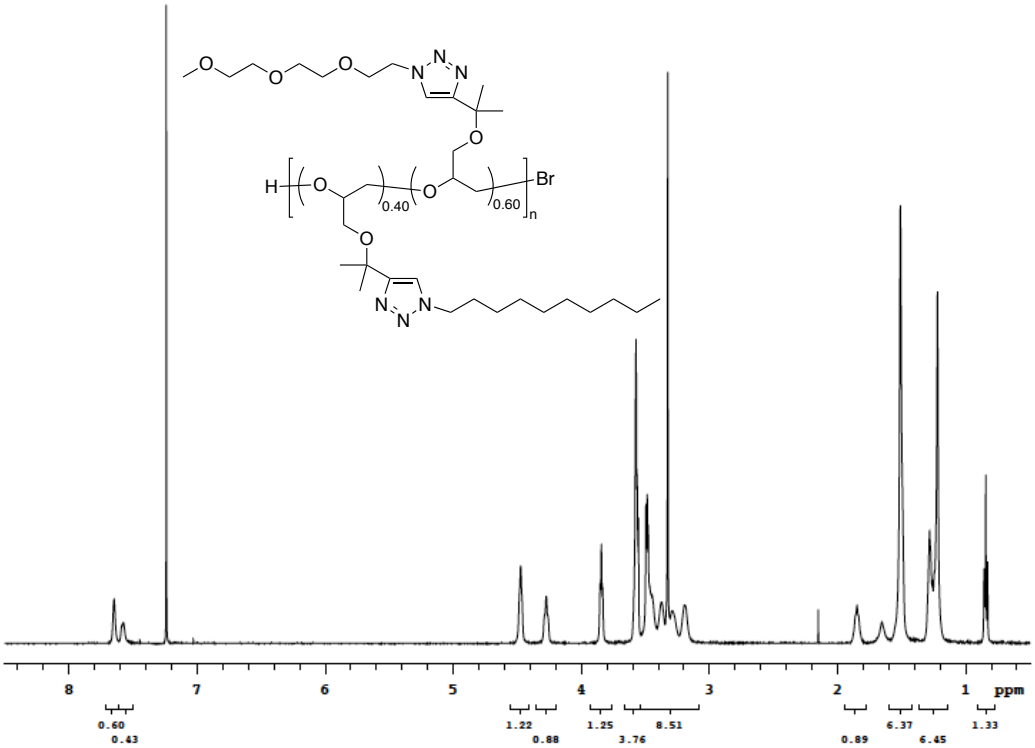

Figure A33. 500 MHz ^{1}H NMR spectra of polymer $\mathbf{4}_{\mathbf{0.60}}$.

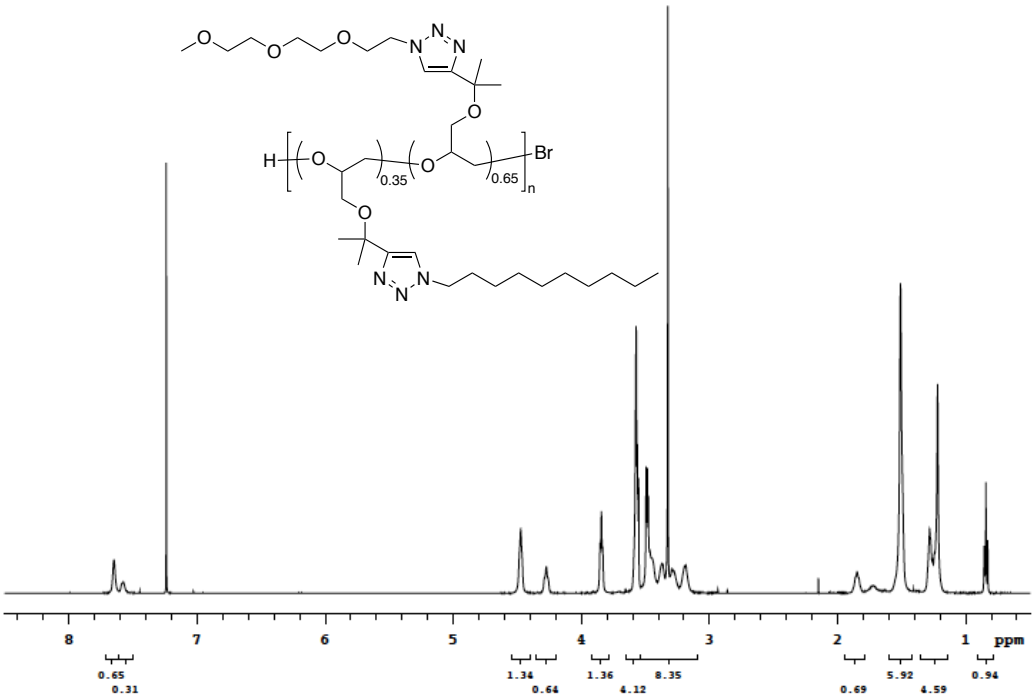

Figure A34. 500 MHz ^{1}H NMR spectra of polymer $\mathbf{4_{0.65}}$.

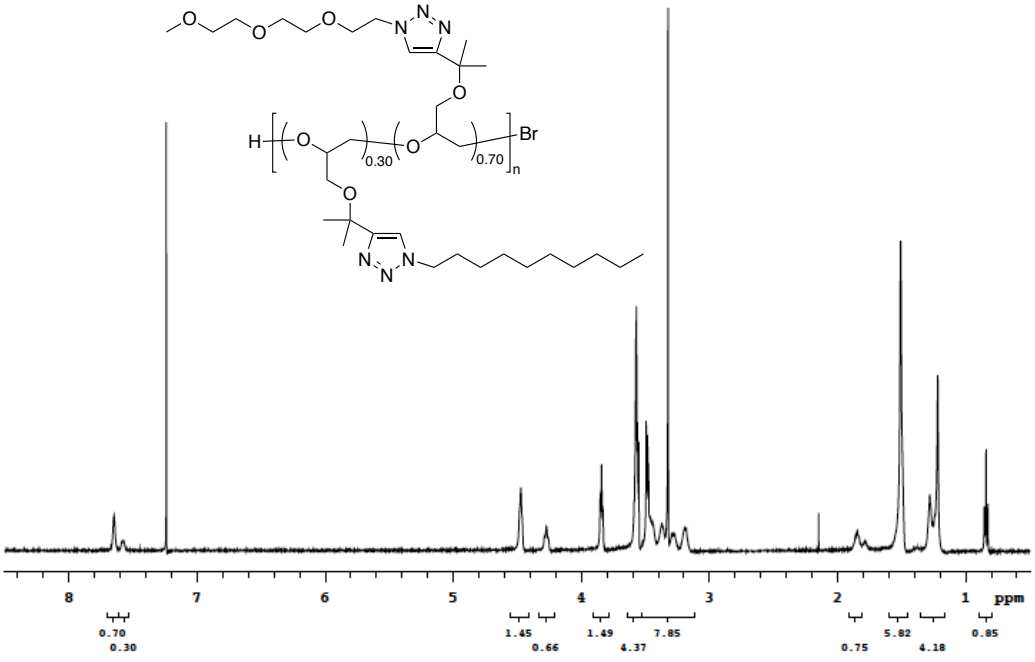

Figure A35. 500 MHz ^{1}H NMR spectra of polymer $\mathbf{4_{0.70}}$.

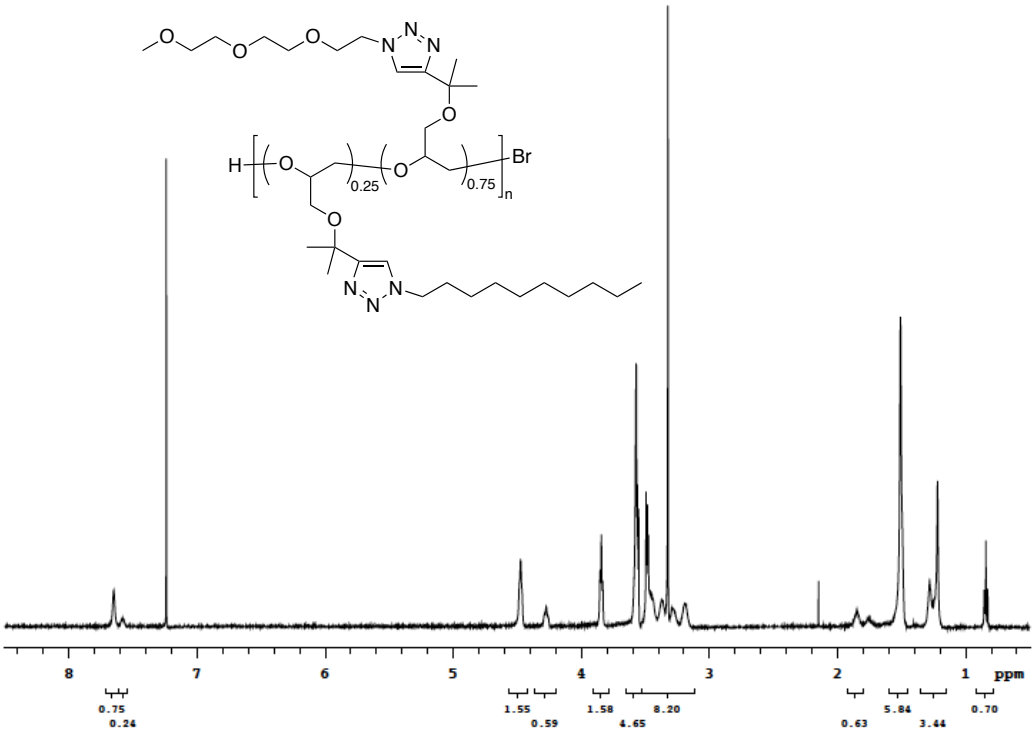

Figure A36. 500 MHz ^{1}H NMR spectra of polymer $\mathbf{4_{0.75}}$.

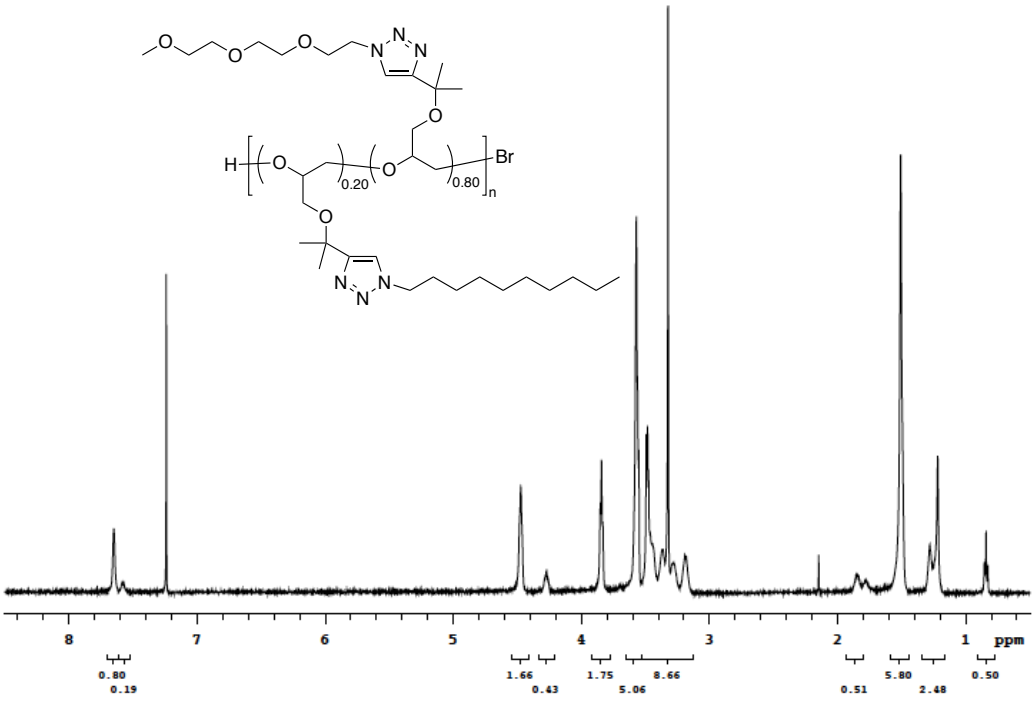

Figure A37. 500 MHz ^{1}H NMR spectra of polymer $\mathbf{4_{0.80}}$.

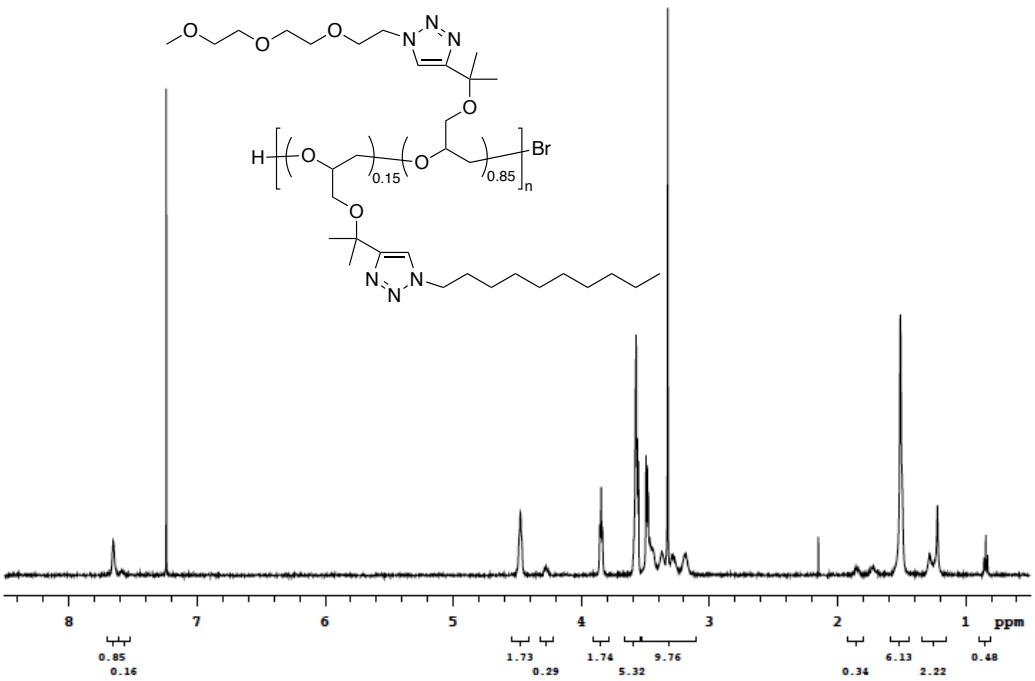

Figure A38. 500 MHz ^{1}H NMR spectra of polymer $\mathbf{4_{0.85}}$.

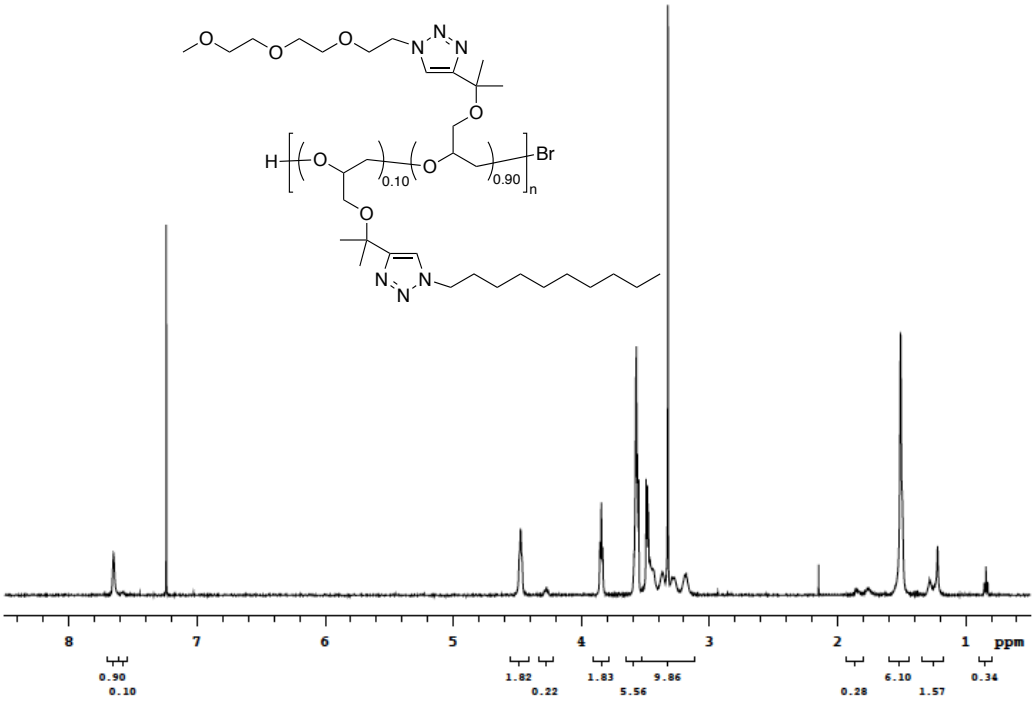

Figure A39. 500 MHz ^{1}H NMR spectra of polymer $\mathbf{4_{0.90}}$.

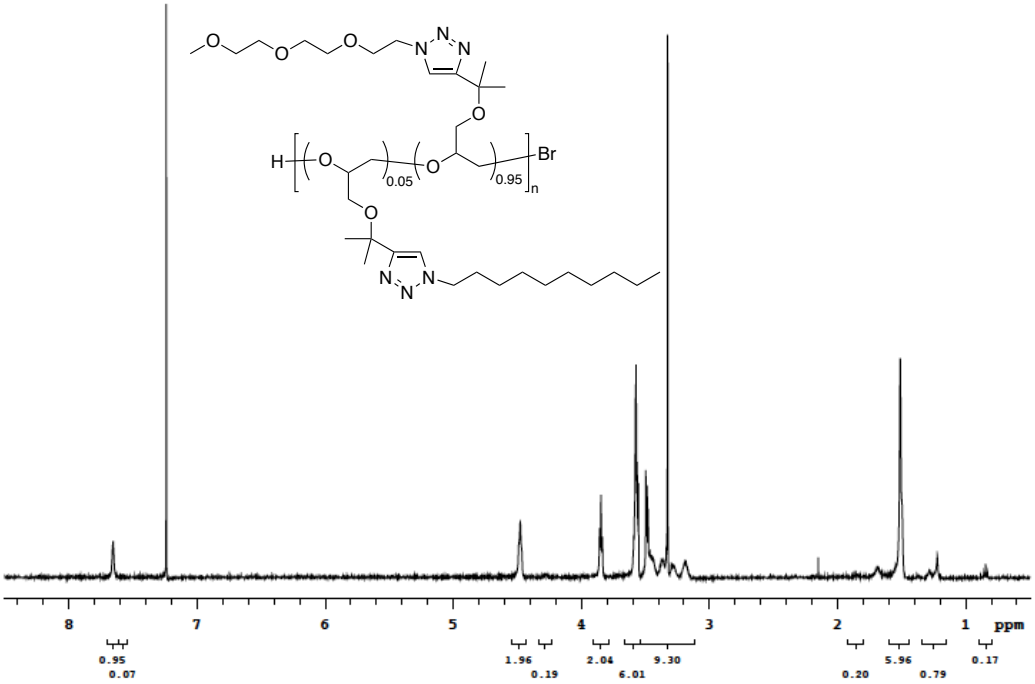

Figure A40. 500 MHz ^{1}H NMR spectra of polymer $\mathbf{4}_{\mathbf{0.95}}$.

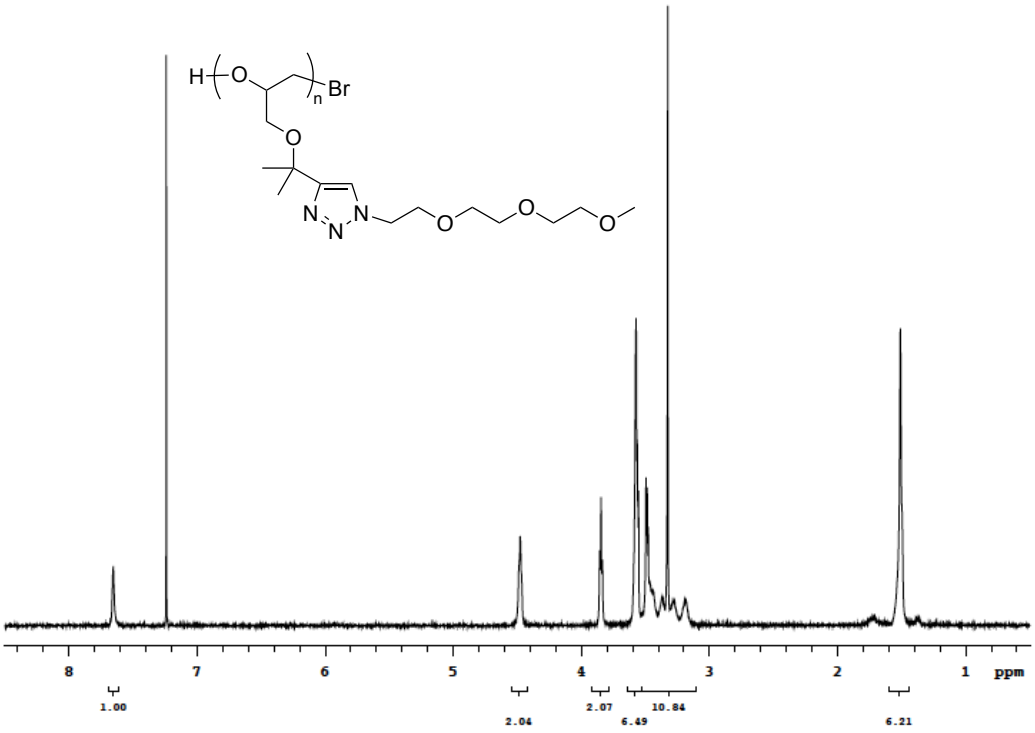

Figure A41. 500 MHz ^{1}H NMR spectra of polymer $\mathbf{4}_{\mathbf{1.00}}$.

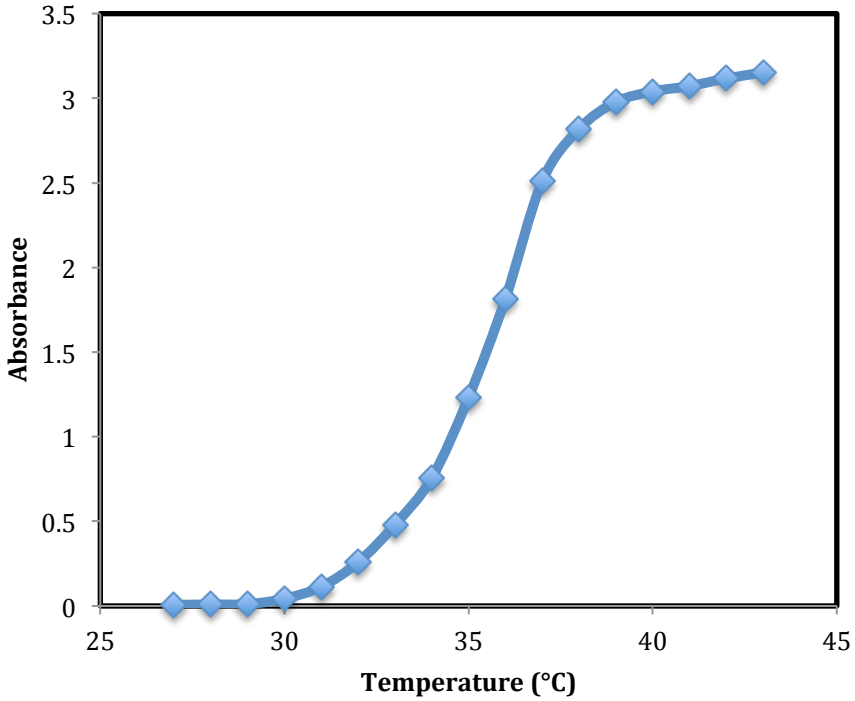

Figure A42. Cloud point determination at 450 nm for polymer $\mathbf{4}_{\mathbf{0.70}}$.

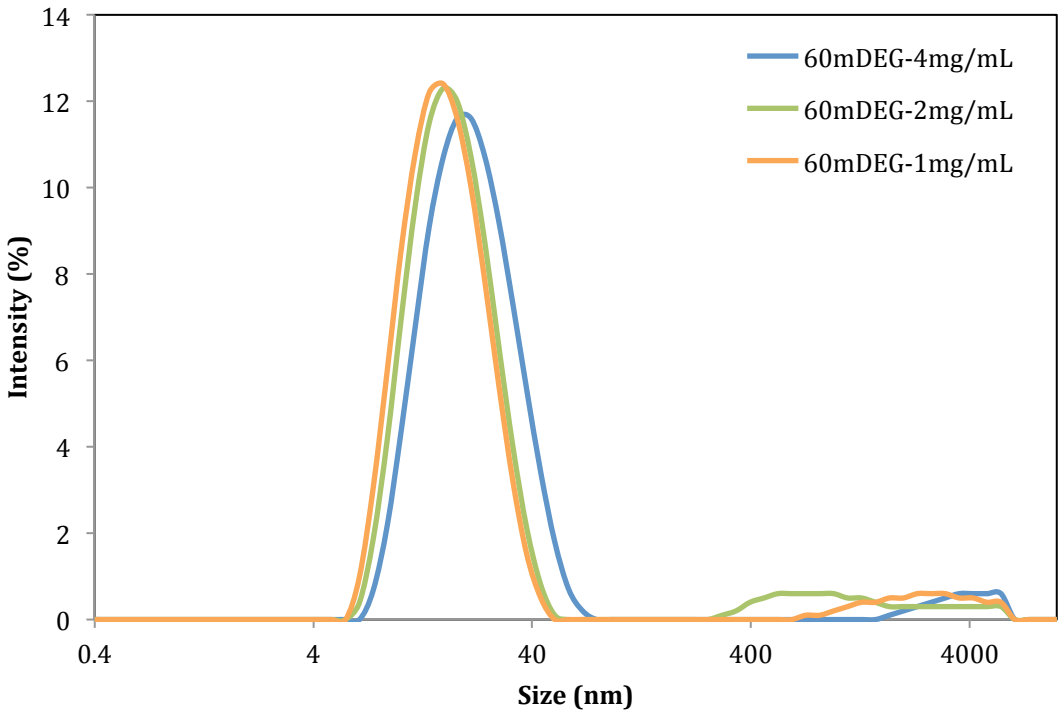

Figure A43. Hydrodynamic radius of polymer $\mathbf{4}_{\mathbf{0.60}}$ determined by DLS.

REFERENCES

REFERENCES

1. Nanamaterials. http://www.niehs.nih.gov/health/topics/agents/sya-nano/ (accessed January 14, 2014).

2. (a) Zhang, L.; Gu, F. X.; Chan, J. M.; Wang, A. Z.; Langer, R. S.; Farokhzad, O. C., *Clin. Pharmacol. Ther.* **2007**, *83*, 761-769; (b) Davis, M. E.; Chen, Z.; Shin, D. M., *Nat. Rev. Drug Discov.* **2008**, *7*, 771-782.

3. (a) Peer, D.; Karp, J. M.; Hong, S.; Farokhzad, O. C.; Margalit, R.; Langer, R., *Nat. Nano.* **2007**, *2*, 751-760; (b) Kiparissides, C.; Kammona, O., *Can. J. Chem. Eng.* **2013**, *91*, 638-651.

4. Barenholz, Y., *Curr. Opin. Colloid. Interface Sci.* **2001**, *6*, 66-77.

5. Woodle, M. C.; Papahadjopoulos, D., Liposome preparation and size characterization. In *Methods Enzymol.*, Sidney Fleischer, B. F., Ed. Academic Press: 1989; Vol. 171, pp 193-217.

6. Torchilin, V. P., *Adv. Drug Deliv. Rev.* **2006**, *58*, 1532-1555.

7. (a) Torchilin, V. P., *Pharm. Res.* **2007**, *24*, 1-16; (b) Sutton, D.; Nasongkla, N.; Blanco, E.; Gao, J., *Pharm. Res.* **2007**, *24*, 1029-1046; (c) Haag, R., *Angew. Chem. Int. Ed.* **2004**, *43*, 278-282; (d) Robb, M. J.; Connal, L. A.; Lee, B. F.; Lynd, N. A.; Hawker, C. J., *Polym. Chem.* **2012**, *3*, 1618-1628.

8. Dechy-Cabaret, O.; Martin-Vaca, B.; Bourissou, D., *Chem. Rev.* **2004**, *104*, 6147-6176.

9. Vermonden, T.; Censi, R.; Hennink, W. E., *Chem. Rev.* **2012**, *112*, 2853-2888.

10. (a) Yasugi, K.; Nagasaki, Y.; Kato, M.; Kataoka, K., *J. Controlled Release* **1999**, *62*, 89-100; (b) Adams, M. L.; Lavasanifar, A.; Kwon, G. S., *J. Pharm. Sci.* **2003**, *92*, 1343-1355.

11. (a) Morishima, Y., *Angew. Chem. Int. Ed.* **2007**, *46*, 1370-1372; (b) Stuart, M. A. C.; Huck, W. T. S.; Genzer, J.; Muller, M.; Ober, C.; Stamm, M.; Sukhorukov, G. B.;

Szleifer, I.; Tsukruk, V. V.; Urban, M.; Winnik, F.; Zauscher, S.; Luzinov, I.; Minko, S., *Nat. Mater.* **2010**, *9*, 101-113.

12. Alarcon, C. d. l. H.; Pennadam, S.; Alexander, C., *Chem. Soc. Rev.* **2005**, *34*, 276-285.

13. Xiong, X.-B.; Binkhathlan, Z.; Molavi, O.; Lavasanifar, A., *Acta Biomaterialia* **2012**, *8*, 2017-2033.

14. (a) Jackson, A. W.; Fulton, D. A., *Polym. Chem.* **2013**, *4*, 31-45; (b) Xu, W.; Burke, J. F.; Pilla, S.; Chen, H.; Jaskula-Sztul, R.; Gong, S., *Nanoscale* **2013**, *5*, 9924-9933.

15. (a) Newkome, G. R.; Moorefield, C. N.; Baker, G. R.; Saunders, M. J.; Grossman, S. H., *Angewandte Chemie International Edition in English* **1991**, *30*, 1178-1180; (b) Liu, H.; Jiang, A.; Guo, J.; Uhrich, K. E., *J. Polym. Sci., Part A: Polym. Chem.* **1999**, *37*, 703-711.

16. (a) Aiertza, M.; Odriozola, I.; Cabañero, G.; Grande, H.-J.; Loinaz, I., *Cell. Mol. Life Sci.* **2012**, *69*, 337-346; (b) Dirlam, P. T.; Kim, H. J.; Arrington, K. J.; Chung, W. J.; Sahoo, R.; Hill, L. J.; Costanzo, P. J.; Theato, P.; Char, K.; Pyun, J., *Polym. Chem.* **2013**, *4*, 3765-3773; (c) Xiao, Y.; Hong, H.; Javadi, A.; Engle, J. W.; Xu, W.; Yang, Y.; Zhang, Y.; Barnhart, T. E.; Cai, W.; Gong, S., *Biomaterials* **2012**, *33*, 3071-3082.

17. (a) Tomalia, D. A.; Baker, H.; Dewald, J.; Hall, M.; Kallos, G.; Martin, S.; Roeck, J.; Ryder, J.; Smith, P., *Polym. J.* **1985**, *17*, 117-132; (b) Esfand, R.; Tomalia, D. A., *Drug Discovery Today* **2001**, *6*, 427-436.

18. (a) Vogel, E. B. Synthesis, Characterization, and Applications of Functionalized Polyglycolides. Michigan State University, 2008; (b) Jiang, X.; Vogel, E. B.; Smith III, M. R.; Baker, G. L., *Macromolecules* **2008**, *41*, 1937-1944; (c) Jiang, X.; Vogel, E. B.; Smith III, M. R.; Baker, G. L., *J. Polym. Sci., Part A: Polym. Chem.* **2007**, *45*, 5227-5236.

19. Dill, K. A.; MacCallum, J. L., *Science* **2012**, *338*, 1042-1046.

20. (a) Sela, M.; Jr, F. H. W.; Anfinsen, C. B., *Science* **1957**, *125*, 691-692; (b) Anfinsen, C. B.; Haber, E., *J. Biol. Chem.* **1961**, *236*, 1361-1363; (c) Kuriyan, J.; Konforti, B.; Wemmer, D., *The Molecules of Life: Physical and Chemical Principles*. 1st ed.; Garland Science, Taylor & Francis Group, LLC: 2012.

21. Hartl, F. U.; Hayer-Hartl, M., *Nat. Struct. Mol. Biol.* **2009**, *16*, 574-581.

22. (a) Dill, K. A., *Biochemistry* **1990**, *29*, 7133-7155; (b) Lim, W. A.; Sauer, R. T., *Nature* **1989**, *339*, 31-36; (c) Matsumura, M.; Becktel, W. J.; Matthews, B. W., *Nature* **1988**, *334*, 406-410; (d) Eriksson, A.; Baase, W.; Zhang, X.; Heinz, D.; Blaber, M.; Baldwin, E.; Matthews, B., *Science* **1992**, *255*, 178-183.

23. Kumar, S.; Nussinov, R., *J. Mol. Biol.* **1999**, *293*, 1241-1255.

24. Burley, S.; Petsko, G., *Science* **1985**, *229*, 23-28.

25. Scheinost, J. C.; Boldt, G. E.; Wentworth, P., Protein Misfolding and Disease. In *Chemical Biology*, John Wiley & Sons, Inc.: 2012; pp 379-400.

26. (a) Walter, S.; Buchner, J., *Angew. Chem. Int. Ed.* **2002**, *41*, 1098-1113; (b) Hildenbrand, Z.; Bernal, R., Chaperonin-Mediated Folding of Viral Proteins. In *Viral Molecular Machines*, Rossmann, M. G.; Rao, V. B., Eds. Springer US: 2012; Vol. 726, pp 307-324; (c) Fink, A. L., *Physiol. Rev.* **1999**, *79*, 425-449.

27. (a) Rozema, D.; Gellman, S. H., *J. Am. Chem. Soc.* **1995**, *117*, 2373-2374; (b) Rozema, D.; Gellman, S. H., *Biochemistry* **1996**, *35*, 15760-15771.

28. (a) Hirakura, T.; Yasugi, K.; Nemoto, T.; Sato, M.; Shimoboji, T.; Aso, Y.; Morimoto, N.; Akiyoshi, K., *J. Controlled Release* **2010**, *142*, 483-489; (b) Sasaki, Y.; Nomura, Y.; Sawada, S.-i.; Akiyoshi, K., *Polym. J.* **2010**, *42*, 823-828; (c) Takahashi, H.; Sawada, S.-i.; Akiyoshi, K., *ACS Nano* **2010**, *5*, 337-345.

29. Takeda, S.; Takahashi, H.; Sawada, S.-i.; Sasaki, Y.; Akiyoshi, K., *RSC Advances* **2013**, *3*, 25716-25718.

30. Liu, X.; Liu, Y.; Zhang, Z.; Huang, F.; Tao, Q.; Ma, R.; An, Y.; Shi, L., *Chem. Eur. J.* **2013**, *19*, 7437-7442.

31. Odian, G., *Principles of Polymerization*. Fourth ed.; John Wiley & Sons, Inc.: 2004.

32. Mangold, C.; Wurm, F.; Frey, H., *Polym. Chem.* **2012**, *3*, 1714-1721.

33. (a) Carlotti, S.; Labbé, A.; Rejsek, V.; Doutaz, S.; Gervais, M.; Deffieux, A., *Macromolecules* **2008**, *41*, 7058-7062; (b) Gervais, M.; Brocas, A.-L.; Cendejas, G.; Deffieux, A.; Carlotti, S., *Macromolecules* **2010**, *43*, 1778-1784; (c) Brocas, A.-L.; Cendejas, G.; Caillol, S.; Deffieux, A.; Carlotti, S., *J. Polym. Sci., Part A: Polym. Chem.* **2011**, *49*, 2677-2684; (d) Labbé, A.; Brocas, A.-L.; Ibarboure, E.; Ishizone, T.; Hirao, A.; Deffieux, A.; Carlotti, S., *Macromolecules* **2011**, *44*, 6356-6364.

34. Baskaran, S.; Baig, M. H. A.; Banerjee, S.; Baskaran, C.; Bhanu, K.; Deshpande, S. P.; Trivedi, G. K., *Tetrahedron* **1996**, *52*, 6437-6452.

35. (a) Gauthier, M. A.; Gibson, M. I.; Klok, H.-A., *Angew. Chem. Int. Ed.* **2009**, *48*, 48-58; (b) Günay, K. A.; Theato, P.; Klok, H.-A., *J. Polym. Sci., Part A: Polym. Chem.* **2013**, *51*, 1-28.

36. Kolb, H. C.; Finn, M. G.; Sharpless, K. B., *Angew. Chem. Int. Ed.* **2001**, *40*, 2004-2021.

37. (a) Meldal, M.; Tornøe, C. W., *Chem. Rev.* **2008**, *108*, 2952-3015; (b) Tornøe, C. W.; Christensen, C.; Meldal, M., *J. Org. Chem.* **2002**, *67*, 3057-3064.

38. Rostovtsev, V. V.; Green, L. G.; Fokin, V. V.; Sharpless, K. B., *Angew. Chem. Int. Ed.* **2002**, *41*, 2596-2599.

39. Worrell, B. T.; Malik, J. A.; Fokin, V. V., *Science* **2013**, *340*, 457-460.

40. Lieber, E.; Chao, T. S.; Rao, C. N. R., *J. Org. Chem.* **1957**, *22*, 238-240.

41. Nossoni, Z.; Wang, W.; Vasileiou, C.; Borhan, B.; Geiger, J., The Extensive 3D Domain Swapped Structure Dimer in CRBP II by a Single Mutation. 2013.